Studies of the Structure and Ultrafast Dynamics of DNA using 2D-IR Spectroscopy

By Gordon Hithell

Department of Physics

University of Strathclyde

A thesis submitted in the requirement for the degree of Doctor of Philosophy

2017

‘This thesis is the result of the author’s original research. It has been composed by the author and has not been previously submitted for examination which has led to the award of a degree.’

Signed:

Date:

Table of Contents

Parts of this thesis are based on the following publications:

(i) Gordon Hithell, Daniel J. Shaw, Gregory M. Greetham, Paul M. Donaldson, Michael Towrie, Glenn A. Burley, Anthony W. Parker and Neil T. Hunt, Ultrafast 2D-IR and Optical Kerr Effect Spectroscopy Reveal the Impact of Duplex Melting on the Structural Dynamics of DNA, *PCCP* 2017, **19**, 10333-10342

(ii) Gordon Hithell, Daniel J. Shaw, Paul M. Donaldson, Gregory M. Greetham, Michael Towrie, Glenn A. Burley, Anthony W. Parker and Neil T. Hunt, Long-Range Vibrational Dynamics Are Directed by Watson–Crick Base Pairing in Duplex DNA, *Journal of Physical Chemistry B* 2016, **120**, 4009-4018

(iii) Gordon Hithell, Paul M. Donaldson, Gregory M. Greetham, Michael Towrie, Glenn A. Burley, Anthony W. Parker and Neil T. Hunt, Effect of Oligomer Length on Vibrational Coupling and Energy Transfer in Double-Stranded DNA, *Chemical Physics*, In Press, Corrected Proof, Available Online

List of Abbreviations

2D-IR – Two-dimensional infrared spectroscopy

A – Adenine

$AgGaS_2$ – Silver Thiogallate

AMP – Adenosine Monophosphate

AOM – Acousto-optic modulator

AT – Adenine-Thymine

BBO – Barium Borate

C – Cytosine

CLS – Centre line slope

D_2O – Deuterium oxide

DFG – Difference Frequency Generation

DFT – Density functional theory

DNA – Deoxyribonucleic acid

'ds-' – double stranded

FFCF – Frequency-frequency correlation function

G – Guanine

GC – Guanine-Cytosine

Ge – Germanium

H-bond – hydrogen bond

He:Ne – Helium:Neon

IR – Infrared

MCT – Mercury Cadmium Telluride

MGBs – Minor groove binders

MIR – Mid infrared

NLS – Nodal line slope

NMR – Nuclear Magnetic Resonance

OPA – Optical Parametric Amplifier

PC1 – Principal Component 1

PC2 – Principal Component 2

PCA – Principal Component Analysis

PTFE –polytetrafluoroethylene

RF – Radio frequency

RNA – Ribonucleic acid

'ss-' – single stranded

T – Thymine

Ti:Sapph – Titanium sapphire

T-jump – temperature jump

T_m – Melting Temperature

TMP – Thymidine Monophosphate

T_W – Waiting Time

Yb:KGW – Ytterbium Potassium Gadolinium Tungstate

Abstract

In this thesis, two-dimensional infrared spectroscopy (2D-IR) spectroscopy is used to study changes in structure and dynamics in deoxyribonucleic acid (DNA) containing only Adenine-Thymine (AT) base pairs. The aims of the studies in this thesis are to demonstrate the ability of 2D-IR spectroscopy to extract unique dynamic information, not accessible via established experimental methods from nucleic acid systems, as it has for protein- and peptide-based systems.

The underlying theory of both linear and nonlinear 2D-IR spectroscopies is described in the initial Chapter, following this the details of the types of information already obtained using these methods from DNA in the current literature is presented.

Chapter (2) describes the experimental setups and methodologies used to acquire the data in this thesis. A description of FTIR spectroscopy as well as the two laser systems used to acquire 2D-IR data (ULTRA and LIFEtime) are presented.

In Chapter (3), the thermal denaturation of an AT DNA sequence 15 base pairs in length is studied with 2D-IR in the spectral region where vibrational modes of the DNA bases are observed. Changes in the unique features observed in these spectra that are sensitive to DNA conformation are described along with the suitability of 2D-IR for accurately following the transition from double- to single stranded DNA compared to established methods. Changes in solvation dynamics experienced by functional groups of the DNA bases are also discussed.

Chapter (4) demonstrates the ability of 2D-IR to explore multiple spectral regions simultaneously using a two-colour 2D-IR method. This allowed examination of communication between the vibrational modes of the DNA bases and those of the DNA backbone in the same DNA sequence used in the previous Chapter. Dynamics extracted from the features linking these two spectral regions present evidence for an energy transfer pathway through DNA that could be responsible for allowing dissipation of excess energy absorbed by DNA, preventing photo-damage of sequences.

Chapter (5) expands on the studies in the previous Chapter by employing the same experimental methodology to AT DNA sequences of lengths varying from 15 bases pairs to a single base mononucleotide. The changes in observed features that link the base and backbone regions for the different sequences is presented along with the effects varying the sequence length has on the timescales of the energy transfer mechanism described in the previous Chapter.

In Chapter (6) the conclusions presented in the Chapters prior to this point are drawn together to highlight progress made in gaining new insights into structure and dynamics of DNA and also presents possible future directions for studying nucleic acid systems with 2D-IR.

1. Introduction

1.1 Dynamic Insights into Nucleic Acids

At the foundation of the complex landscape of biology lies the most fundamental of all biological molecules – deoxyribonucleic acid (DNA). DNA is Nature's hard drive, storing genetic information of cells within the DNA base sequence.[1] DNA is made up of a sequence of individual building blocks –nucleotides. Each nucleotide contains three components, the first two of which are ribose and phosphate groups which form the sugar-phosphate backbone of a longer chain oligomer. The final component of a nucleotide is the base which can be one of four options, pyrimidine bases Thymine (T) and Cytosine ™ or purine bases Adenine (A) or Guanine (G). Cellular DNA molecules can contain several hundred million bases[2] and the base dictates the sequence of the DNA molecule. DNA is typically found in the double-stranded form, where the two strands are linked by hydrogen bonds between the DNA bases. The traditional Watson-Crick base pairs are formed by the pairing of T with A and C with G. An example of double stranded DNA and a nucleotide building block is depicted in Figure 1.1 below.

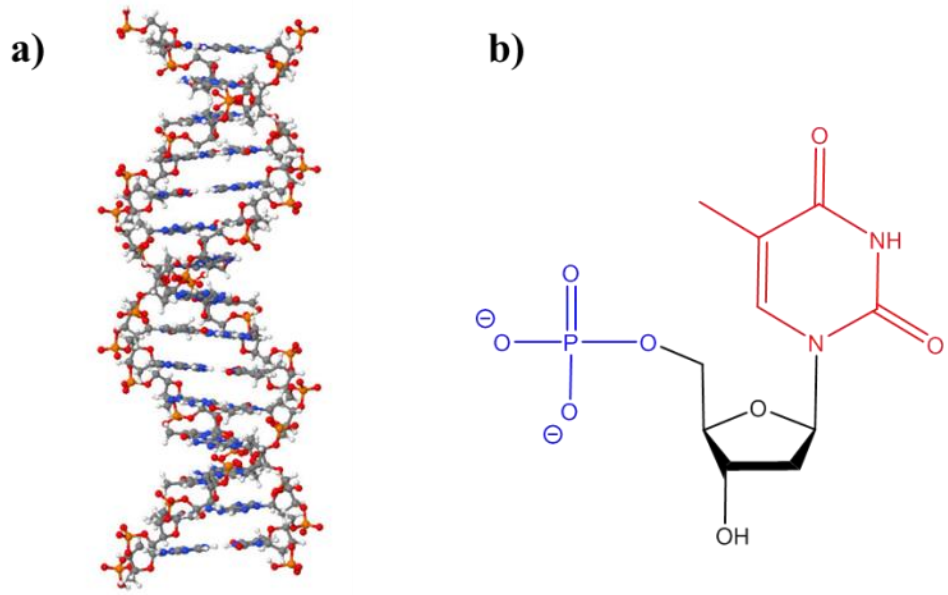

Figure 1.1 *– a) Molecular Structure of the DNA double helix b) Molecular structure of Thymidine nucleotide. Phosphate moiety highlighted in blue and the base in red.*

DNA in its most common conformation, that is the double stranded helix, is dependent on two primary types of interaction between atoms. Strong covalent bonding that holds together the atoms in a DNA strand (~836 kJ/mol), and also the comparatively weak hydrogen bonds that hold two strands together (~4-8 kJ/mol), indeed the structure of DNA is dependent on many of these weak hydrogen bonds to remain double stranded as the strength of one of these weak hydrogen bonds is comparable to room temperature energy (~2.6 kJ/mol).[1] Furthermore interactions between biomolecules are facilitated by these weak hydrogen bonds. When considering that all cellular processes take place in water, a unique substance whose nature is defined by its continually evolving hydrogen bonding network on the a picosecond timescale,[3,4] then hydrogen bonds between biomolecules and water must be considered to play an important role in biological processes, but this complication presents a significant uncertainty when trying to model interactions between large biomolecules.[1] The mechanisms through which biomolecules are able to read the sequence specific code of DNA with high efficiency has garnered great interest for the potential to utilise DNA for both biomedical[5,6] as well as technological advances[7]; however, the physical mechanisms that underpin these interactions are not well understood. The crossover between the physical and biological sciences is growing ever larger with the continued development of physical tools and techniques to aid in interrogating the intricate processes that are vital for biological function.

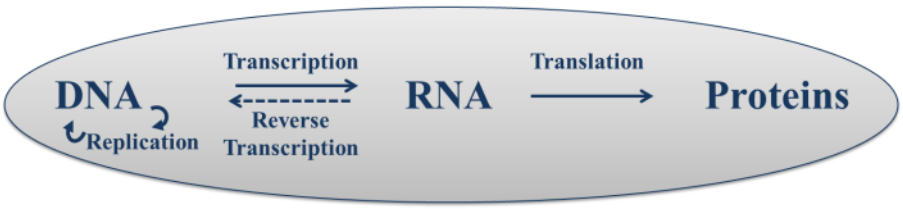

***Figure 1.2** – 'Central Dogma' of molecular biology – Outline of major biological processes.*

Figure 1.2 is a demonstration of the 'Central Dogma' of molecular biology, summarising the major processes in transferring genetic information from DNA.[2] DNA plays a role in two significant processes. The first is the process by which DNA can be copied exactly in order to preserve genetic information in new cells – replication. The second process is transcription where the genetic code in DNA is transcribed into ribonucleic acid (RNA) which then allows the genetic code from the original DNA sequence to be translated into proteins. RNA can also undergo reverse transcription in order to produce template DNA, this is a crucial process in retroviruses which contain no DNA, reverse transcription allows the virus'

genetic code to be replicated, facilitating the spreading of the virus.[2] Both replication and transcription are highly dynamic, for example for DNA strands replicating in eukaryotic cells (Figure 1.3) replication occurs at a rate 50 nucleotides per second with incredibly low error rates of around 10^{-7}–10^{-8}.[2,8] Another key point of note is that DNA is biologically silent when in the double stranded form. In both the replication and transcription processes mentioned above, one of the initial steps in these processes is the unwinding of the DNA double helix in order for the DNA bases to be exposed and the genetic code to be read.

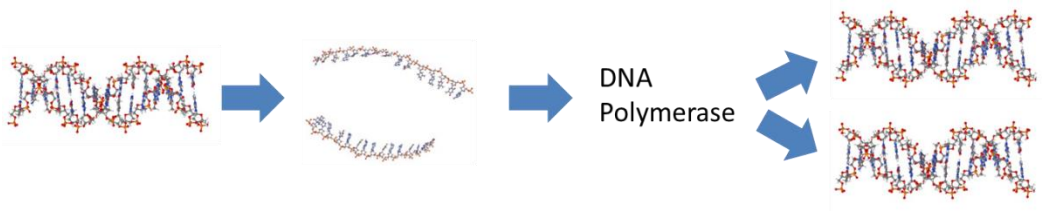

Figure 1.3 *– Simplified outline of DNA replication scheme.*

X-ray crystallography has become the most widely used technique for determining both protein and nucleic acid structures.[9] Indeed it was through this technique that the now iconic double helical structure of DNA was first resolved.[10] While X-ray crystallography offers a powerful insight into biological structure, there are some limitations to this technique. Crystallisation of biological systems can be extremely difficult and if a system is unable to form crystals then it cannot be used in this technique. Furthermore while this technique offers extremely high spatial resolution, the static crystal structures observed with this method may not correlate exactly with the same in the solution phase where biological systems can undergo dynamic motion.

Nuclear magnetic resonance spectroscopy (NMR), in particular multidimensional NMR spectroscopy,[11,12] overcomes one of the disadvantages of X-ray crystallography as molecular structures can be analysed in the solution phase,[13,14] meaning that systems found to be unable to be crystallised can now be investigated. Although this problem is also being overcome by using x-ray sources from a free electron laser to perform diffraction experiments on microcrystals.[15,16] NMR uses radio-frequency (RF) radiation in order to interrogate nuclear spins of a given system. By tuning the frequency of the excitation radiation, the experiment can focus on responses specific from specific elements such as H^1 and C^{13}.[17] NMR spectroscopy has been used to gain structural information about the solution phase conformations of various DNA sequences[18,19] as well as DNA-ligand binding

complexes.[20,21] A further benefit to NMR spectroscopy is the ability to extract dynamic information on a range of timescales from nanoseconds to minutes. Biological processes such as DNA replication and translation are highly dynamic and therefore techniques providing this type of insight are of great value. Within the timescales accessible by NMR, information on processes such as protein conformational[22] changes as well as DNA –ligand binding[23–25] interactions can be obtained. However, the temporal resolution of NMR based techniques is limited to the order of nanoseconds, owing to the pulse duration of RF pulses used. While this allows insight into a number of dynamic processes for biological systems it does not yield insight into the ultrafast dynamics that occur on the picosecond timescales.

Two-dimensional infrared spectroscopy (2D-IR) is a recently developed laser-based spectroscopy technique following the advent of femtosecond laser pulses.[26] The technique is analogous to multidimensional NMR experiments, however, instead of using a RF radiation to interrogate nuclear spins, short pulses of mid-infrared (MIR) light are used to excite molecular vibrations within a given system and generate a 3rd order nonlinear signal.[27] As in 2D-NMR the 2D-IR spectrum produced, (this will be discussed in more detail later), is a correlation map of excitation frequency versus detection frequency. This map provides information on the interactions between the molecular vibrations of the excited system; this is gained in the off-diagonal region of the 2D spectrum. These off-diagonal features provide information on coupling and/or energy transfer between the different vibrational modes. Vibrational coupling can occur either mechanically through bonding interactions or electrostatically through space, depending on the relative orientation of transition dipoles of the vibrational modes and has a strong dependence on distance. By utilising the sensitivity of the 2D-IR signals to the polarisation of the interrogating laser pulses, angles between transition dipoles can be extracted and this can be translated into structural information about the given system.

The ultrafast duration of the MIR pulses used in 2D-IR, typically on the order of hundreds of femtoseconds, offers 2D-IR the ability to access molecular processes occurring on the sub-picosecond timescales, such as fluctuation of hydrogen bonds, motions thought to be critical in underpinning biological functionality. Altering the time delay between the excitation events used in 2D-IR experiments allows evolution of solvation or structural dynamics or energy transfer between vibrational modes in the system under investigation to take place and be subsequently measured. Access to this dynamic information also

allows the possibility to utilise 2D-IR to investigate non-equilibrium processes, such as light-activated reactions or, indeed, processes initiated by changes in temperature.[28–32] The ultrafast time-resolution of 2D-IR leads to the possibility of so called 'molecular movies' of these processes.

Since its development, 2D-IR has been applied to study a number of biological systems,[33–37] however, these have primarily focussed on protein or peptide systems and there have been far fewer studies performed on nucleic acids using this technique. There remains a number of key aspects of nucleic acid structure and dynamics yet to be explored using 2D-IR spectroscopy. For example, as unwinding of double stranded DNA is crucial for the transfer of genetic information, then gaining a dynamic insight into this process will be central to controlling this process via the design of more effective drug molecules which function by preventing the genetic code in DNA bases from being read. 2D-IR spectroscopy affords the opportunity to gain insights into the structural dynamics of biomolecules and the role they play in the structure-function relationship.

1.2 Infrared Spectroscopy

Infrared spectroscopy is commonly used for identification of the chemical composition of a given substance and utilises the fact that absorptions of infrared light are characteristic of the chemical structure of that substance. It is therefore important to understand the origins of these absorptions and how they can be used to investigate structural dynamics of nucleic acids.

1.2.1 Molecular Vibrations

Two covalently bonded atoms can be treated as a classic Morse oscillator. As such the potential energy between the two atoms is at a minimum for an atomic separation that is equal to the natural bond length. An example of the Morse potential is shown in Figure 1.4.

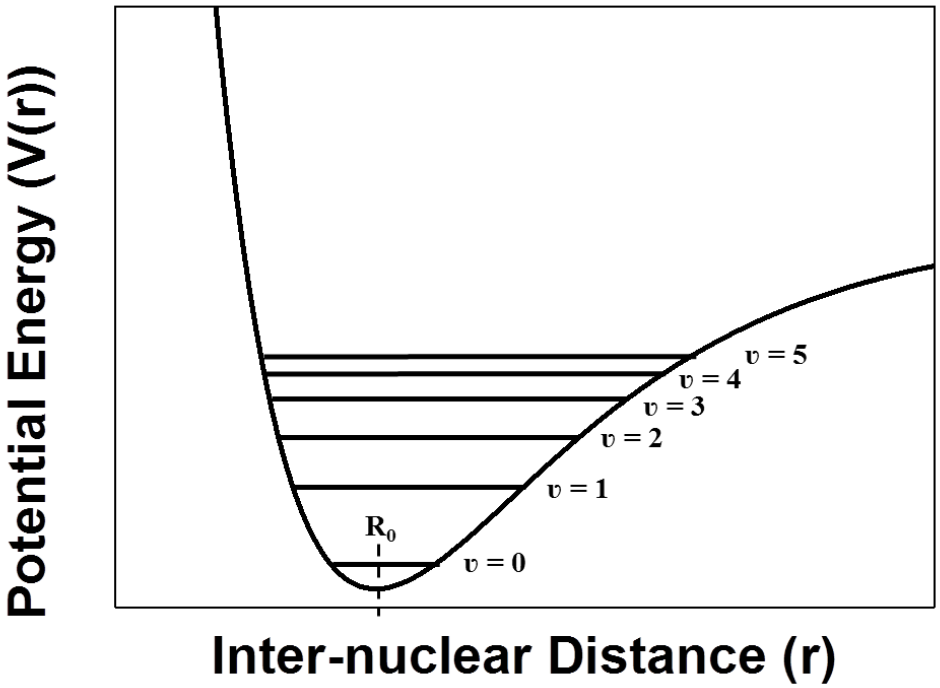

Figure 1.4 *– Morse potential of a chemical bond between two nuclei. Allowed vibrational energy levels depicted along with the vibrational ground state which defines the natural bond length.*

As this is a description of atoms and not macro scaled objects then this must also be described quantum mechanically and is done so by discrete energy levels within the potential. The energy of the discrete levels in the potential well (E_v) are described as follows:

$$E_\upsilon = \left(v + \tfrac{1}{2}\right) v_e + \left(v + \tfrac{1}{2}\right)^2 x_e v_e + \left(v + \tfrac{1}{2}\right)^3 y_e v_e \qquad (1.1)$$

Here v is the vibrational quantum number, v_e is the harmonic energy and x_e and y_e are anharmoncity constants of the Morse potential. The anharmonicity of vibrational modes is crucial for 2D-IR spectroscopy and as such the normal mode description for vibrations, where the potential energy between atoms is described by a harmonic oscillator, cannot be used to describe the vibrational transitions. Indeed the third order response, which is responsible for generating signals in 2D-IR experiments, from a harmonic system is in general zero.[38,39] As will be shown later, without anharmonicty in the vibrational potential, the features in 2D-IR spectra resulting from interactions with the v = 0–1 and v = 1–2 would overlap exactly and so cancel one another out.[27] Anharmonicity is also key to resolving off-

diagonal 2D-IR spectral features between coupled vibrational modes. The anhramonicity of the vibrational modes also allows for transitions to occur between potential energy manifolds, which in turn introduce a perturbation of the coupled states. This perturbation of the coupled vibrational energy levels then leads to the off-diagonal anharmonicities.[38] The off-diagonal anharmonicity that results in the shift of the combination band also allows transitions to the combination band of coupled modes to appear as off-diagonal features in 2D-IR spectra.

The fundamental vibration frequency of a diatomic molecule can be calculated using the following equation:

$$\bar{\upsilon} = \frac{1}{2\pi c}\sqrt{\frac{f(m_1+m_2)}{(m_1 m_2)}} \tag{1.2}$$

Where υ is the unit notation for the frequency unit commonly used in IR spectroscopy – wavenumber in cm^{-1}, c is the speed of light, f is the force constant and m_1, m_2 are the respective masses of the two bonded atoms. Small displacements from the bond length of a diatomic molecule are the simplest example of molecular vibration. As molecules become larger and more complex they can undergo a range of different vibrational motions or modes. The number of vibrational modes available to a structure is governed by the rule 3N-5 modes for a linear molecule and 3N-6 modes for a nonlinear molecule where N is the number of atoms present in the molecule. For large complex molecules such as DNA these vibrational modes can take a number of forms, examples of these are depicted in Figure 1.5 below.

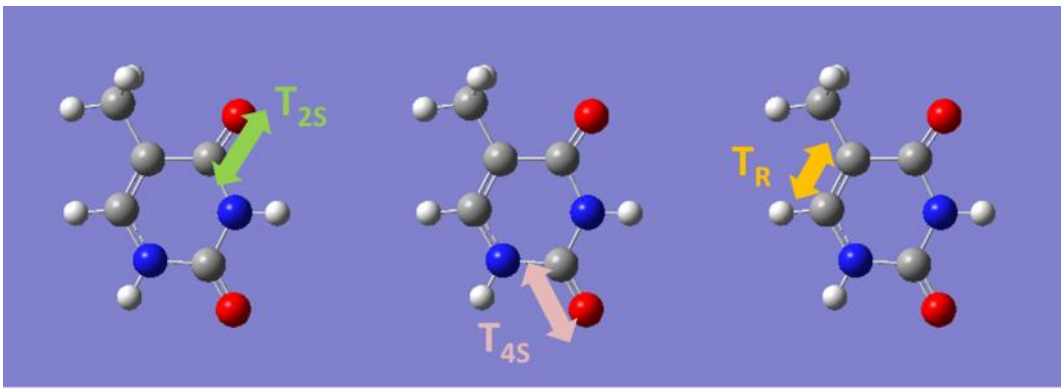

Figure 1.5 *– Illustration of the various types of molecular vibration exhibited by the DNA base Thymine. Illustration created using Gaussview and uses nomenclature described by Cho et al.*[40]

While each of the vibrational modes illustrated in Figure 1.5 are common in most types of molecules, the vibrational frequency of these modes is determined by the masses of the two bonded atoms and the neighbouring functional groups which influence the electron density across the covalent bond and subsequently the vibrational frequency is unique to different molecular structures. This offers IR spectroscopy the ability to distinguish between various moieties which are part of a larger molecular structure. For example, vibrational modes from the base moiety of DNA building blocks (shown in red Figure 1.1) in the form of carbonyl stretching modes or C=N ring vibrations are found in the 1500-1700 cm^{-1} spectral region[41–43] while vibrational modes from the phosphate backbone moiety (shown in blue Figure 1.1) are found at lower frequencies in the 1000-1300 cm^{-1} spectral region.[43,44] The chemical environment surrounding one of these active vibrational modes can also influence the infrared spectroscopy by creating differing distributions around the central peak frequency and causing a broadening effect on absorbance peaks in an IR spectrum.

Linear IR spectroscopy has demonstrated that these vibrational modesare sensitive to formation of the DNA double helix or the reverse process of denaturation where the helix is unwound into component single strands.[43] While linear methods have been shown to be sensitive to these changes in the nucleic acid structure, the data is essentially a time averaged picture and give no dynamic insight to these processes. Nor do linear methods provide any insight into how the different vibrational modes of the different components of the nucleic acid structure interact with one another. 2D-IR spectroscopy has the ability to

fill both of these voids with the combination of structural and dynamic information available from these experiments.

1.2.2 IR Absorption Spectroscopy

The absorption of light resonant with the difference in energy between the ground and first excited vibrational energy levels by a dielectric medium induces a polarisation of the charges within that given medium. The charge separation created causes an oscillating dipole moment within the medium at a frequency matching that of the excitation radiation. This oscillation of the polarisation results in the emission of a signal from the medium which recombines with the excitation medium.[45] The phase between the excitation and signal radiation will be π/2 out of phase, resulting in destructive interference at frequencies corresponding to bond vibrational frequencies and therefore features in a detected absorption spectrum.[27]

The polarisation P(t) induced by an electric field E(t) in a given medium can be described as follows:

$$P(t) = \epsilon_0 \chi E(t) = \epsilon_0 (\chi^{(1)} E(t) + \chi^{(2)} E^2(t) + \chi^{(3)} E^3(t) + \cdots \chi^{(n)} E^n(t)) \qquad (1.3)$$

Where ε_0 is the permittivity of free space and χ is the optical susceptibility of the dielectric medium. For the case of linear optics, the intensity of the excitation light is insufficient to generate significant higher order terms and this equation can be reduced to the form:[46]

$$P(t) = \epsilon_0 \chi^{(1)} E(t) \qquad (1.4)$$

As optical susceptibility of the dielectric medium χ is directly related to the 11olarizability of that medium then it is also related to the transition dipole moment of the fundamental transition v=0–1 (μ_{01}).[27] In the classical picture it is vibration of the oscillating charges that results in the emission of the signal field. However the quantum mechanical description is that the excitation field creates a coherent superposition between the ground and first excited vibrational states which creates the macroscopic polarisation in the medium oscillating at the frequency of the fundamental transition and thus results in the signal being emitted with energy equal to that transition. Maxwell's Equations state that oscillating charges will emit radiation that is π/2 out of phase with respect to the

polarisation,[47] this causes the signal to interfere destructively with the excitation radiation at frequencies corresponding to the vibrational transition in the medium.

Over time the macroscopic polarisation decays back to equilibrium according to the molecular response function R(t) as the polarisation is related to the linear response function according to the following equation:

$$P^{(1)}(t) = \int_0^\infty dt_1 E'(t - t_1) R^{(1)}(t_1) \tag{1.5}$$

R(t) contains information unique to the molecular structure being measured, this can be extracted by Fourier transformation of R(t) to the frequency domain, giving the signal field S(ω).

The emitted signal field S(ω) contains both real and imaginary components. While the imaginary component yields information of the dispersive vibrational lineshape D(ω) the real component contains information on the absorptive component of the lineshape A(ω). The phase of D(ω) means that only A(ω) interferes with E(t) and therefore can be detected. D(ω) and A(ω) are given by the following:

$$D(\omega) \propto -\mu_{01}^2 \frac{\omega - \omega_{01}}{(\omega - \omega_{01})^2 + (0.5\gamma)^2} \tag{1.6}$$

$$A(\omega) \propto \mu_{01}^2 \frac{0.5\gamma}{(\omega - \omega_{01})^2 + (0.5\gamma)^2} \tag{1.7}$$

Where ω is the frequency of the emitted light, ω_{01} is the frequency of the fundamental transition and γ is the natural linewidth of the transition. The detected absorption spectrum of A(ω) has a Lorentzian distribution as shown in Figure 1.6.

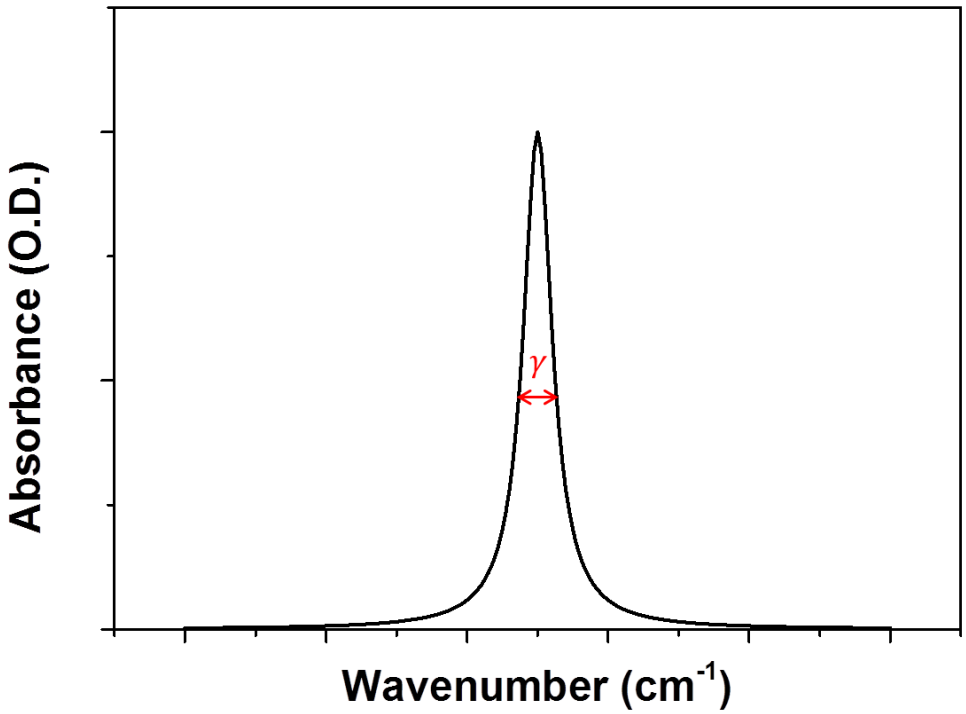

Figure 1.6 *– Graph depicting an absorption peak with a Lorentzian distribution highlighting the natural linewidth γ.*

Absorption features have a natural linewidth and cannot be infinitely narrow. As population of the v=1 vibrational state has an associated error in the time in which this state is occupied or the vibrational lifetime (T_1), therefore there is an error in the energy of the state as per the Heisenberg uncertainty principle:

$$\partial E \cdot \partial t \geq \frac{h}{4\pi} \tag{1.8}$$

Where ∂E is the uncertainty in the energy of the vibrational energy level, ∂t is the time spent in the excited state (vibrational lifetime T_1) and h is Planck's constant. As the frequency of an oscillation is directly related to the difference in energy between the initial and excited states, then an error in the energy will have a direct impact on the error in the oscillation frequency:

$$\partial E = hc \cdot \partial v \tag{1.9}$$

Substitution into equation (1.8) yields:

$$\partial v \geq \frac{1}{4\pi c \partial t} \tag{1.10}$$

Here the error in the frequency of vibration ∂v is directly impacted by the associated vibrational lifetime. The vibrational lifetime T_1 allows for the decay of the induced macroscopic polarisation as the system relaxes back to the ground state. However this decay from the excited state is also subject to other dephasing processes. Rapid fluctuations in the oscillation frequency of a single molecule causes further loss of coherence between the ground and excited state wavefunctions, inducing further decay in the polarisation.[48,49] This process is known as pure-dephasing and occurs on a timescale T_2^*. These two processes contribute to the overall width of the spectral features and therefore the overall natural linewidth is given by the total dephasing rate $1/T_2$:[48]

$$\gamma \sim \frac{1}{T_2} = \frac{1}{2T_1} + \frac{1}{T_2^*} \tag{1.11}$$

Here γ is the natural linewidth of the vibrational transition. A spectral feature with width that depends solely on T_2, then it is said to be homogeneously broadened.

While the minimum linewidth of features in an IR spectrum has been established, features observed in real spectra are often much broader. In a solution phase, the environment around a vibrating oscillator has a significant impact on its dephasing due to the number of conformations available due to interactions with solvent molecules. Hydrogen bonding between an oscillator and solvent changes the electron distribution between the bonded molecules of the oscillator. This in turn changes the potential energy well shown in Figure 1.4, altering the energy of the first excited vibrational state and therefore changing the frequency of the vibration associated with v=0-1 transition. For each oscillator, its vibrational frequency can fall anywhere within a probability distribution with a Gaussian profile determined by the different solvation conformations available to the oscillator.

For an ensemble of oscillators each of these conformations is likely to be occupied, this results in a range of potential vibration frequencies resulting in absorption features that are significantly broader than the natural linewidth. Peaks from a solution phase system are essentially made up a series of overlapping Lorentzian lineshapes resulting in the so-called ‘inhomogeneously broadened’ Gaussian profile as demonstrated in Figure 1.7 below:

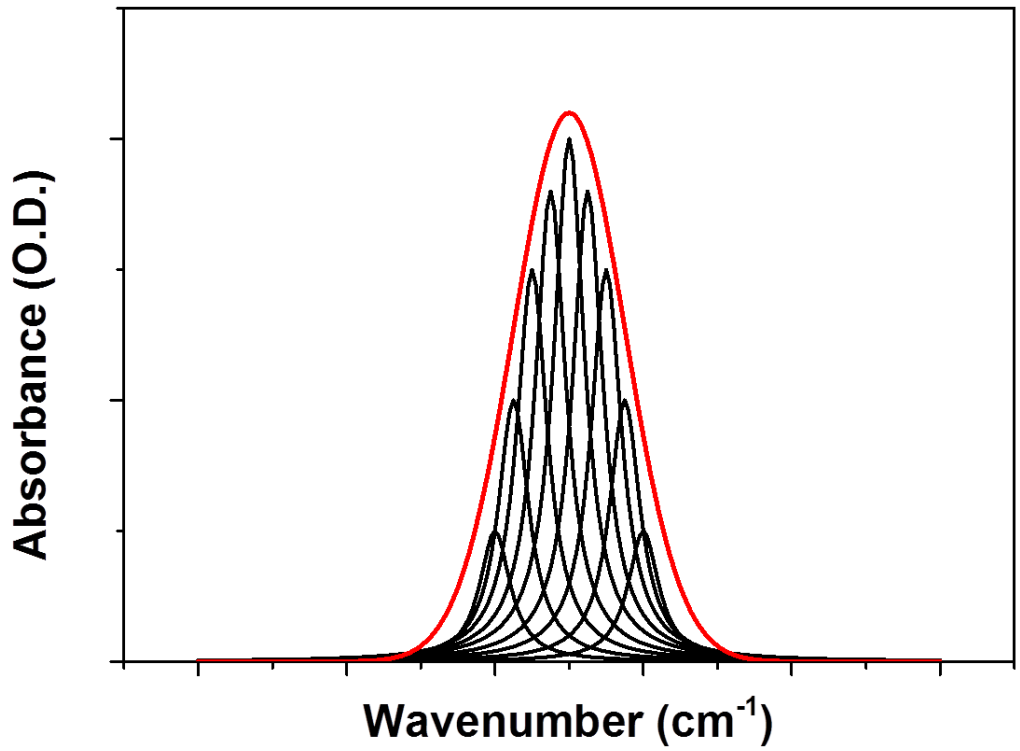

Figure 1.7 *– Example of an inhomogeneously broadened lineshape where a series of Lorentzian lineshapes of various molecular conformations contribute to the broadened Gaussian distribution.*

In practice the interactions that cause inhomogeneous broadening are highly dynamic. The hydrogen bonding network within the liquid water is continually changing and evolving on the sub-picosecond timescale. This means that a vibrating oscillator is continually undergoing fluctuations with its solvent environment resulting in the evolution of the frequency of that vibration with time. This process is known as spectral diffusion. The lineshape of vibrational modes are therefore probes of their local solvation environment. In theory this information is available from linear information spectroscopy. However the contributions from homogenous and inhomogeneous broadening are convoluted and completely inseparable.[27] Furthermore, linear IR spectroscopy does not have sufficient temporal resolution to capture these processes in action and linear IR spectra are essentially a time averaged picture of these processes. 2D-IR spectroscopy offers the possibility of differentiating between these different contributions by providing a greater amount of accessible information by spreading it over a second frequency access. This allows vibrational modes to be used as probes of their solvent environment which can be important in understanding conformations of biological molecules such as nucleic acids

where interaction with their solvent environment can be crucial for nucleic acids to carry out their functions in cellular biological sources.

1.3 Nonlinear Spectroscopy

1.3.1 3rd Order Non Linear Signal

As mentioned previously, linear spectroscopy only requires consideration of the first order optical susceptibility $\chi^{(1)}$ as described in (1.4). However, in order to observe change sin structure and dynamics that influence molecular vibrations, then laser pulses with duration shorter than the timescales these processes occur on are required. Subsequently, use of this high intensity excitation source results in the macroscopic polarisation induced in the medium by the excitation source being no longer able to be considered as linear as the higher order terms of equation (1.3) are now sufficiently large to require consideration. The measured response R(t) from a system excited by laser pulses will therefore contain contributions from $\chi^{(1)}$, $\chi^{(3)}$ and higher order odd-power terms. The higher order odd terms (> $\chi^{(3)}$)are small enough that they are not considered here. Even power terms of the optical susceptibility do not contribute to these responses as in non-centrosymmetric media they are equal to zero ($\chi^{(2n)}$=0).[46]

The most common method whereby 3rd order signals are extracted from a medium is using a 'four-wave mixing' approach, where three excitation fields (laser pulses in this case) are separated temporally by intervals t_1, t_2 and t_3. This approach results in a much more complicated response function than that observed in linear spectroscopy. This response is related to the 3rd order polarisation by the following relationship:

$$P^{(3)}(t) \propto \int_0^\infty dt_3 \int_0^\infty dt_2 \int_0^\infty dt_1 E_3(t-t_3)\, E_2(t-t_3-t_2) E_1(t-t_3-t_2-t_1) R^{(3)}(t_3,t_2,t_1) \quad (1.12)$$

Deconvolution of the 3rd order response from the excitation fields is achieved by using phase matching of the pulse sequence.[27] In four-wave mixing the three excitation fields are referred to by their respective wave-vectors ($2\pi/\lambda$) $\vec{k}_1$, $\vec{k}_2$ and $\vec{k}_3$ with the emitted signal field referred to as $\vec{k}_4$. The numbered subscript indicates the temporal order of each of the fields.

In order to fully describe interaction of the laser pulses with a given system containing an ensemble of oscillators, both quantum mechanics as well as statistics must be incorporated. To do this, density matrix representation is used which describes the statistical average of the ensemble. When one of the excitation pulses interacts with the ensemble, the transition dipole operator μ is applied to the density matrix. Depending on the sign of the excitation pulse ($\pm\vec{k}$) then the interaction with the density matrix will be different, with positive wave vectors exciting the *ket* state of the ensemble and negative wave vectors exciting the *bra* state. De-excitation of the *bra* and *ket* states is the opposite to this with positive or negative wave-vectors de-exciting the opposing bra or *ket* state to that which it is initially excited.[27]

The interaction of three excitation fields with an ensemble therefore presents a number of pathways through which the density matrix can evolve. However these multiple pathways can result in one of two cases and examples of these are depicted in Figure 1.8 below using Feynman diagrams as a graphical way to represent the temporal evolution of the density matrix. If the sign of the first excitation field causes excitation of the *bra* state of the ensemble and the signal field $\vec{k}_4$is emitted by de-excitation of the *ket* state of the ensemble then this is said to be a 'rephasing' pathway.[27] Response functions that contains a rephasing pathway are able to restore the macroscopic polarisation incurred by the initial excitation field and so emits a 'photon-echo' signal.[27]

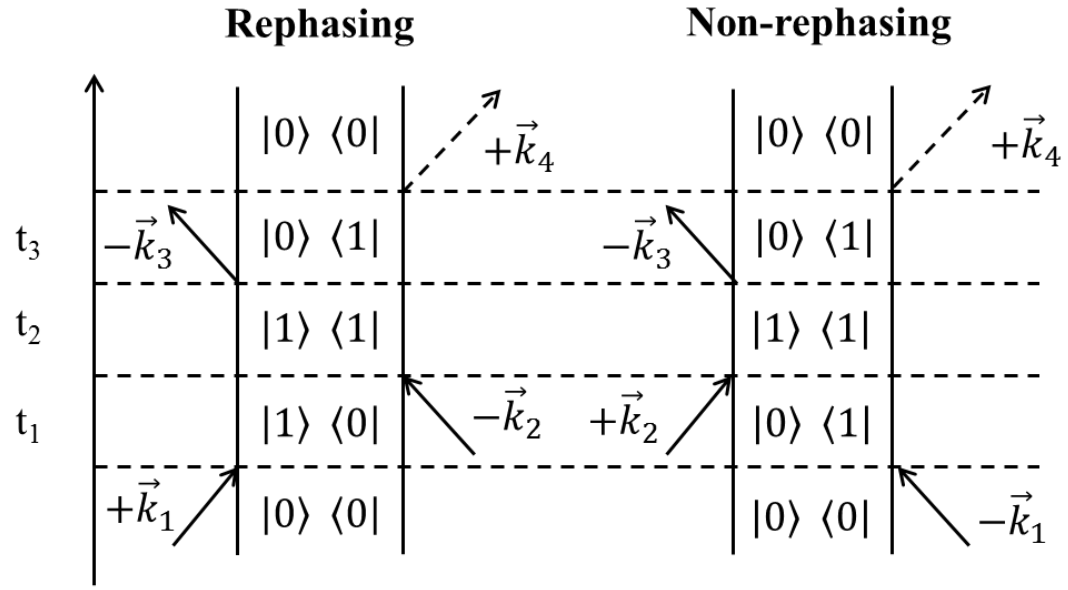

Figure 1.8 *– Feynman diagrams for cases of rephasing and non-rephasing pathways.*[27]

In contrast to this, a pathway which has initial excitation in either *bra* or *ket* and which is de-excited from the same state after interaction with the third excitation field is said to be a 'non-rephasing' pathway. Non-rephasing pathways are insensitive to inhomogeneous dephasing and therefore collecting data from both rephasing as well as non-rephasing pathways is necessary for separation of homogeneous and inhomogeneous linewidths and even for preventing distortion of lineshapes from 3rd order responses.[27]

Now that a formalism for the pathways for the molecular ensemble as they interact with the laser pulses has been detailed, a description of how 3rd-order nonlinear responses are emitted from the ensemble is detailed below.

- The ensemble is initially in the ground state.

- The first pulse, $\vec{k}_1$, interacts with the system, exciting either the *bra* or *ket* of the ensemble, creating a coherent superposition of the ground and first excited states, which oscillates with a frequency ω_{01}.

- During the time t_1 between the first and second pulses, the macroscopic polarisation created by $\vec{k}_1$, decays as a result of dephasing between molecules.

- The second pulse, $\vec{k}_2$, converts the superposition state into a population state by either de-excitation of the previously excited *bra* or *ket* or excitation of the opposite state to that initially excited.

- During the time t_2 between the second and third pulses, the population state evolves with time, this can be vibrational relaxation, spectral diffusion or the transfer of energy between coupled modes.

- The third pulse, $\vec{k}_3$, induces a second superposition state by exciting or de-exciting either the *bra* or *ket* state of the ensemble, this restores the macroscopic polarisation of the system. For rephasing pathways, the coherence between the molecule returns after a time t_3, this time is approximately equal to the time t_1, as the time taken to restore coherence is of the molecules is equivalent to reversing the initial dephasing.

- Following the time t_3 then the signal field $\vec{k}_4$, is emitted from the ensemble.

With the information contained within the emitted signal field directly relating to the pathway explored by the ensemble during the steps above, this information then gives rise to the features observed in a 2D-IR spectrum. The origins of these spectral features will be explained further in the following section; however, it is interesting for now to note that the number of laser pulses used in generation of 3rd-order nonlinear signals allows the possibility of the molecular ensemble climbing the vibrational ladder to access quantum states higher than v=1.[27] While access to these states is possible in linear spectroscopy, transitions such as v=0-2 are very weak as the transition dipole for this transition, μ_{02}, is very small due to vibrational selection rules.[27] However, when accessing these higher states by climbing the vibrational ladder through 3rd order spectroscopic techniques, the size of the associated transition dipole for the v=1-2 (μ_{12}) transition is much greater, making this an ideal way of accessing higher quantum states that are otherwise extremely weak in linear spectroscopies. A number of possible pathways for the molecular ensemble are shown in Figure 1.9, including pathways in which the v=2 quantum state is accessed and coherences between the v=1 and v=2 states are obtained.

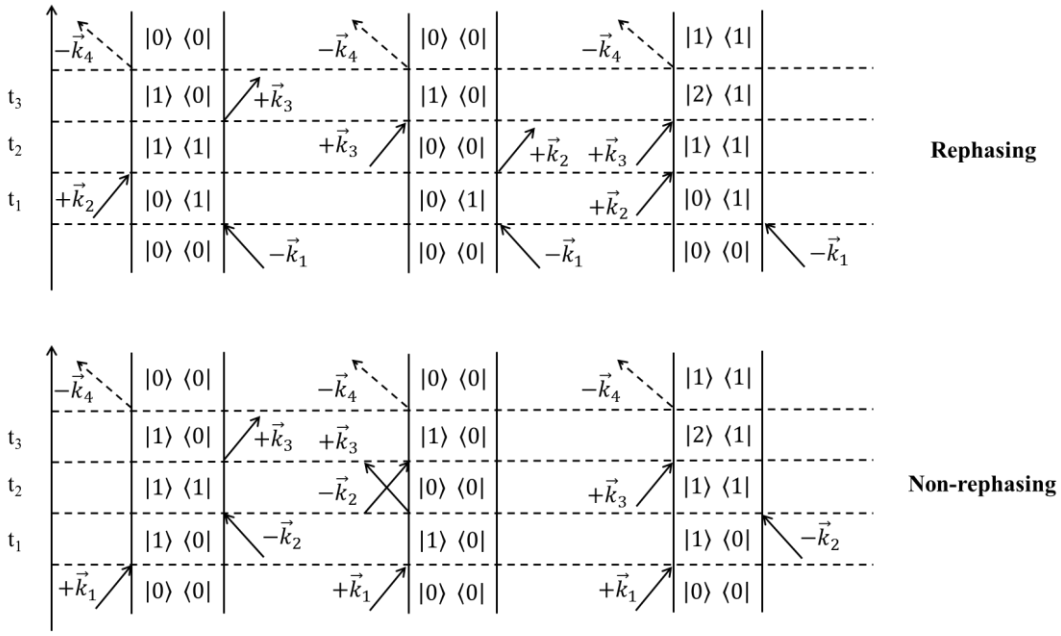

Figure 1.9 *– Six possible Feynman diagrams for pathways in 2D-IR spectroscopy. The top row of diagrams represents rephasing pathways and non-rephasing pathways are shown on the bottom row.*

As the propagation of these pathways are dependent on the sign of the wave vector of each laser field, then some pathways produced via this four-wave mixing process can be discriminated over others by a process called 'phase matching'.[27] This direction of the emitted signal field from the interaction is determined by the wave vectors of the initial three laser fields. In particular this technique can be used to discriminate between rephasing and non-rephasing pathways should this be desired, however, collecting both of these pathways yields so called purely absorptive 2D-IR spectra which preserves the sign of the measured response function as well as offering the highest possible frequency resolution.[27] In the experiments used throughout this thesis, a laser pulse geometry is used such that the first two laser pulses are collinear ($\overrightarrow{k_1} = \overrightarrow{k_2}$) which results in rephasing and non-rephasing pathways to be emitted in the same direction which simplifies the experimental setup required to capture the complete 3rd-order signal.[50] As such the phase matching condition utilised in the experiments in this thesis is as follows:

$$\overrightarrow{k_4} = -\overrightarrow{k_1} + \overrightarrow{k_2} + \overrightarrow{k_3} \tag{1.13}$$

A further benefit of using a pulse geometry where the first two laser fields are collinear, is that the signal field produced by the four wave-mixing process is emitted collinear with $\overrightarrow{k_3}$, which allows for $\overrightarrow{k_3}$ to act as a local oscillator and self-heterodyne the signal. This phase information is retained when the signal is collected, ensuring that spectra produced can be correctly phased. This will be discussed further in Chapter 2. In the next section the features produced in a 2D-IR spectrum are discussed along with how they relate to the Feynman diagram formalism presented in this section.

1.3.2 2D-IR Spectroscopy

2D-IR spectroscopy is an example of a four-wave mixing technique which is able to extract information on the molecular ensemble as described in the previous section. By spreading the information contained in the molecular response over a second frequency axis, as well as use of ultrafast laser pulses as a light source, then information that is inaccessible in linear IR spectroscopy can now be obtained. Construction of the second frequency axis required in 2D-IR spectroscopy can be achieved using two methods. The first method is a frequency domain approach which is the simpler approach experimentally and uses narrow bandwidth pulses where the centre frequency is scanned to generate the second frequency axis.[37] Narrow bandwidth pulses have an increased pulse duration which subsequently results in a diminished temporal resolution using this method.[51] This makes this approach less suitable for interrogation of ultrafast processes in biological systems and as such details on the frequency-domain approach will not be described here. The second approach is a time-domain based approach[52] and this approach is the methodology used for the experiments throughout this thesis.

The time-domain 2D-IR approach utilises broadband laser pulses to extract 3rd order responses from a molecular ensemble, resulting in a greater temporal resolution than that available in the frequency domain approach. These excitation fields result in the emission signal field which is detected by dispersion of the signal via a spectrometer onto an array detector. Dispersion of the signal field yields one frequency axis of the 2D-spectrum, referred to as the detection or probe frequency axis. The second frequency axis in the time-domain approach is constructed via control of the temporal delay between the first two excitation fields (pump pulses) in the sequence. This can be performed either by use of an interferometer set-up, controlling the pulses with variable optical delay lines, or by

acousto-optical modulation using a 'pulse shaper' to replicate the effects of an interferometer but also reducing acquisition time due to there no longer being a need to wait on movement of mechanical stages.[53,54] By recording the emitted signal field as a function of the time delay between the pump pulses and performing a Fourier transform the frequency domain data can be recovered. This process will be discussed further in Chapter 2 relative to the laser systems used in the experiments presented in this thesis.

Shown below is an example 2D-IR spectrum of two coupled vibrational modes recorded at a very short time interval between the second and third laser pulse interaction, referred to as the waiting time (T_W). Accompanying this spectrum is an energy level diagram for the two vibrational modes. In this energy level diagram, ground state is denoted as $|00\rangle$. Five other energy levels are considered, the first excited state of each of the two modes, $|01\rangle$ and $|10\rangle$, the two second excited states,$|02\rangle$ and $|20\rangle$ and the combination band between the two modes $|11\rangle$.

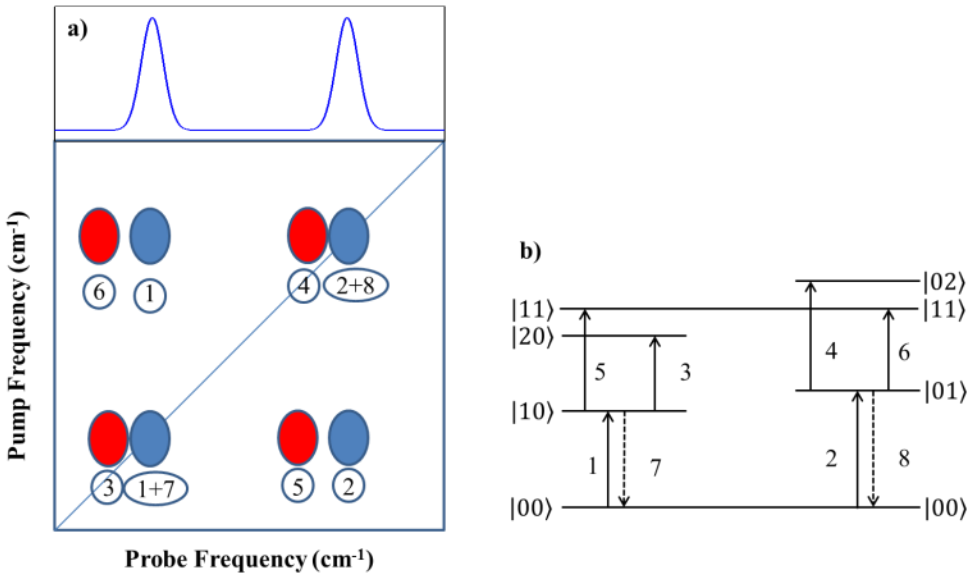

Figure 1.10 *– a) Example linear IR spectrum of two coupled vibrational modes (upper panel) and corresponding example 2D-IR spectrum of the same two coupled vibrational modes (lower panel) b) Energy level diagram indicating excitation pathways undergone to create each of the features in the example spectrum.*

In the example spectrum shown, there are two regions that must be considered – the on-diagonal region and the off-diagonal region. First we will consider the peaks labelled (1+7) and (2+8) in Figure 1.10a). In terms of Feynman pathways discussed previously, these

features are the result of a pathway which contains the same coherence between the ground and first excited vibrational state (i.e. $|00\rangle\langle 01|$ or $|01\rangle\langle 00|$) during both t_1 and t_3. Accompanying each on-diagonal feature is a second feature with opposite sign to the diagonal feature. For pathways that generate a population state of the v=1 vibrational energy level during the period t_2 ($|10\rangle\langle 10|$ or $|01\rangle\langle 01|$) which allows the third laser interaction to generate a coherence during t_3 between the first and second excited states ($|20\rangle\langle 10|$ or $|01\rangle\langle 02|$) and result in features labelled 3 and 4 appearing in the example spectrum. The v=1-2 features are found at a lower detection frequency than the v=0-1 features due to the anharmonicity of the vibrational potential. Were the system investigated a completely harmonic one, then the v=1-2 feature would lie on top of the v=0-1and cancel each other out exactly, meaning a 2D-IR spectrum would for a system of this sort would be featureless. The sign here is opposite to the on-diagonal as the result of the Feynman diagram carries a $(-1)^n$ term where n is the number of interactions that act upon the right side of the diagram.[27] For pathways that manifest themselves in 2D-IR spectral features with the phase matching geometry used, the number of interactions with the right side of the of the diagram will be even for features that result from a v=0-1 transition giving a positive a result, while for features from v=1-2 transitions will have an odd number of interactions with the right hand side yielding a negative response.

The second region to consider in 2D-IR spectra is the off-diagonal region. In the example spectrum in Figure 1.10a) it should be noted that the value of T_W=0. Features observed in this region are due to coupling between vibrational modes. Coupling between vibrational modes arises when two oscillating chemical bonds are close enough that the vibrational potentials influence one and another and as such if vibration of one oscillator influences the other such that vibrations in the second oscillator occur.[27] If two modes are vibrationally coupled then they can be thought of as sharing a common ground state as shown in the energy level diagram in Figure 1.10b).[34] This means that excitation of the $|00\rangle \rightarrow |10\rangle$ transition results in a depletion of the shared ground state and so a negative off-diagonal feature is observed at a detection frequency equal to the $|00\rangle \rightarrow |01\rangle$ transition frequency and results in the feature labelled 1 in Figure 1.10a) and also the feature labelled 2 if the case is reversed and the $|00\rangle \rightarrow |01\rangle$ transition is the initially excited one. The accompanying positive feature labelled 6 is due to the transition $|01\rangle \rightarrow |11\rangle$ (or feature labelled 5 for the $|10\rangle \rightarrow |11\rangle$ transition) to the anharmonically shifted combination band. The anharmonicty of the combination band is not equal to that

of the v=1-2 transition and as such the separation of the off-diagonal features yields the off-diagonal anharmonicty. Off-diagonal features are crucial in the extraction of structural information from 2D-IR spectra as their peak intensity depends on the distance and relative angle between the transition dipole moments of the two vibrational modes in question and therefore understanding how coupled modes are interacting with one another allows interpretation of molecular structure.

A single 2D-IR spectrum is recorded with a fixed value of T_w. Recording a series of spectra at a range of waiting times yields dynamic information from the system under investigation. For on-diagonal features, as T_w is increased then the probability of the population state created, following the first two laser field interactions, decaying back to the ground state increases, this results in a decrease of the amplitude of these features at longer delay times. At a sufficiently a long value of T_w then the population state will have completely relaxed to the ground state and so the amplitude of the 2D-IR features will be zero. Plotting the amplitudes of these features as a function of T_w yields the vibrational lifetime of that particular vibrational mode.

Further information can be observed through dynamics in off-diagonal spectral features. When mentioned previously in this section, these features were considered only due to coupling between vibrational modes and therefore present in the earliest recorded 2D-IR spectra and will decay in amplitude in accordance with their associated diagonal peak amplitudes. However 2D-IR spectroscopy has also been used to study the transport of vibrational energy within a molecular structure.[55–62] In these experiments off-diagonal features between vibrational modes exhibit intensity profiles which initially grow as the waiting time increases. This is due to population relaxation from one mode into another mode. In terms of the energy level diagram considered previously in Figure 1.10b), following population of the $|10\rangle$ vibrational level, population transfer allows the transition from $|10\rangle \rightarrow |01\rangle$ to be possible. Subsequently this means that the $|01\rangle \rightarrow |02\rangle$ becomes possible and results in another peak appearing in the 2D-IR spectrum found in this case between peaks 6 and 1 of Figure 1.10a).[49,51] This is due to the anharmonicty of the $|01\rangle \rightarrow |02\rangle$ transition (the receiving mode in the energy transfer example) differing from that of the $|10\rangle \rightarrow |20\rangle$ which results in the initial cross-peak labelled 6 in Figure 1.10a). The presence of these spectral features is indicative of energy being transported from one mode to another. These experiments can typically employ laser pulses centred in two

different spectral regions in order to excite vibrational motion in one part of a molecule and probe at a frequency resonant with a second part of the molecule in order to observe the vibrational energy transfer between the modes.[55,62] Information from these experiments can provide useful insight into interactions between vibrational probes that are separated by distances that are typically too far apart to experience vibrational coupling as well as identifying pathways for energy transport through a molecular structure.

Recording 2D-IR spectra at a series of waiting times also allows for evolution of the lineshapes of spectral features via dynamic processes. The example spectrum in Figure 1.10 did not consider any dynamic evolution, another example system consisting of a single vibrational mode is considered. 2D-IR spectra recorded at two values of T_w and that show lineshape changes with increasing value of T_W is shown in Figure 1.11 below.

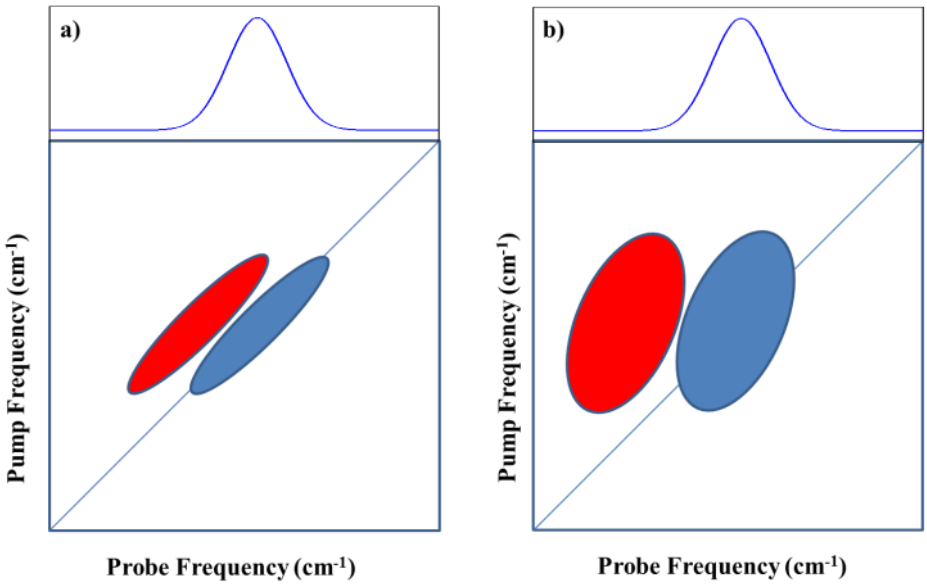

Figure 1.11 *– Example 2D-IR spectra of a single vibrational mode recorded at (a) T_w=0 and (b) T_w>0. The upper window in (a) and (b) depicts the linear IR spectrum of the example single vibrational mode while the lower window shows the corresponding 2D-IR spectrum. Increasing T_W results in broadening of the spectral features in the 2D-IR spectrum in (b).*

At short values of T_w approaching T_w=0 as represented in Figure 1.11a), the on-diagonal v=0-1 feature along with the accompanying v=1-2 feature are elongated along the diagonal while the anti-diagonal width of the features are much narrower. The anti-diagonal width reflects the homogenous linewidth of the vibration. A much narrower anti-diagonal width than the diagonal width implies that the vibrational mode is inhomogeneously broadened

as if homogenous broadening was the only contribution to the linewidth then the diagonal and anti-diagonal linewidths would be equal. At such short waiting times such as is considered in Figure 1.11a), a vibrating oscillator will experience a 'static' environment. This means that following a waiting time period which is shorter than the fluctuation of solvent molecules around the oscillator, then the frequency of the oscillator cannot evolve.

In order to observe effects of fluctuations in the environment then the vibrating oscillator must be given more time to experience those fluctuations. This is achieved by increasing the waiting time and measuring the spectrum at these longer times, an example of which is shown in Figure 1.11b). In this example the anti-diagonal width of the spectral features has increased and the features become broadened and more circular. At longer waiting times, the vibrating oscillator will experience a range of vibrational frequencies as the solvent molecules around the oscillator continually re-orientate, giving rise to a greater probability of the oscillator having a detected vibrational frequency which is different from that which it was initially excited. This process is known as spectral diffusion.

For an oscillator that is undergoing inhomogenous broadening, spectral diffusion will cause the lineshape of 2D-IR spectral features to become increasingly more circular as the waiting time is increased. The rate at which spectral diffusion occurs can be quantified by measuring the change in the lineshape at a series of waiting times. This is a measure of how well the excitation frequency of a vibration is correlated with the detection frequency. There are a number of methods through which this quantification can be achieved. Three such methods are the central line slope approach (CLS),[63] the nodal line slope approach (NLS)[64,65] and fitting of two-dimensional Gaussian features.[66] Each of these methods fundamentally extracts the same information, a measure of how well correlated the frequency of a given oscillator following an initial excitation is with the frequency observed for that oscillator after a given time to interact with its environment (the waiting time). This result is known as the frequency-frequency correlation function (FFCF) a description of how this information is extracted from 2D-IR spectra using some of the analysis methods mentioned is presented below.

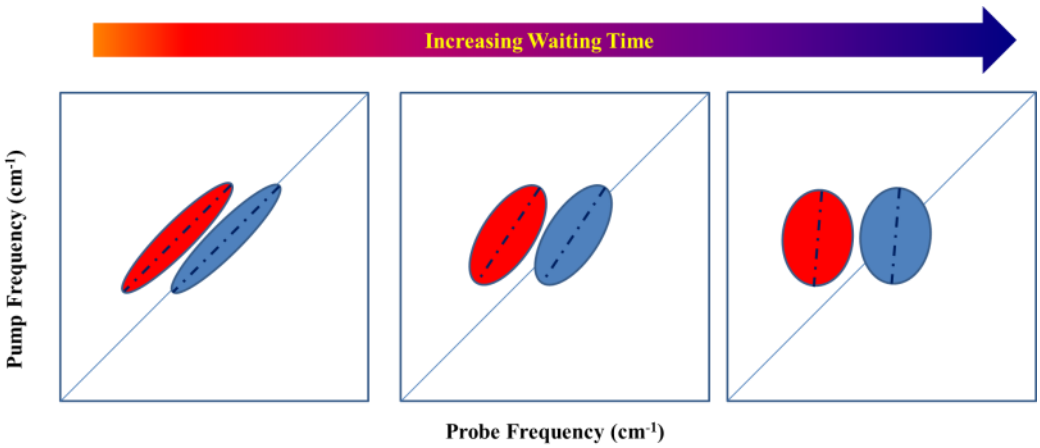

Figure 1.12 *– Example of CLS analysis extracted from spectra undergoing spectral diffusion with increasing waiting time. The CLS for each spectral feature at a given value of* T_W *is depicted by the dot-dash line through the red and blue features.*

CLS analysis (demonstrated in Figure 1.12) is performed by extracting the probe frequency at which the maximum amplitude of a 2D-IR feature is found at a given pump frequency. This can be performed on either negative v=0-1 features or positive v=1-2 features. By extracting this probe frequency value at which the maximum amplitude is found at a series of pump frequencies through the spectral feature, a straight line can be overlaid onto that feature. At short waiting times, little to no spectral diffusion is observed and the CLS obtained should lie parallel to the diagonal line through the spectrum and has a gradient of 1 relative to the pump and probe frequencies. As the waiting time is increased and the vibration undergoes spectral diffusion, this line becomes increasingly more vertical until a maximum gradient of ∞ is reached. At this point the correlation between the initial and final vibrational frequencies is zero.

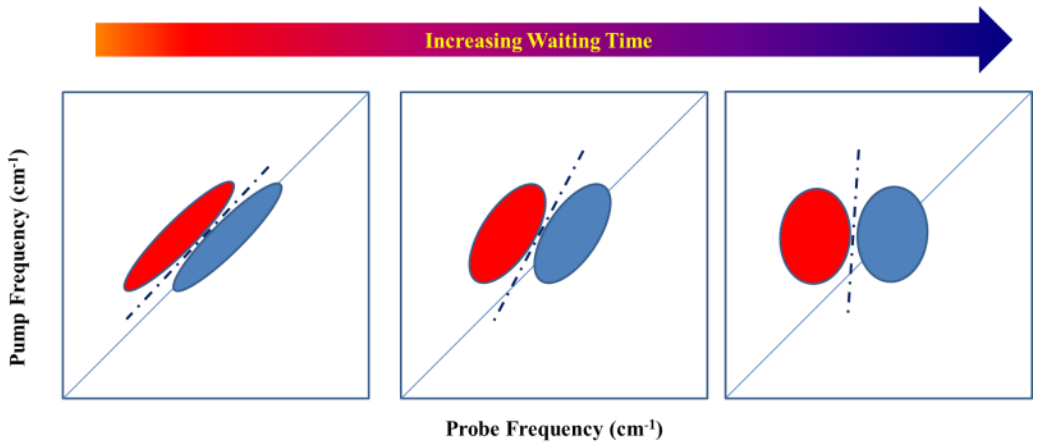

Figure 1.13 *– Example of NLS analysis extracted from spectra undergoing spectral diffusion with increasing waiting time. The NLS for each spectrum at a given value of T_W is depicted by the dot-dash line between the red and blue features.*

NLS analysis uses a similar approach (Figure 1.13). However in this method, instead of recording the point at which amplitude is a maximum, the frequency recorded at each pump frequency is the one where the sign of the signal changes from the negative v=0-1 feature to the positive v=1-2 feature. In both CLS and NLS analysis methods, the inverse of the gradient that is overlaid onto the spectrum gives the time dependent correlation of the vibrational frequencies.

If 2D Gaussian fitting is used for spectral diffusion analysis, then the positive and negative features in a 2D spectrum are fit with a sum of Gaussian lineshapes along both the pump and probe axes. From this the relative correlation of the diagonal and anti-diagonal widths can be extracted from the fitting function used.

Regardless of the analysis method used, they should each extract the same dynamic information from the spectra, the FFCF. However it has been shown that some methods are more suited than others to different types of 2D-IR spectra.[67] For example 2D Gaussian fitting can become unreliable in spectra that have a number of overlapping features or the anharmonicity of a mode is too small, resulting in overlap of the v=0-1 and v=1-2 features. Meanwhile NLS analysis has been shown to become unreliable for spectra where the anharmonicty is too large and positive and negative feature pairs become too far apart.

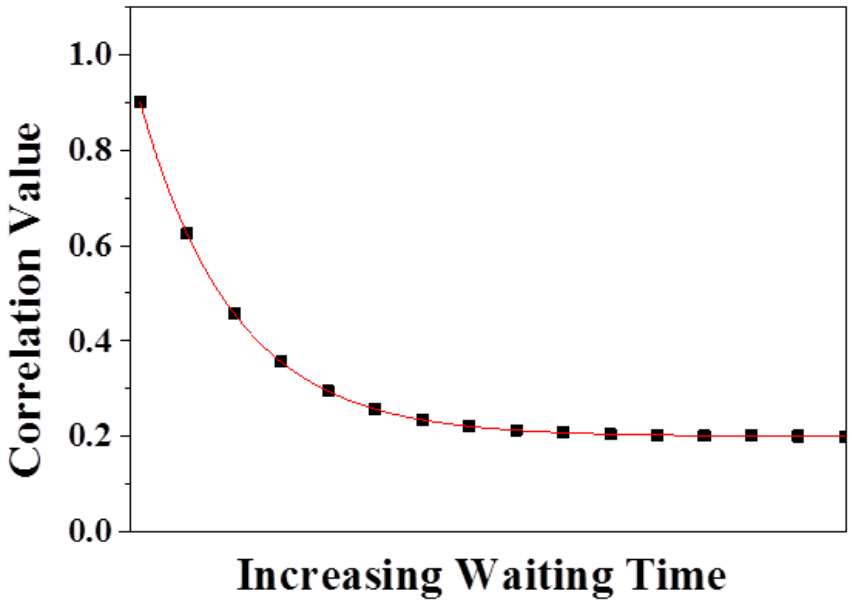

Figure 1.14 *– Example of FFCF plot obtained from spectral diffusion analysis.*

Figure 1.14 shows an example of FFCF which is a result obtained from spectral diffusion analysis for a vibrational mode that is undergoing inhomogeneous broadening. A number of pieces of information can be obtained from this plot. Firstly, the main piece of information gleaned from this analysis is the timescale over which the correlation value decays. This is typically described by one or more exponential decays functions in order to extract time constants which can then be assigned to different physical processes. The next piece of information is gained from the end point of the correlation plot. A vibrational mode that is given sufficient time to explore all possible interactions with its environment should theoretically reach a correlation value of zero. However it has been observed that some FFCF plots reach a non-zero static region at longer waiting times,[68,69] which are indicative processes with a timescale too slow for the experiment to observe. The final piece of information comes from the initial correlation value recorded at a waiting time equal to zero. While spectra recorded at such a short waiting time can be unreliable due to the temporal overlap of laser pulses convoluting the nonlinear signals emitted, an initial value smaller than one can be indicative of rapid processes such as rapid structural fluctuations that occur on timescales faster than typical laser pulse durations of around 200 fs.

Interpretation of timescales obtained from FFCF plots is typically aided by some prior knowledge of the environment around the vibrational probe group. Thus allowing ready

interpretation of timescales reflecting a probe that is free in solution or indeed one which is incorporated into a groove or binding site of a biological molecule.

With the range of structural and dynamic information available from 2D-IR spectroscopy, it is therefore an extremely useful method for investigating interactions and processes in biomolecules, in particular in nucleic acids on which there has been distinctly fewer 2D-IR studies than compared to proteins and peptide systems. The details on the information available from 2D-IR spectra presented here is by no means exhaustive, but are intended to provide background for the principles that are prominent in the experiments applying 2D-IR spectroscopy to study changes in structure and observe molecular dynamics previously inaccessible to other experimental methodologies which are presented throughout this thesis.

1.3.3 Application of 2D-IR to DNA

A number of 2D-IR investigations have already been performed on DNA systems yielding to new insights into the behaviour of DNA in the solution phase and, in particular, ultrafast dynamic information relating to how it interacts with its solvent environment. The details of these investigations and the properties investigated in each one are detailed in the following section.

The first 2D-IR measurement of DNA was performed in 2003 by Krummel and co-workers.[70] In this work the 2D-IR spectrum was recorded for a 10mer DNA duplex containing only Guanine-Cytosine (G-C) base pairs in the 1550-1750cm^{-1} spectral region where vibrational modes from the DNA bases are found. Spreading this information along the second frequency axis however allows observation of off-diagonal features indicating coupling between the on-diagonal modes. This coupling was observed between each of the Guanine and Cytosine carbonyl modes; however, the origin of this coupling, whether inter or intra-strand coupling was not obvious.

The origin of the coupling patterns observed by Krummel et al.[70] was investigated using an exitonic coupling model used previously to describe coupling in Amide-I vibrations of peptides.[37] Simulated 2D-IR spectra of the two carbonyl modes are presented with and without inter-strand coupling included. When only one of either inter- or intra-strand coupling are considered in the simulation then the experimental spectrum is not fully

reproduced, indicating that both base pairing between the strands as well as base stacking interactions through the strand are contributing to the off diagonal features observed. Krummel and co-workers were the next to revisit DNA 2D-IR spectra in 2006.[71] Further spectra recorded again in the 1550-1750 cm^{-1} this time for two G-C only DNA oligomers, one the G_5C_5 sequence measured in their previous work which produces an A-form type duplex and a longer 16 base sequence with alternating G/C base content whose structure is found to be a B-form duplex. Differences in the off-diagonal features in the 2D-IR spectra of the two duplexes indicates that hydrogen bonding between the bases is not the only mechanism that is responsible for the coupling patterns but the differing stacking geometries of the A and B-form duplexes must also play a role. In this work the authors look to further investigate the mechanism though which the coupling between the DNA base modes occurs. Computational modelling has allowed a comprehensive calculation of the various coupling constants between stacked and hydrogen-bonded bases. These results do not take into account hydration and charge transfer effects and also do not consider the more complex cases of duplex that also include adenine and thymine bases. The first experiments performed by Zanni and co-workers showed the sensitivity of 2D-IR as a tool for investigation of DNA structure while its inherent high time resolution make it a strong candidate to explore the fast structural dynamics of DNA that could be crucial to its biological functions.

Following on from the first experimental data recorded on DNA with 2D-IR, Lee and co-workers published a series of papers utilising computational methods to simulate linear IR and 2D-IR spectra in the 1400-1800cm^{-1} region for of a range of DNA lengths and base content. The first paper in this series focuses on Density Functional Theory (DFT) calculations performed on DNA bases, base-pairs and stacks of base pairs for G-C and Adenine-Thymine (A-T) base sequences.[40] These calculations produced simulated IR spectra for each of these cases. Coupling constants between each of the calculated base modes was then calculated using a Hessian matrix reconstruction method. These coupling constants were found to be highly sensitive to WC hydrogen bonding. This work also first presented vibrational base modes as base paired modes when part of a hydrogen-bonded double helix structure.

The second paper in this series by Lee et al., expands on the work in the first article by considering the case more resembling typical experimental conditions where DNA IR

spectra are recorded in heavy water (D_2O). In this case labile protons are exchanged with deuterium atoms which causes a shift in the vibrational modes of the DNA bases.[72] The IR spectra and coupling constants were again calculated for the deuterated variants of those in the first article and compared to available experimental data, showing good agreement. The deuterated spectra and coupling constants found in this work are what is then used in the subsequent calculation of the 2D-IR spectra in the proceeding articles in this series.

Lee and co-workers then went on to calculate simulated 2D-IR spectra of G-C and A-T duplexes with oligomer lengths varying from 1 to 10 bases using the frequencies and coupling constants from the previous studies.[73] 2D-IR spectra displayed reasonable agreement with the experimental data of Krummel et al., despite the difference in duplex conformations between the two studies, with the experimental study using DNA in the A-form conformation as opposed to the B-form configuration considered in the simulations. It was found that the length of the DNA sequences did not have a large impact on the resultant 2D-IR spectrum for that DNA sequence; however this study only considers duplexes in the B-form configuration. This work demonstrated the viability of producing simulated 2D-IR spectra of DNA and is a useful base for prediction and comparison of other experimentally measured spectra of DNA sequences.

The final paper in the series of computational IR studies on DNA builds on the successful calculation of simulated DNA 2D-IR spectra by looking at the 2D-IR spectra and coupling constants produced by A-, B- and Z-form DNA duplexes.[74] These simulations showed that vibrational coupling constants are strongly correlated with duplex conformation due to the variation of the distance between bases in neighbouring base-pair layers. Distinct marker modes of each of the duplex forms also can be useful for assignment of features in future 2D-IR spectra in this region for different DNA sequences as well as another allowing 2D-IR to become another method for characterising the conformation of DNA duplexes in solution. These computational studies carried out by Lee et al. would serve as an invaluable guide for future 2D-IR measurements in this spectral region, along with providing indications of the vibrational modes no longer being considered locally in double-stranded DNA, but delocalised across the base pair.

With an aim of stripping back the complexity of nucleic acid spectroscopy, Peng et al. carried out a study measuring the 2D-IR spectra of the building blocks of nucleic acids – the individual nucleotide monophosphates that make up DNA and RNA oligomers.[75] Spectra

were recorded for each of the five primary nucleotides at parallel and perpendicular polarisations and revealed coupling between each of the various carbonyl stretches and ring deformation vibrations present in each base. A comparison with DFT calculated spectra for each of the bases showed good agreement in terms of both the on- and off-diagonal features observed. Calculations also agreed that a number of the ring vibrational modes are delocalised over the rings, shifting the paradigm from the traditional local mode description. This work can be used as a basis for modelling a range of nucleic acid structures.

All experiments and simulations on 2D-IR spectroscopy of DNA to this point in the literature have focused on the 1500-1700cm^{-1} spectral region. Yang et al. were the first to perform 2D-IR spectroscopy of NH and NH_2 stretching modes located in the 3000-3500cm^{-1} region with an investigation of these modes amongst A-T base pairs in DNA.[76] NH and NH_2 groups are important moieties of the DNA duplex structure as they are directly involved in WC base-pairing, which governs duplex formation. By measuring 2D-IR spectra of a 23 base pair AT duplex prepared in a humidity controlled environment, at a serious of population times, allowed the NH modes of the adenine and thymine bases to be distinguished from one another. Spectral diffusion analysis was carried out on the NH_2 adenine stretch located at 3350cm^{-1} and the thymine NH stretch at 3200cm^{-1} using the centre line slope (CLS) method[77]. The two modes displayed contrasting behaviour with the NH stretch of Thymine becoming homogeneously broadened by a population time of 1 ps while the Adenine NH_2 stretch showed inhomogeneous broadening, indicating disorder in the duplex structure. Authors of this work also observed some vibrational energy transfer from the NH_2 adenine stretch to the thymine NH stretch.

Yang et al. then followed on from this this study with another which explored the NH stretching vibrations of GC base pairs in chloroform.[78] Features in the 2D spectra are assigned using a local mode description to hydrogen bonded and free NH vibrations of the guanosine and cytosine base pairs. Coupling between the Guanosine and Cytosine NH stretching modes are revealed in the off-diagonal region of the spectra while dynamic data show a dramatic decrease in the vibrational lifetime of the NH_2 modes upon hydrogen bonding. As was also observed in the experiments for AT DNA, evidence for energy transfer between the modes from each of the respective bases in the pair is observed in the dynamic data.

An investigation on the interaction of DNA with its solvent environment has also been carried out by the Yang et al..[79] Using the same AT DNA sequence in their previous work, 2D-IR spectra of the NH stretching vibrations as well as spectrally resolved OH stretching vibrations were recorded at various levels of relative humidity to investigate the interactions between the DNA structure and the surrounding solvent molecules. The spectra of the NH stretching vibrations exhibit little change with increased hydration, indicating that the interaction between the DNA modes and the solvated water is limited. Using the CLS analysis method as previous, the spectral diffusion of the OH stretching modes displayed spectral diffusion times slower than observed for bulk H_2O.

Similar to the work on GC base pairs performed previously, Greve et al. and Fidder et al. carried out further and more comprehensive studies on NH stretching modes of AT as well as revisiting GC base pairs in chloroform.[80,81] The work performed on chemically modified Adenosine-Thymidine base pairs in chloroform focuses on the features in the 2D-IR spectrum due to various base pairing geometries other than traditional WC base pairing, including Hoogsteen and reverse-Hoogsteen base pairing where the adenosine base is flipped. A larger number of features than the number of NH modes are observed in the 2D-IR spectrum and can be described by coupling with other low frequency modes and Fermi resonances. The results in this work showed a local mode description of the NH modes is inadequate and that a model taking into account coupling to lower frequency modes of the AT base pairs is required to describe the observed results.

In an extension to the previous work on GC base pairs by Greve et al. and Fidder et al., a higher resolution 2D-IR spectrum has revealed a number of previously unobserved features. The complex set of features observed is assigned to Fermi resonances between the NH modes and lower frequency modes. Like the AT base-pairs, the data strengthens the case for a model of these modes other than a local mode description. Shifting of the description of the NH vibrations to delocalised modes across the base pair as opposed to the previous local mode descriptions is also in agreement with the work focused on vibrational modes in the 1500-1700 cm^{-1} which indicates some general behaviour for the vibrational modes of the DNA bases in the hydrogen-bonded duplex configuration.

The spectroscopic measurements with 2D-IR in a sense then come full circle with a similar study to that previously performed on the NH and OH stretching vibrations in AT DNA duplexes carried out on a 23 base pair GC duplex at different degrees of hydration.[82] Thin

film samples of high optical quality were prepared on Si_3N_4 substrates by replacing the sodium counterions of the oligomers with cetyltrimethyl- ammonium chloride (CTMA chloride) which forms a complex with the oligomers. A custom stainless steel humidity cell was constructed to control the water content of the film. A channel connected the sample chamber to a reservoir where various agents could be placed to control the sample chamber r.h. The sample on the Si_3N_4 membrane was sealed into the humidity cell with P_2O_5 in the reservoir to maintain 0% r.h. inside of the chamber. For DNA at 0% relative humidity, CLS analysis exhibited little change in spectral diffusion by upon reaching a population time of 1 ps. This indicates limited interaction with the limited number of water molecules per base per present under such conditions. At 92% relative humidity with the number of water molecules per base pair greatly increased, more spectral diffusion is seen and the decay constant obtained from the OH band is similar but notably slower than that observed for bulk H_2O. This is consistent with the behaviour seen in the previous work with AT DNA oligomers under the same conditions.

Another important spectral region in DNA spectroscopy is the 1000-1250 cm^{-1} region which contains backbone vibrations sensitive to DNA structure. Siebert and co-workers have measured this spectral region and vibrational modes of the backbone are used as probes of the phosphate-solvent interactions.[44] 2D-IR measurements revealed coupling between the phosphate, phosphodiester linkages and sugar ring vibrational modes. Energy transfer between the modes was also found to occur on the picosecond timescale. Dynamic measurements also revealed a rapid component of the frequency-frequency correlation function (FFCF) of 300 fs, an indication of the direct interaction of the backbone modes with the solvent environment. This work shows that the backbone vibrational modes act as an efficient sink for energy transfer in DNA duplex, dissipating energy into the solvent.

Further experiments have also been performed on the backbone-phosphate region at different hydration levels.[83] At both 0% and 92% relative humidity, spectral diffusion timescales of 300 fs are observed. At the higher hydration levels, the amplitude of the relevant component of the FFCF is double that what is seen at 0% relative humidity, indicative of water molecules playing an important role in the structural fluctuations seen in the spectral diffusion analysis.

One of the most important biological processes undergone by DNA is the transition from double to single-stranded conformation in order for the genetic code contained in the DNA

base sequence to be read, for example when the process of transcription is initiated by transcription factors. A thorough understanding of the denaturation process is therefore of direct importance to understanding the behaviour of DNA in solution and from there its interaction with other biological molecules and machinery. Using temperature-jump (T-jump) 2D-IR spectroscopy, Tokmakoff and co-workers have revealed differences in denaturation mechanisms for different DNA sequences.[84] In general, this study shows that the general mechanism for duplex melting comes first through fraying of the ends of the strands, occurring on a timescale of around 100 ns while complete dissociation of the duplex occurs on timescales of around 10-30 μs. The information from these experiments could prove to be vital in the understanding of future time-resolved studies of DNA-ligand complexes, potentially revealing the timescales and mechanisms through which small molecules such as minor groove binders (MGBs) identify and bind to their target sequences.

An equilibrium state study of a DNA-MGB interaction has already been performed by Ramakers et al.[85] Here the binding of an archetypal MGB, Hoechst 33258, to optimal and sub-optimal binding sites in DNA duplexes has been investigated using 2D-IR. Subtle shifts in the centre frequencies of the bands in the 1500-1700 cm^{-1} region of the 2D-IR spectrum follow behaviour consistent with that observed for the DNA-MGB complex in crystallography and NMR experiments due to propeller twisting of the DNA bases. Comparisons are made between spectra of the MGB bound to two different DNA sequences, one with an optimal binding site while the other contains a sub-optimal binding site. Differences in the 2D-IR spectra of both the bound and unbound sequences do not support the conventional model of a 'lock and key' fitting mechanism but in fact agree with an induced fit mechanism where the binding site undergoes differing amounts of structural changes in order to accommodate the MGB.

As a technique, 2D-IR can serve as a valuable complement to established techniques such as X-ray crystallography and NMR, providing insight into structure and dynamics of biological systems. The early studies on nucleic acid based systems show the great potential of 2D-IR as an avenue for gaining an insight into the fundamental mechanisms that dictate the behaviour of this important molecule and how it can potentially be exploited or controlled as a crucial player in biological processes.

1.4 References

1. Sneppen, K. & Zocchi, G. *Physics in Molecular Biology*. (Cambridge University Press, 2005). doi:10.1017/CBO9780511755699

2. Allison, L. A. *Fundamental Molecular Biology*. (Wiley, 2009).

3. Eaves, J. D. *et al.* Hydrogen bonds in liquid water are broken only fleetingly. *Proc. Natl. Acad. Sci. U. S. A.* **102,** 13019–13022 (2005).

4. Kraemer, D. *et al.* Temperature dependence of the two-dimensional infrared spectrum of liquid H2O. *Proc. Natl. Acad. Sci. U. S. A.* **105,** 437–442 (2008).

5. Neidle, S. DNA minor-groove recognition by small molecules. *Nat. Prod. Rep.* **18,** 291–309 (2001).

6. White, C. M., Heidenreich, O., Nordheim, A. & Beerman, T. A. Evaluation of the effectiveness of DNA-binding drugs to inhibit transcription using the c-fos serum response element as a target. *Biochemistry* **39,** 12262–12273 (2000).

7. Su, W., Schuster, M., Bagshaw, C. R., Rant, U. & Burley, G. A. Site-specific assembly of DNA-based photonic wires by using programmable polyamides. *Angew. Chem. Int. Ed. Engl.* **50,** 2712–2715 (2011).

8. Kunkel, T. A. DNA Replication Fidelity. *J. Biol. Chem.* **279,** 16895–16898 (2004).

9. Callaway, E. The Revolution Will Not Be Crystallized. *Nature* **525,** 172–174 (2015).

10. Watson, J. & Crick, F. Molecular structure of nucleic acids. *Nature* **171,** 737–738 (1953).

11. Aue, W. P., Bartholdi, E. & Ernst, R. R. Two-dimensional spectroscopy. Application to nuclear magnetic resonance. *J. Chem. Phys.* **64,** 2229–2246 (1976).

12. Davis, D. G. & Bax, A. Assignment of Complete 1H NMR Spectra via Two-Dimensional Homonuclear Hatmann-Hahn Spectroscopy. *J. Am. Chem. Soc.* **107,** 2820–2821 (1985).

13. Furtig, B., Richter, C., Wohnert, J. & Schwalbe, H. NMR spectroscopy of RNA.

ChemBioChem **4,** 936–962 (2003).

14. Wüthrich, K. NMR - This Other Method for Protein and Nucleic Acid Structure Determination. *ACTA Crystallogr. Sect. D-BIOLOGICAL Crystallogr.* **51,** 249–270 (1995).

15. Kern, J. *et al.* Room temperature femtosecond X-ray diffraction of photosystem II microcrystals. *Proc. Natl. Acad. Sci.* **109,** 9721–9726 (2012).

16. Lyubimov, A. Y. *et al.* Capture and X-ray diffraction studies of protein microcrystals in a microfluidic trap array. *Acta Crystallogr. Sect. D Biol. Crystallogr.* **71,** 928–940 (2015).

17. Roberts, J. D. *Nuclear Magnetic Resonance - Applications to Organic Chemistry*. (McGraw-Hill Book Company, Inc., 1959).

18. Engman, K. C. *et al.* DNA adopts normal B-form upon incorporation of highly flourescent DNA base analogue tC: NMR structure and UV-Vis spectroscopy characterization. *Nucleic Acids Res.* **32,** 5087–5095 (2004).

19. Lin, Z., Hung, K. N., Grollman, A. P. & De Los Santos, C. Solution structure of duplex DNA containing an extrahelical abasic site analog determined by NMR spectroscopy and molecular dynamics. *Nucleic Acids Res.* **26,** 2385–2391 (1998).

20. Bunkenborg, J., Behrens, C. & Jacobsen, J. P. NMR characterization of the DNA binding properties of a novel Hoechst 33258 analogue peptide building block. *Bioconjug. Chem.* **13,** 927–936 (2002).

21. Spielmann, H. P., Wemmer, D. E., Peter, J. & Ji, J. Solution Structure of a DNA Complex with the Fluorescent Bis-Intercalator TOTO Determined by NMR Spectroscopy. *Biochemistry* **34,** 8542–8553 (1995).

22. Kay, L. E. NMR studies of protein structure and dynamics. *J. Magn. Reson.* **173,** 193–207 (2005).

23. Palmer, A. G., Ranee, M. & Wright, P. E. Intramolecular Motions of a Zinc Finger DNA-Binding Domain from Xfin Characterized by Proton-Detected Natural Abundance 13C Heteronuclear NMR Spectroscopy. *J. Am. Chem. Soc.* **113,** 7863–

7863 (1991).

24. Anderson, K. M. *et al.* Direct Observations of the Ion-Pair Dynamics at a Protein-DNA Interface by NMR Spectroscopy. *J. Am. Chem. Soc.* **135,** 3613–3619 (2013).

25. Lieblein, A. L., Buck, J., Schlepckow, K., Fürtig, B. & Schwalbe, H. Time-resolved NMR spectroscopic studies of DNA i-motif folding reveal kinetic partitioning. *Angew. Chemie - Int. Ed.* **51,** 250–253 (2012).

26. Hochstrasser, R. M. Two-dimensional spectroscopy at infrared and optical frequencies. *Proc. Natl. Acad. Sci. U. S. A.* **104,** 14190–14196 (2007).

27. Hamm, P. & Zanni, M. T. *Concepts and Methods of 2D Infrared Spectroscopy*. (Cambridge University Press: Cambridge, 2011).

28. Hunt, N. T. Transient 2D-IR spectroscopy of inorganic excited states. *Dalt. Trans.* **43,** 17578–17589 (2014).

29. Bredenbeck, J., Helbing, J., Kolano, C. & Hamm, P. Ultrafast 2D-IR spectroscopy of transient species. *ChemPhysChem* **8,** 1747–1756 (2007).

30. Bredenbeck, J. & Hamm, P. Peptide structure determination by two-dimensional infrared spectroscopy in the presence of homogeneous and inhomogeneous broadening. *J. Chem. Phys.* **119,** 1569–1578 (2003).

31. Chung, H. S., Khalil, M., Smith, A. W., Ganim, Z. & Tokmakoff, A. Conformational changes during the nanosecond-to-millisecond unfolding of ubiquitin. *Proc. Natl. Acad. Sci. U. S. A.* **102,** 612–617 (2005).

32. Zhang, X.-X. *et al.* Studying Protein–Protein Binding through T-Jump Induced Dissociation: Transient 2D IR Spectroscopy of Insulin Dimer. *J. Phys. Chem. B* **120,** 5134–5145 (2016).

33. Simpson, N. & Hunt, N. T. Ultrafast 2D-IR spectroscopy of haemoproteins. *Int. Rev. Phys. Chem.* **34,** 361–383 (2015).

34. Hunt, N. T. 2D-IR spectroscopy: ultrafast insights into biomolecule structure and function. *Chem. Soc. Rev.* **38,** 1837–1848 (2009).

35. Adamczyk, K. *et al.* Measuring protein dynamics with ultrafast two-dimensional infrared spectroscopy. *Meas. Sci. Technol.* **23,** 62001 (2012).

36. Ganim, Z. *et al.* Amide I two-dimensional infrared spectroscopy of proteins. *Acc. Chem. Res.* **41,** 432–441 (2008).

37. Hamm, P., Lim, M. & Hochstrasser, R. M. Structure of the Amide I Band of Peptides Measured by Femtosecond Nonlinear-Infrared Spectroscopy. *J. Phys. Chem. B* **5647,** 6123–6138 (1998).

38. Hamm, P., Lim, M., DeGrado, W. F. & Hochstrasser, R. M. The two-dimensional IR nonlinear spectroscopy of a cyclic penta-peptide in relation to its three-dimensional structure. *Proc. Natl. Acad. Sci. U. S. A.* **96,** 2036–2041 (1999).

39. Mukamel, S. *Principles of Nonlinear Optical Spectroscopy*. (Oxford University Press, 1995).

40. Lee, C., Park, K.-H. & Cho, M. Vibrational dynamics of DNA. I. Vibrational basis modes and couplings. *J. Chem. Phys.* **125,** 114508 (2006).

41. Taillandier, E. & Liquier, J. Infrared Spectroscopy of DNA. *Methods Enzymol.* **211,** 307–335 (1992).

42. Tsuboi, M. Application of Infrared Spectroscopy to Structure Studies of Nucleic Acids. *Appl. Spectrosc. Rev.* **3,** 45–90 (1969).

43. Banyay, M., Sarkar, M. & Graslund, A. A library of IR bands of nucleic acids in solution. *Biophys. Chem.* **104,** 477–488 (2003).

44. Siebert, T., Guchhait, B., Liu, Y., Costard, R. & Elsaesser, T. Anharmonic Backbone Vibrations in Ultrafast Processes at the DNA–Water Interface. *J. Phys. Chem. B* **119,** 9670–9677 (2015).

45. Smith, F. G., King, T. A. & Wilkins, D. *Optics and Photonics: An Introduction*. (John Wiley & Sons Ltd., 2007).

46. Boyd, R. W. *Nonlinear Optics*. (Academic Press, 2008).

47. Jackson, J. D. *Classical Electrodynamics*. (John Wiley & Sons Ltd., 1999).

48. Zewail, A. H. Optical Molecular Dephasing - Principles of and Probings by Coherent Laser Spectroscopy. *Acc. Chem. Res.* **13,** 360–368 (1980).

49. Khalil, M., Demirdöven, N. & Tokmakoff, A. Vibrational coherence transfer characterized with Fourier-transform 2D IR spectroscopy. *J. Chem. Phys.* **121,** 362–373 (2004).

50. DeFlores, L. P., Nicodemus, R. a & Tokmakoff, A. Two-dimensional Fourier transform spectroscopy in the pump-probe geometry. *Opt. Lett.* **32,** 2966–2968 (2007).

51. Cervetto, V., Helbing, J., Bredenbeck, J. & Hamm, P. Double-resonance versus pulsed Fourier transform two-dimensional infrared spectroscopy: An experimental and theoretical comparison. *J. Chem. Phys.* **121,** 5935–5942 (2004).

52. Asplund, M. C., Zanni, M. T. & Hochstrasser, R. M. Two-dimensional infrared spectroscopy of peptides by phase-controlled femtosecond vibrational photon echoes. *Proc. Natl. Acad. Sci. U. S. A.* **97,** 8219–8224 (2000).

53. Shim, S., Strasfeld, D. B., Fulmer, E. C. & Zanni, M. T. Femtosecond pulse shaping directly in the mid-IR using acousto-optic modulation. *Opt. Lett.* **31,** 838–840 (2006).

54. Strasfeld, D. B., Shim, S. & Zanni, M. T. Controlling Vibrational Excitation with Shaped Mid-IR Pulses. *Phys. Rev. Lett.* **38102,** 1–4 (2007).

55. Rubtsova, N. I. & Rubtsov, I. V. Vibrational Energy Transport in Molecules Studied by Relaxation-Assisted Two-Dimensional Infrared Spectroscopy. *Annu. Rev. Phys. Chem.* **66,** 717–738 (2015).

56. Qasim, L. N. *et al.* Energy Transport in PEG Oligomers: Contributions of Different Optical Bands. *J. Phys. Chem. C* **120,** 26663–26677 (2016).

57. Kasyanenko, V. M., Tesar, S. L., Rubtsov, G. I., Burin, A. L. & Rubtsov, I. V. Structure dependent energy transport: Relaxation-assisted 2DIR measurements and theoretical studies. *J. Phys. Chem. B* **115,** 11063–11073 (2011).

58. Keating, C. S., McClure, B. A., Rack, J. J. & Rubtsov, I. V. Sulfoxide stretching mode as a structural reporter via dual-frequency two-dimensional infrared spectroscopy. *J. Chem. Phys.* **133,** 144513 (2010).

59. Kasyanenko, V. M., Lin, Z., Rubtsov, G. I., Donahue, J. P. & Rubtsov, I. V. Energy transport via coordination bonds. *J. Chem. Phys.* **131,** 154508 (2009).

60. Rubtsov, I. V. Relaxation-assisted two-dimensional infrared (RA 2DIR) method: accessing distances over 10 å and measuring bond connectivity patterns. *Acc. Chem. Res.* **42,** 1385–1394 (2009).

61. Naraharisetty, S. R. G., Kasyanenko, V. M. & Rubtsov, I. V. Bond connectivity measured via relaxation-assisted two-dimensional infrared spectroscopy. *J. Chem. Phys.* **128,** 104502 (2008).

62. Kurochkin, D. V, Naraharisetty, S. R. G. & Rubtsov, I. V. A relaxation-assisted 2D IR spectroscopy method. *Proc. Natl. Acad. Sci. USA* **104,** 14209–14214 (2007).

63. Kwak, K., Park, S., Finkelstein, I. J. & Fayer, M. D. Frequency-frequency correlation functions and apodization in two-dimensional infrared vibrational echo spectroscopy: A new approach. *J. Chem. Phys.* **127,** 124503 (2007).

64. Kwac, K. & Cho, M. Molecular dynamics simulation study of N-methylacetamide in water. II. Two-dimensional infrared pump-probe spectra. *J. Chem. Phys.* **119,** 2256–2263 (2003).

65. Ghosh, A. & Hochstrasser, R. M. A peptide's perspective of water dynamics. *Chem. Phys.* **390,** 1–13 (2011).

66. Adamczyk, K. *et al.* The effect of point mutation on the equilibrium structural fluctuations of ferric Myoglobin. *Phys. Chem. Chem. Phys.* **14,** 7411–7419 (2012).

67. Guo, Q., Pagano, P., Li, Y.-L., Kohen, A. & Cheatum, C. M. Line shape analysis of two-dimensional infrared spectra. *J. Chem. Phys.* **142,** 212427 (2015).

68. Hunt, N. T., Greetham, G. M., Towrie, M., Parker, A. W. & Tucker, N. P. Relationship between protein structural fluctuations and rebinding dynamics in ferric haem nitrosyls. *Biochem. J.* **433,** 459–468 (2011).

69. Brookes, J. F., Slenkamp, K. M., Lynch, M. S. & Khalil, M. Effect of solvent polarity on the vibrational dephasing dynamics of the nitrosyl stretch in an FeII complex revealed by 2D IR spectroscopy. *J. Phys. Chem. A* **117,** 6234–6243 (2013).

70. Krummel, A. T., Mukherjee, P. & Zanni, M. T. Inter and Intrastrand Vibrational Coupling in DNA Studied with Heterodyned 2D-IR Spectroscopy. *J. Phys. Chem. B* **107,** 9165–9169 (2003).

71. Krummel, A. T. & Zanni, M. T. DNA vibrational coupling revealed with two-dimensional infrared spectroscopy: insight into why vibrational spectroscopy is sensitive to DNA structure. *J. Phys. Chem. B* **110,** 13991–14000 (2006).

72. Lee, C. & Cho, M. Vibrational dynamics of DNA. II. Deuterium exchange effects and simulated IR absorption spectra. *J. Chem. Phys.* **125,** 114509 (2006).

73. Lee, C., Park, K.-H., Kim, J.-A., Hahn, S. & Cho, M. Vibrational dynamics of DNA. III. Molecular dynamics simulations of DNA in water and theoretical calculations of the two-dimensional vibrational spectra. *J. Chem. Phys.* **125,** 114510 (2006).

74. Lee, C. & Cho, M. Vibrational dynamics of DNA: IV. Vibrational spectroscopic characteristics of A-, B-, and Z-form DNA's. *J. Chem. Phys.* **126,** 145102 (2007).

75. Peng, C. S., Jones, K. C. & Tokmakoff, A. Anharmonic vibrational modes of nucleic acid bases revealed by 2D IR spectroscopy. *J. Am. Chem. Soc.* **133,** 15650–15660 (2011).

76. Yang, M., Szyc, Ł. & Elsaesser, T. Femtosecond two-dimensional infrared spectroscopy of adenine-thymine base pairs in DNA oligomers. *J. Phys. Chem. B* **115,** 1262–1267 (2011).

77. Kwak, K., Rosenfeld, D. E. & Fayer, M. D. Taking apart the two-dimensional infrared vibrational echo spectra: More information and elimination of distortions. *J. Chem. Phys.* **128,** 204505 (2008).

78. Yang, M. *et al.* Dynamics and couplings of N-H stretching excitations of guanosine-cytidine base pairs in solution. *J. Phys. Chem. B* **115,** 5484–5492 (2011).

79. Yang, M., Szyc, Ł. & Elsaesser, T. Vibrational dynamics of the water shell of DNA studied by femtosecond two-dimensional infrared spectroscopy. *J. Photochem. Photobiol. A Chem.* **234,** 49–56 (2012).

80. Greve, C. *et al.* N-H stretching excitations in adenosine-thymidine base pairs in

solution: Pair geometries, infrared line shapes, and ultrafast vibrational dynamics. *J. Phys. Chem. A* **117,** 594–606 (2013).

81. Fidder, H. *et al.* N-H stretching vibrations of guanosine-cytidine base pairs in solution: Ultrafast dynamics, couplings, and line shapes. *J. Phys. Chem. A* **117,** 845–854 (2013).

82. Greve, C. & Elsaesser, T. Ultrafast two-dimensional infrared spectroscopy of guanine-cytosine base pairs in DNA oligomers. *J. Phys. Chem. B* **117,** 14009–14017 (2013).

83. Guchhait, B., Liu, Y., Siebert, T. & Elsaesser, T. Ultrafast vibrational dynamics of the DNA backbone at different hydration levels mapped by two-dimensional infrared spectroscopy. *Struct. Dyn.* **3,** 43202 (2016).

84. Sanstead, P. J., Stevenson, P. & Tokmakoff, A. Sequence-Dependent Mechanism of DNA Oligonucleotide Dehybridization Resolved through Infrared Spectroscopy. *J. Am. Chem. Soc.* **138,** 11792–11801 (2016).

85. Ramakers, L. A. I. *et al.* Optimised DNA Minor Groove Binding Follows an Induced Fit Model. *J. Phys. Chem. B* **121,** 1295–1303 (2017).

2. Experimental Methods

This chapter will focus on describing the primary methods and experimental setups used throughout this thesis, namely FTIR spectroscopy and 2D-IR spectroscopy using the ULTRA and LIFEtime laser systems housed at the Rutherford Appleton Laboratories. Supplemental techniques and measurements will be discussed in each individual chapter when required.

2.1 Linear FTIR Spectroscopy

FTIR spectroscopy is a fast and robust method for recording IR spectra. FTIR spectrometers use blackbody radiation and a He:Ne continuous wave laser in conjunction with a Michelson interferometer in order to measure IR intensity. The source of infrared radiation comes from passing an electric current through a silicon carbide filament (Globar). This causes the element to heat up and emit IR light as a continuous blackbody source with a frequency range from 600-7000cm^{-1} (16.7-1.4 µm). This light is passed through an aperture and collimated by a parabolic before being passed through the interferometer shown in the figure below.

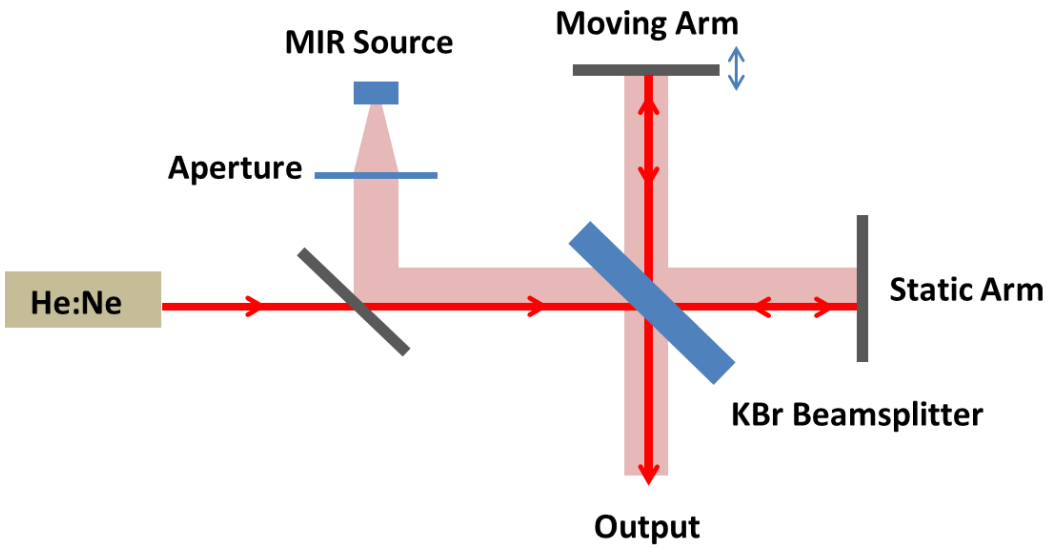

Figure 2.1 *– Typical Michelson interferometer setup found in FTIR Spectrometer.*

A potassium bromide beamsplitter is used to divide the IR radiation into two arms set at 90^{o} to one another. One arm has a stationary mirror while the other has a periodically moving mirror translating in the plane of propagation of the radiation at a fixed scanning velocity. The displacement of the moving mirror creates an interference pattern (interferogram) as the radiation in the two arms are recombined with the intensity of the recombined light being dependent on the moving mirror position at a given time. At different mirror positions, different frequencies of light will interfere constructively or destructively creating a time dependent frequency profile of the IR light. In order to convert this time based signal into the frequency domain, the exact path difference between the two interferometer arms must be known. This is achieved by the use of a helium-neon laser beam (He:Ne) as a reference. The He:Ne is directed through the same optical path and experiences the same path difference as the IR light through the interferometer. Interference of the recombined He:Ne light generates a series of fringes that can be 'counted' as the moving mirror translates, providing the spectrometer with a reference for the path difference at any given time.

In general, the absorbance of a sample is related to the relative intensity of the light before and after passing through a medium as follows:

$$A = \log_{10} \frac{I_0}{I} \tag{2.1}$$

Here *A* is the absorbance in optical density (O.D.) and *I* and I_0 are the relative intensities of the light before and after the medium. For a medium of molecules dissolved in solution the absorbance is also related to the concentration of molecules in the sample by the Beer-Lambert law:

$$A = \varepsilon c l \tag{2.2}$$

Where *c* is the concentration of molecules in the sample (mol L^{-1}), *l* is the path length (cm) and ε is the molar extinction coefficient (mol^{-1} Lcm^{-1}). The relative concentration and path length of samples used in the experiments in this work was chosen to offer appropriate absorption intensities of the peaks measured.

Samples in this work were all made in the same manner. After dissolving molecules into solvent, small amounts of liquid sample were housed between two calcium fluoride (CaF_2)

windows, separated by a thin polytetrafluoroethylene (PTFE) spacer ring. Construction of the sample cell used is shown in Figure 2.2 below.

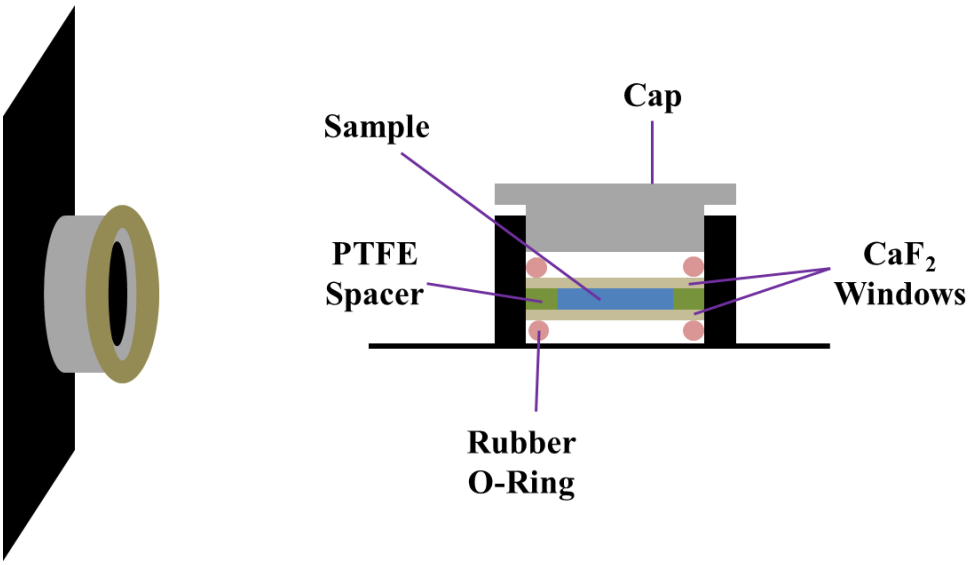

Figure 2.2 *– Harrick sample cell and cross section for all samples used in this thesis.*

2.2 2D-IR Spectroscopy

Two different laser set ups were used in the experiments shown in this thesis. 2D-IR spectra in Chapter 3 were recorded on the ULTRA laser system which uses the Michelson interferometer based method for generating the pump frequency axis. 2D-IR experiments in Chapters 4 and 5 were carried out on the LIFEtime laser system which uses a MIR pulse shaper to create pulse sequences and generate the pump axis. Both laser systems utilise the same basic principles of operation and have a large number of similarities and both these and the differences in the two set-ups are described separately below.

2.2.1 ULTRA Laser System

The ULTRA laser system[1,2] begins with a custom-built titanium sapphire oscillator (Ti:Sapph) that produces laser pulses centred at 800 nm with a pulse duration of 20 fs, bandwidth of 50 nm and at a repetition rate of 65 MHz.

The laser pulses from the oscillator are then fed into a regenerative amplifier to increase the average power of the laser pulses. Amplification of short pulses can result in dangerous peak intensities causing damage to the Ti:sapph gain medium. Pulses are therefore

'stretched' temporally by means of a grating before entering the amplification cavity. The Ti:Sapph gain medium is pumped by two Nd:YAG lasers each with a power output of 55 W. In order to prevent thermal effects damaging the gain medium, cooling of the crystal is employed by means of cryogenic cooling pumps.[3] Entry and exit to the amplification cavity are dictated by means of electro-optic modulators (Pockels cells). After a sufficient amplification is achieved following a number of round trips through the gain medium the exit Pockels cell polarisation is switched to allow the pulse to be ejected from the cavity. Following this step ejected pulses undergo pulse compression again by means of a second grating which compensates for the effects of the initial pulse stretching. Following amplification in the ULTRA system, the result is 800nm laser pulses with average pulse energy of 0.8 mJ, pulse duration of 40-80 fs at a repetition rate of 10 kHz.

In order to convert the amplified 800 nm pulses into MIR light, an optical parametric amplifier (OPA) is required. Optical parametric amplification allows for the manipulation of the wavelength of the amplified laser pulses in order to bring them into resonance with molecular vibrations of interest. In the case of the experiments in this thesis, experiments in Chapters 3,4 and 5 all employ laser pulses centred at 1650 cm^{-1} (~6 um) while chapters 4 and 5 also require pulses centred at 1090 cm^{-1} (~9 um).

Optical parametric amplification begins by dividing the light from the regenerative amplifier with a 50:50 beam splitter into two pump beams. One of these pump beams is incident onto a further beam splitter that reduces the pump intensity to 5% of its original value. This low intensity light is then focussed onto a sapphire plate. At the point where the beam is focussed, the now high intensity light is now sufficient to contribute to the refractive index of the sapphire medium and causes further self-focusing of the light. This self-focusing effect is balanced out by multiphoton ionisation creating free electrons in the crystal. This effect decreases the overall refractive index of the medium. The intensity-dependent component of the refractive index introduces an intensity dependent phase-shift in the light as it passes through the medium which in turn alters the frequency of the light. Controlling the intensity of the light as it passes through the medium therefore offers intensity dependent frequency broadening of the light:

$$\omega = \omega_0 + n_2 \frac{\omega_0}{c} L \frac{\delta I(t)}{\delta t} \tag{2.3}$$

Where ω_0 and ω are the initial and final frequencies of the light, n_2 is the nonlinear contribution of the refractive index, c is the speed of light, L is the length of the medium and I is the intensity of the light at a given time. As the laser pulses pass through the medium, the temporal profile of the pulses induces broadening to both lower and higher frequencies. The leading edge of the pulse has a temporal increase in intensity, resulting in an increase in refractive index and subsequent shift of the light to lower frequencies. Following the point of maximum intensity at the temporal centre of the laser pulse, the nonlinear refractive index decreases and a resulting shift to higher frequencies occurs. The broadened 'white light' pulses can span up to 1000 nm.

White light pulses are broadened temporally before focussing onto a 2nd order nonlinear optical barium borate (BBO) crystal, along with the other half of the initial 800 nm pump light. The pump and white light travel non-collinearly through the crystal. The BBO crystal allows the process of optical parametric amplification to occur, converting photons of 800 nm light (pump) into lower frequency 'signal' and 'idler' radiation where the idler radiation is produced as a by-product of the conversion of energy from the pump to the signal[4]:

$$\omega_3 = \omega_1 + \omega_2 \tag{2.4}$$

Where ω_3 is the frequency of the pump light, ω_1 is the signal frequency which is the amplified frequency components of the white light seed and ω_2 is the idler frequency which is the photon of light produced with frequency equal to the difference between those of the pump and signal fields . The white light pulses act as a seed for the amplification of a broad range of potential frequencies and selection of a specific wavelength to be amplified is controlled by adjusting the temporal delay between the pump and signal fields and the relative angle of the BBO crystal. Efficient energy conversion is only achievable when the phase of the pump and signal fields are well matched.[5,6] The signal from the OPA is collimated; however, the signal and idler beams are dumped following this interaction.

The signal beam is passed through a second amplification stage in order to generate more signal power. The only difference between this stage and the first OPA stage is that the signal and pump pass collinearly through the BBO crystal resulting in the production of a collinear idler beam.

MIR light is finally achieved through difference frequency generation (DFG) of the signal and idler beams.[6,7] A silver thiogallate ($AgGaS_2$) crystal allows the production of photons of

light at a frequency which is equal to the difference in frequency between the signal and idler beams. Using this method light with a wavelength range tuneable from 2.4 um to 12 um is achievable.[6] The resulting output of the ULTRA system with laser pulses centred at 6 um as in the experiments in Chapter 3 have a temporal duration of around 100 fs and bandwidth greater than 200 cm^{-1}.

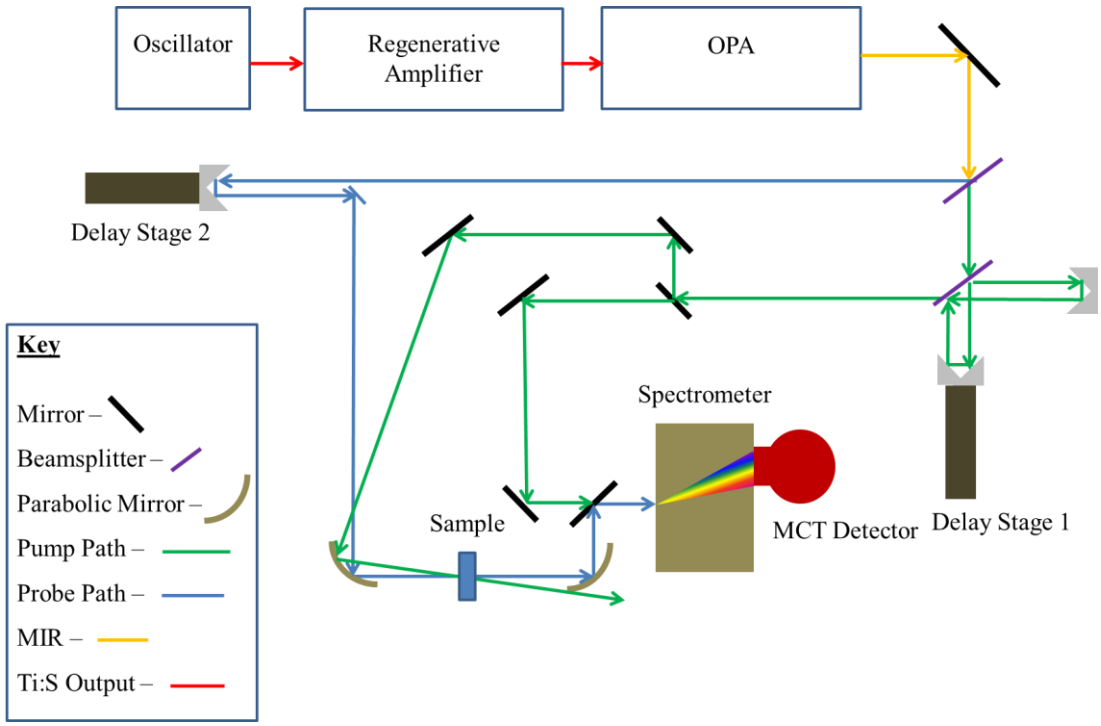

***Figure 2.3** – Schematic diagram of the ULTRA laser system.*

Following generation of MIR laser pulses at the desired wavelength, the OPA output is directed on to a 90:10 beam splitter creating what is referred to as pump ($\vec{k}_1$, $\vec{k}_2$) and probe ($\vec{k}_3$) beams respectively. The pump beam is passed through a Michelson-type interferometer. A 50:50 beam splitter divides the pump beam into a stationary arm and a moving arm. The moving arm of the interferometer is controlled by a variable delay stage (Figure 2.3 Delay Stage 1) which scans during data acquisition and defines the time period t_1 between the first two laser pulses in a measurement. As the stage is scanned, the different frequency components of light being recombined from the two arms of the interferometer will shift in and out of phase depending on the relative path difference between the two arms. The timing of the delay t_2 between the pump pulses and the probe pulse is also controlled via a delay stage (Figure 2.3 Delay Stage 2) and defines the waiting time (T_w) for the collected 2D-IR spectrum.

High precision is required in the movement of the delay stage in the interferometer. During a 2D-IR measurement, this delay stage is scanned which alters the time t_1 between the two pump pulses. The step sizes taken by the delay stage as well the maximum value of t_1 recorded defines the resolution of the pump frequency axis of the measured 2D-IR spectrum. The step size also defines the maximum frequency that is detectable from the Fourier transform of the collected time domain data also known as the Nyquist frequency (ω_N) defined by the equation:

$$\frac{\omega_N}{2\pi} = \frac{1}{2\Delta t} \tag{2.5}$$

Where Δt is the step size. For vibrational modes such as a carbonyl stretch which vibrates at a frequency of around 1600 cm^{-1}, this translates to a vibrational period of the carbonyl bond of about 20 fs. Therefore step sizes of less than 10 fs are required to properly capture the frequency components in the emitted signals although this can be overcome by under-sampling methods as used in the LIFEtime set-up discussed in the next section.[8] During measurements performed for this thesis on ULTRA, step sizes of 3 fs are used to acquire 2D-IR data and this correlates to a physical movement of the delay stage of around 0.45 um.

Scanning t_1 is also required for collecting of a pump-field autocorrelation which is in turn necessary for calculating the pump frequency axis as well as properly 'phasing' the 2D-IR spectrum. As t_1 is scanned then the two pump pulses will interfere with one another. At the value of t_1 where the two pulses are completely in phase then all frequency components interfere constructively resulting in an intensity maximum. This time is known as t_0, the defining of which is important for processing of the data following acquisition. An example of a collected autocorrelation is shown in Figure 2.4 below.

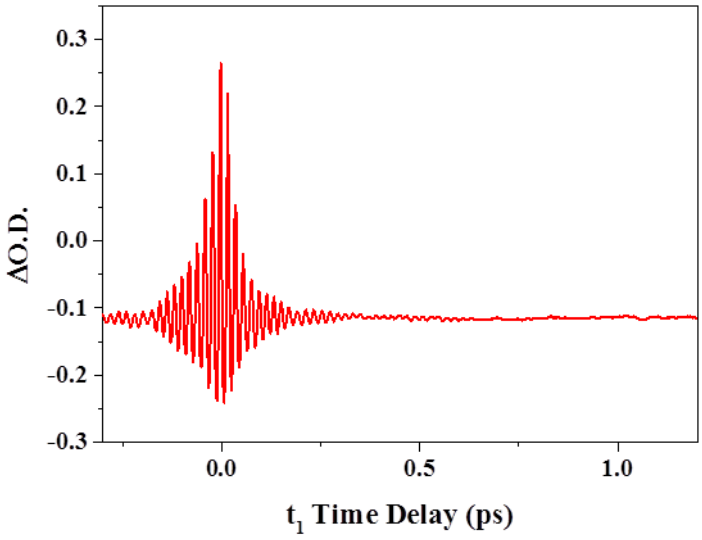

Figure 2.4 *– Pump field-autocorrelation collected during 2D-IR data acquisition on ULTRA.*

The pump-field autocorrelation is collecting by isolating a portion of the pump light following recombination of the two arms of the interferometer and directing this light onto a single pixel on the MCT detector (Figure 2.3). As the time delay between the pump pulses is scanned the intensity of the recombined light is recorded as a function of t_1. In order to record the full interference pattern between the two pump pulses, data is recorded for negative t_1 values (i.e. the ordering of the pump pulses is initially reversed) as well as positive values. During 2D-IR measurements presented in this thesis, signals are recorded for t_1 values from -0.3 ps out to a maximum value of 4 ps.

Following the interferometer stage, the pump and probe beams are both directed onto the sample by a gold parabolic mirror which also focusses the beams. Following interaction with the sample the residual probe light and the emitted signal is re-collimated by a second parabolic mirror before entering a custom built spectrometer and being dispersed spectrally by a diffraction grating (75 lines/mm) onto a liquid nitrogen cooled 128 pixel mercury cadmium telluride (MCT) detector array which yields the probe frequency axis of the 2D-IR spectrum. Spectral resolution achieved on the probe axis for the ULTRA system is around 1.5 cm^{-1}. The residual pump light is directed onto a non-reflective surface following sample interaction. Signals are extracted by recording probe spectra across the detector both with and without preceding pump pulse interactions. Pump pulses are modulated by a beam chopper, synchronised to the output of the regenerative amplifier at half of the repetition rate (5 kHz), which blocks alternate pump pulses and allows the probe spectrum

to be recorded without the pump. An example of the signal collected by each pixel in the MCT array is shown below. In the experiments in Chapter 3, each point in the recorded signal is averaged over 4000 laser shots to increase signal to noise. The signal itself is also averaged over three scans of t_1 in order to compensate for any long term drift effects in the laser alignment.

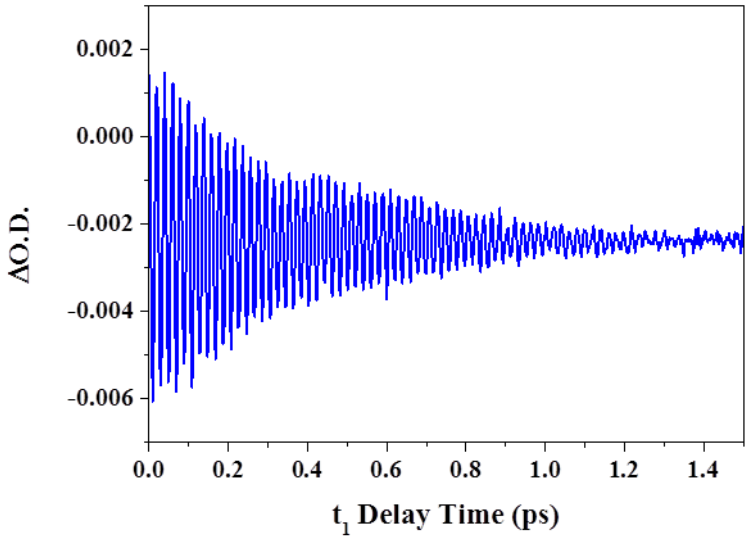

Figure 2.5 *– Collected signal from one of the pixels in the 128 pixel MCT detector during a 2D-IR data acquisition on ULTRA.*

As mentioned previously, signals are collected beginning with negative values of t_1. However the time points before t_0, defined from the autocorrelation, for pixels other than the autocorrelation pixel are removed. This ensures that any unwanted information from the signal that comes from the interactions prior to t_0 is not present in the resulting spectrum. Fourier transformation of the signal shown in Figure 2.5 with respect to t_1 yields a value for the intensity of the signal at each excitation frequency. Following Fourier transformation slices of the transformed signal at each excitation frequency (probe slices) can be compiled into a 2D-IR spectrum. Figure 2.6 shows an example of a probe slice obtained from Fourier transformation of the signal recorded for a given probe pixel.

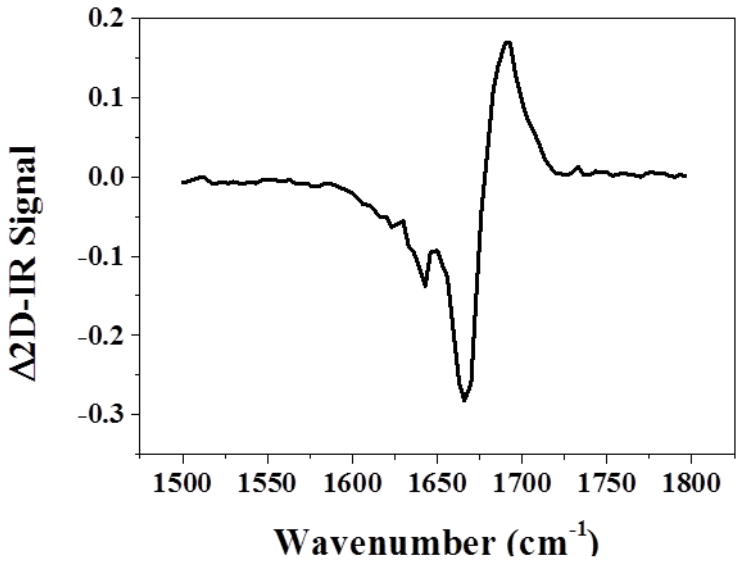

Figure 2.6 *– Example result of Fourier transformation of probe pixel interferogram.*

Fourier transformation and generation of 2D-IR spectra is performed with data processing software created on LabVIEW by By Dr Gregory M. Greetham, adapted from a previous version authored by Dr Neil Hunt, Dr Rafal Kania, Dr Katrin Adamczyk. This program extracts the collected auto-correlation data, generates the pump-frequency axis in 2D spectra and allows for phasing of 2D-IR data.

2D-IR spectra recorded on the ULTRA laser system presented in this thesis are the result of averaging of three repeated measurements with each measurement the result of scanning t_1 from -0.3 to 4 ps in 3 fs steps as mentioned above. Each of these scans takes around 15 minutes to perform and as such small amounts of laser beam drift can occur in this time, effecting the measurements. Repeated measurements and averaging are therefore used help to counteract this problem. The recording of repeated scans also means that three autocorrelation measurements are performed. The average autocorrelation signal is calculated in the program to allow more accurate determination of t_0 before the data is interpolated, the reason for which will be described later.

In order to perform the t_0 calculation and calculate the pump frequency axis, a small temporal window of the autocorrelation signal is isolated (around -0.2 to 0.2 ps) which contains the 'centre burst' of the auto-correlation field. This intensity of the signal measured in this temporal region is defined by the relative phase of the two pump pulses.[9] Fourier transformation of the signal within the isolated window yields the power spectrum of the laser pulses as well as the phase spectrum.

Accurately defining t_0 is important to ensure dispersive components found in signals measured prior to t_0 are not included in 2D-IR spectra, causing distortion in the observed linshapes.[8] This is accomplished by removing the data points recorded in each probe recorded before t_0. An estimate of t_0 is obtained from the phase slope of the phase spectrum generated from the Fourier transform of the autocorrelation signal ($\delta\varphi/\delta t_1$). At the point where all frequency components of the two laser pulses are in phase, $\delta\varphi/\delta t_1$ is equal to zero and so this point in the phase slope is taken as the t_0 estimate. A more accurate value of t_0 is then obtained using the additional points added via the interpolation of the autocorrelation signal. This allows for fine tuning of the spectral phase in the each of the probe signals obtained. Determination of the final value of t_0 used to phase the spectrum is achieved using the 'projection slice theorem'.[8] This involves overlaying a slice of the 2D-IR spectrum projected onto the probe axis with a pump-probe signal also recorded during the measurement (details of which are presented in the following section).The value of t_0 can then be adjusted through the interpolated data points and observing the effect on the projected 2D slice. When the spectrum is correctly phased the projected slice should overlay exactly the pump-probe signal, indicating that no dispersive components are present to distort the lineshapes.

Zero-padding is also implemented using the data processing software, allowing increased resolution of the obtained pump frequency axis.[10] This process is performed by adding a number of data points with an intensity equal to zero to the recorded signals prior to the Fourier transformation. This therefore increases the maximum value of t (t_{max}) in the Fourier transform which in turn increases the resolution of the subsequent frequency domain data. Figures (2.7-2.9) below provide a visualisation of the data processing performed to obtain 2D-IR spectra.

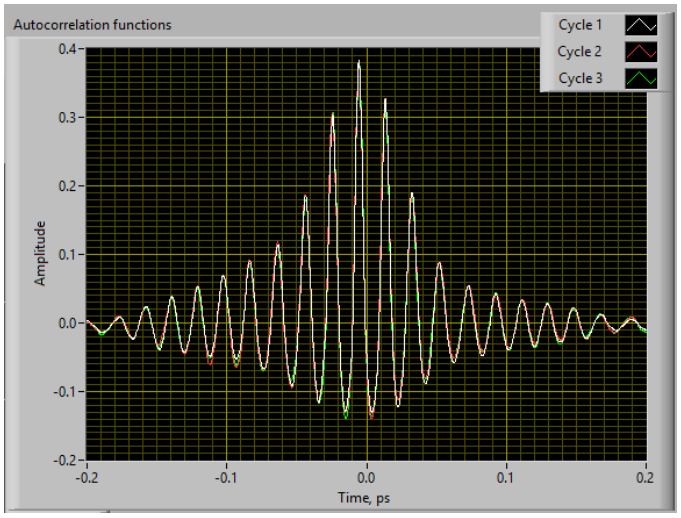

Figure 2.7 *– Centre burst of three measured autocorrelation fields, the average of these signals is obtained and Fourier transformed to obtain phase spectrum and subsequent phase slope, allowing estimation of* t_0.

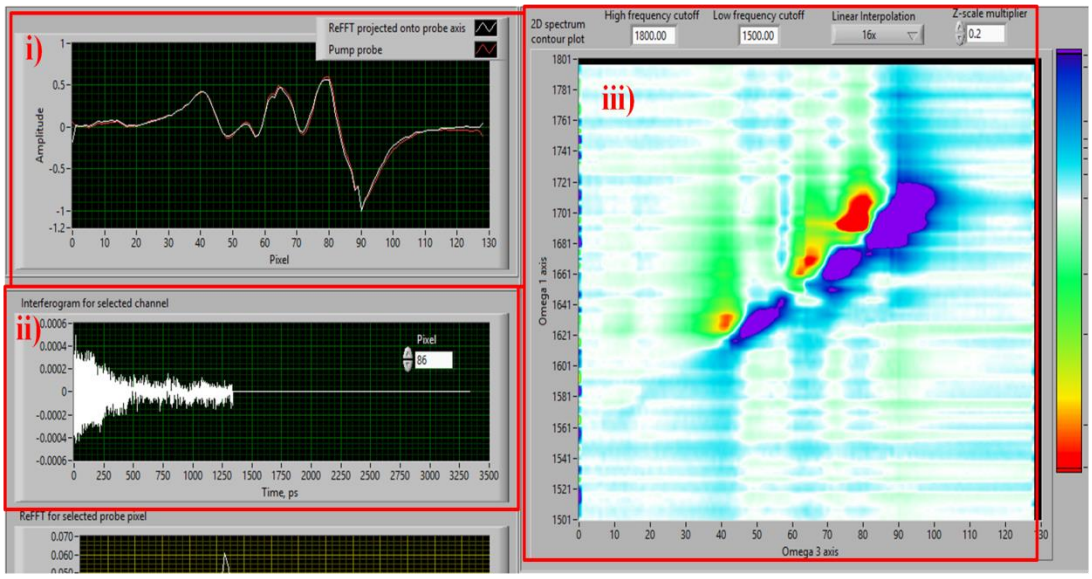

Figure 2.8 *– Fine tune phasing of 2D-IR data via projection slice theorem. Window i) directly shows the projected slice overlapped with a pump probe signal. In this case the correct value of* t_0 *has been used and all the features in the two traces overlap almost exactly. Window ii) shows interferogram recorded on a single detector pixel, zero padding has been used here and can be seen by the long section of y=0 values. Window iii) shows the resulting 2D-IR spectrum following phasing. In correctly phased spectra, no dispersive contributions are present to distort the lineshapes.*

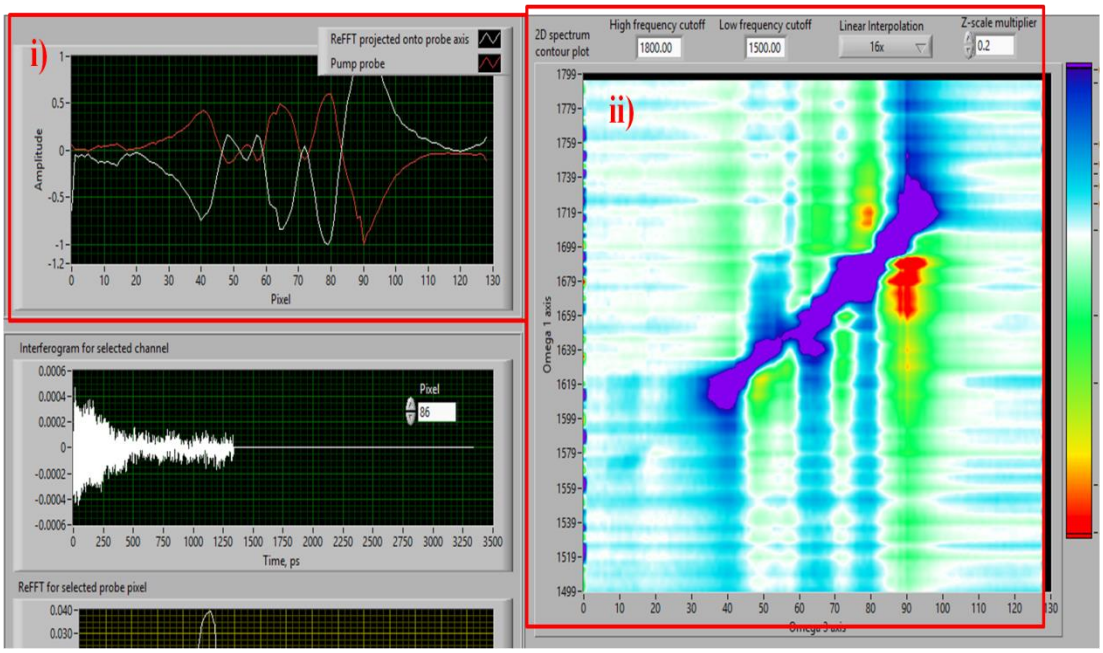

Figure 2.9 *– Fine tune phasing of 2D-IR data via projection slice theorem. Window i) directly shows the projected slice overlapped with a pump probe signal. In this case an incorrect value of* t_0 *has been used and the two traces are not overlapping, indeed the two traces are completely out of phase. Window ii) shows the resulting 2D-IR spectrum following phasing. In incorrectly phased spectra, dispersive contributions are present to distort the lineshapes, splitting the features into quadrants.*

2.2.1.1 Pump-Probe Spectroscopy on ULTRA

In addition to acquiring 2D-IR data as described in the previous section, pump-probe experiments are also readily performed on the ULTRA laser system with minimal adjustments to the experimental set-up required. Pump-probe signals are also considered to be a four wave mixing interaction although in this case the first two excitation fields ($\vec{k}_1, \vec{k}_2$) are considered to be degenerate and temporally overlapped.[8] This combined excitation field is referred to as the 'pump' pulse and $\vec{k}_3$ is referred to as the 'probe' pulse. As the time interval between the excitation fields is zero (t_1 =0) the separation of the Feynman pathway during the excitation is not impossible. As such, the pump creates a population state in the molecular ensemble following the interaction. The probe pulse can therefore interact with either a $|0\rangle\langle 0|$ or a $|1\rangle\langle 1|$ population state following t_2 in this case referred to as the pump-probe delay time. During pump-probe delay time, vibrational relaxation can occur, and the longer the delay time the greater probability of relaxation

occurring. The final coherent state in the ensemble created by interaction with the probe pulse is therefore dependent on the amount of relaxation that has occurred during the delay time allowing for direct measurements of the vibrational lifetime of a given mode.

Pump-probe signals are acquired by an absorption difference methodology. Absorption spectra of the probe beam are recorded for the case where the system has been excited by the pump (pump on) and again when it has not (pump off). The difference between these two signals yields a change in absorbance as a result of the excitation by the pump pulse. This results in the extraction of transient absorption features which have an amplitude dependent on the relaxation of the modes during the delay time. Recording pump-probe signals at a series of pump-probe delay times allows extraction of the vibrational lifetime of a mode (T_1) which is given by the intensity of the features found in the difference spectrum as a function of temperature.

In practice on the ULTRA setup, pump-probe spectroscopy is achieved by blocking the light in the moving arm of the interferometer, with the light in the other arm then acting as the pump pulse in the experiment. The delay stage in the interferometer is also not scanned during measurement, instead the stage that controls the waiting time in 2D-IR experiments is scanned as this now controls the separation between the pump and probe pulses. Pump probe signals are also subject to phase matching conditions and as such behave as they do in the pump-probe 2D-IR geometry previously described. The signals are overlapped with residual probe light allowing for heterodyne detection of the signals. Signals are dispersed onto the same 128 pixel MCT detectors used in 2D-IR experiments.

Pump probe signals are also inherently present when collecting 2D-IR spectra. One as a result of the interactions of $\vec{k}_1$ and $\vec{k}_3$ with the ensemble and $\vec{k}_2$ and $\vec{k}_3$ interacting with the ensemble. These can however be removed from the desired 2D-IR signal. The first of these pump probe signals is subtracted from the signal by subtraction of the equivalent signal obtained when the pump is 'off' caused by modulation of $\vec{k}_2$ by the chopper at each value of t_1. This results in a signal in the form of a free induction decay as shown in Figure 2.5. The second pump-probe signal is removed during the Fourier transformation of the free induction decay obtained for each pixel. The contribution of this pump-probe signal to the free induction decay is a single exponential with a decay constant T_1, which when

Fourier transformed becomes a Lorentz lineshape with width equal to the to the natural linewidth as determined by the lifetime.[8]

2.2.2 LIFEtime Laser System

The LIFEtime laser system[11] operates on number of the same principles as the ULTRA set up however there a number of differences in experimental hardware which have a significant impact on the performance of each laser system when measuring 2D-IR spectra. Most notable are the number of components used in the production of the IR pulses used in 2D-IR experiments. Two ytterbium potassium gadolinium tungstate (Yb:KGW) regenerative amplifiers are used to seed 3 OPAs. Amplifier-A (pump amplifier) produces pulses centred at 1030 nm with pulse duration of 260 fs at a repetition rate of 100 kHz and a total power output of 15 W. Amplifier-B (probe amplifier) has a slightly lower output power of 6 W but also generates laser pulses centred at 1030 nm with a duration of 180 fs at a rate of 100 kHz. The pump amplifier drives a similar OPA-DFG process (OPA 1 (Light Conversion Orpheus-HP)) as described for the ULTRA set-up to provide pump pulses tuneable from 2100-13000 nm. Amplifier-B drives two more OPA-DFG setups (OPA 2 and OPA 3 (Light Conversion Orpheus-One)) providing two separate probe outputs that can range from 4000-13000 nm which allows for probing of two different spectral regions simultaneously.

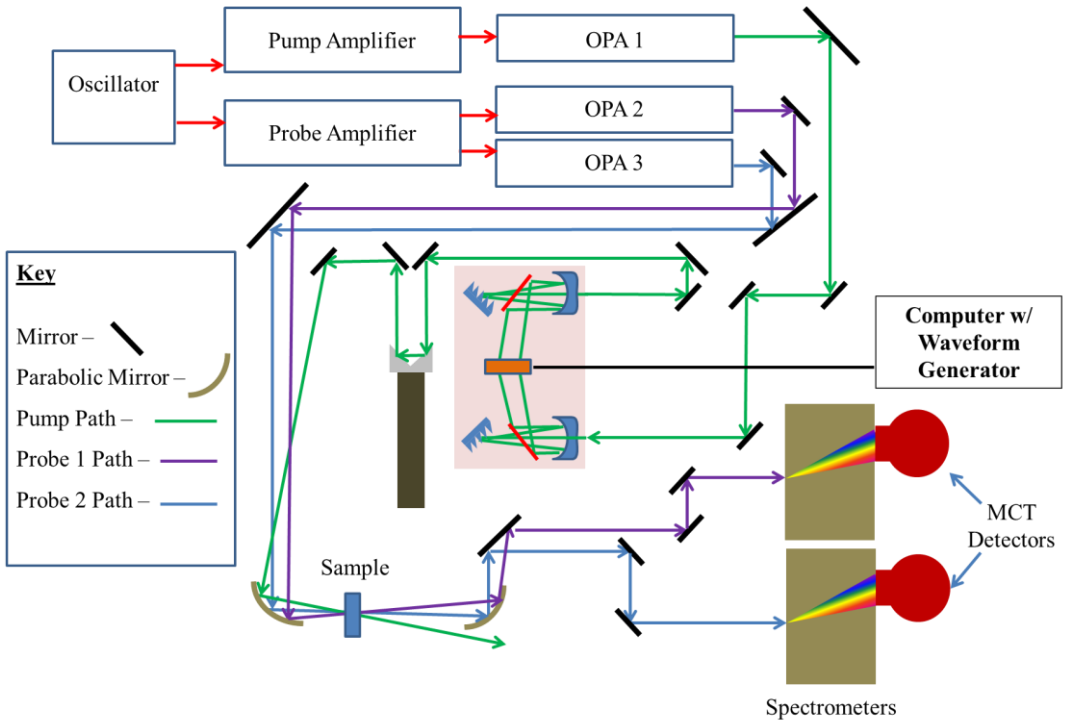

Figure 2.10 *– Schematic diagram of the LIFEtime laser system.*

Another major difference between the ULTRA and LIFEtime systems is the use of a MIR pulse shaper (highlighted in the pink box in Figure 2.10) to control the phase and amplitude of the pump light as an alternative to an interferometer.[12,13] The output from OPA 1 is directed into the pulse shaper and is dispersed by a grating before being collimated by a cylindrical mirror. The collimated light is then incident on an acousto-optic modulator (AOM) made of germanium (Ge). A programmable acoustic wave passes along the Ge crystal dictated by an attached waveform generator in a computer. The wave in the Ge crystal acts as a grating which diffracts desired MIR frequencies with exact intensity and phase.[8] Following interaction with the Ge AOM, a second mirror and grating serve to convert the transformed light back into a temporal pulse which is output from the pulse shaper. By altering the acoustic wave in the AOM, the shaper can be used to mimic the output of an interferometer. With each programmed wave yielding a pulse pair output, varying the AOM input alters the relative timing between the pulse pair reduced.

Following generation of the desired pump pulses by the pulse shaper, the output is overlapped along with both probe beams onto the sample with a gold parabolic mirror. The same pump-probe beam geometry as used in the ULTRA setup with ($\vec{k}_1 = \vec{k}_2$) resulting in signals emitted collinearly with the respective residual probe light allowing for self-

heterodyne detection of signals. Following interaction with the sample each probe beam is focussed again on a second parabolic and directed onto a separate grating based spectrometer to disperse the signals across two 128 pixel MCT detector arrays. Signal frequencies detected at each pixel are collected as a function t_1 as described for the ULTRA system such that the signal can be Fourier transformed to yield the pump frequency axis of the 2D-IR spectrum.

Due to the increased higher repetition rate in the LIFEtime laser system (100 kHz compared to 10 kHz in ULTRA), data acquisition is much faster with greater signal to noise levels achievable due to the ability to record data from a large number of laser shots in a short time. Spectra presented in thesis that were acquired on LIFEtime were obtained with an total acquisition time of 80 s. This affords the opportunity to collect large numbers of spectra very quickly which proved invaluable for collecting the large datasets presented in Chapters 4 and 5 of this thesis.

In the previous section, it was stated that in order to accurately capture signal components of a given frequency, then the signal must be sampled with a step size below the Nyquist limit which is around 10 fs for vibrations found in the 1600 cm^{-1} region. One disadvantage of the LIFEtime system lies in the limited number of points that can be collected for scanning t_1. This is due to a memory capacity issue that stems from the higher repetition rate of the laser and subsequent rate and volume of data points acquired. In order to cover a range of t_1 values sufficient to capture all the information generated in the four wave mixing process in the sample, much larger step sizes than the maximum dictated by the Nyquist frequency are required to cover the same range of values with a fewer number of points. In LIFEtime measurements performed in this thesis, 24 fs step sizes are employed compared to 3 fs steps in the ULTRA data sets. This means that the data is being comparatively under sampled. An example of under-sampling is shown in Figure 2.11 below.

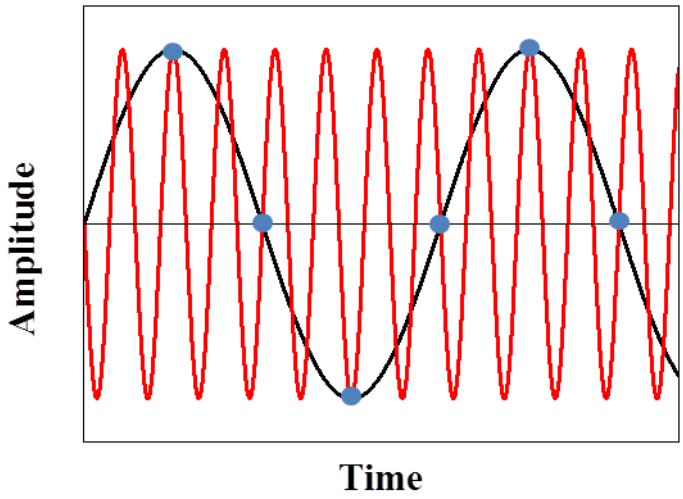

Figure 2.11 *– Example of signal under-sampling, red trace represents regular sampling of a signal, black trace shows under-sampled signal.*

If fewer points are recorded to properly sample the frequency of the signal, then frequency components higher than the Nyquist frequency for that step size are 'aliased'.[8] The correct frequencies for features found in the spectrum can be retrieved given that the measured as the region interrogated is dictated by the frequency spectrum of the laser spectrum. The aliased frequencies (ω) are an integer number of their correct values (ω_0) and therefore can be recovered from the following relationship for even integers:

$$\omega_0 = \omega + m \cdot \omega_N \tag{2.6}$$

And for odd integers by:

$$\omega_0 = -\omega + m \cdot \omega_N \tag{2.7}$$

Where ω_N is the Nyquist frequency and m is an integer number.

There are some further differences in the method of data acquisition used in the LIFEtime setup. The method of phase cycling is employed to help reduce background noise and scatter effects in 2D-IR spectra. Phase cycling is a technique where additional data points are collected for each value of t_1 where the phase between the pump pulses is varied typically by a factor of π. The desired information in the signal will be out of phase when compared between the two recorded phase points while background noise in the signal is phase independent and is therefore unchanged between the recorded signals.[8] Subtraction of the additional signals removes artefacts, such as scattering of the pump light into the

signal field, from the recorded signal as these are phase independent and would therefore be unchanged in all signals measured.

Processing of data recorded on the LIFEtime laser system is notably simpler than in the ULTRA setup. One of the key advantages gained from use of a pulse-shaper to generate pump pulse sequences is that the relative phase of the excitation fields are inherently known as they are dictated by the pulse shaper. As such the phasing process using the projection slice theorem outlined in the ULTRA data processing section is not required to produce spectra from LIFEtime data, LIFEtime spectra are in effect automatically correctly phased and no dispersive contributions will be present in the 2D-IR spectral features. All that remains is for Fourier transformation of the collected probe interferograms to generate frequency slices which are compiled to construct 2D spectra.

A final area consideration for recording 2D-IR spectra is the effects of relative polarisation of the laser pulses in the 2D-IR pulse sequence. For a long time in pump-probe spectroscopies, different polarisations have been used to measure rotational motion of molecules or indeed remove effects of rotational motion from measured data.[8] Polarisation effects on on-diagonal peaks in 2D-IR spectra offer these same benefits however there is much more information that can be extracted from 2D-IR spectroscopy by use of different polarisation geometries. Relative polarisation of the laser pulses in a 2D-IR pulse sequence is an effective way of enhancing or suppressing different Feynman pathways and subsequently the features that appear in a measured 2D-IR spectrum due to the relative angles of transition dipoles involved in the transitions observed in the Feynman pathways. This subsequently alters the intensity of on-diagonal and off-diagonal 2D-IR spectral features. Observing these effects allows extraction of relative angles between transition dipoles which can be used to interpret molecular structure.[14–16] While this is consideration that can be applied to any 2D-IR experimental setup, it is considered only here as in the data recorded on the ULTRA setup presented in this thesis, the same polarisation is used throughout all measurements. In the LIFEtime data contained within this thesis, different polarisations are used and so the effects of polarisation will now be discussed briefly.

The most common polarisation geometry used is referred to as ‘parallel polarisation’ or ‘ZZZZ polarisation’ where each of the four Zs in this notation denote the four laser pulses in the pulse sequence ($\vec{k}_1$, $\vec{k}_2$, $\vec{k}_3$ and $\vec{k}_4$) and refers to each of the pulses being linearly

polarised in the same direction. All measurements performed on ULTRA in this thesis utilise this polarisation geometry. An alternate polarisation geometry that can be used which enhances off-diagonal features in 2D-IR spectra is the 'perpendicular polarisation' or 'ZZYY polarisation'. Under this condition the probe and signal fields ($\vec{k}_3$ and $\vec{k}_4$) polarised at a relative angle of 90 degrees to the two pump fields. Under this polarisation condition, on-diagonal peak intensities are reduced by a factor of 3 while off-diagonal peaks will decrease by less than this provided that the angle between the two respective coupled transition dipoles that generate the off-diagonal peak is not equal to zero.[8] This effectively leads to an enhancement of off-diagonal peaks in 2D-IR spectra which in some cases allows for more accurate measurement of off-diagonal peaks.

2.3 References

1. Greetham, G. M. *et al.* ULTRA laser system: a new dual-output 10 kHz Ti:Sapphire amplifier with UV–IR generation for time-resolved spectroscopy. *Cent. Laser Facil. Annu. Rep.* 249–250 (2008).

2. Greetham, G. M. *et al.* ULTRA : A Unique Instrument for Time-Resolved Spectroscopy. *Appl. Spectrosc.* **64,** 1311–1319 (2010).

3. Backus, S., Read, K., Murnane, M. & Kapteyn, H. Cryogenic cooling multiplies output of Ti:sapphire output. *Laser Focus World* **41,** 65–68 (2005).

4. Boyd, R. W. *Nonlinear Optics*. (Academic Press, 2008).

5. Baumgartner, R. A. & Byer, R. Optical Parametric Amplification. *IEEE J. Quantum Electron.* **15,** 432–444 (1979).

6. Cerullo, G. & De Silvestri, S. Ultrafast optical parametric amplifiers. *Rev. Sci. Instrum.* **74,** 1–18 (2003).

7. Brida, D. *et al.* Generation of broadband mid-infrared pulsesfrom an optical parametric amplifier. *Opt. Express* **15,** 15035–15040 (2007).

8. Hamm, P. & Zanni, M. T. *Concepts and Methods of 2D Infrared Spectroscopy*. (Cambridge University Press: Cambridge, 2011).

9. Deflores, L. P., Nicodemus, R. a & Tokmakoff, A. Two-dimensional Fourier transform spectroscopy in the pump-probe geometry. *Opt. Lett.* **32,** 2966–2968 (2007).

10. Dorrer, C., Belabas, N., Likforman, J.-P. & Joffre, M. Spectral resolution and sampling issues in Fourier-transform spectral interferometry. *J. Opt. Soc. Am. B-Optical Phys.* **17,** 1795–1802 (2000).

11. Greetham, G. M. *et al.* A 100 kHz time-resolved multiple-probe femtosecond to second infrared absorption spectrometer. *Appl. Spectrosc.* **70,** 645–653 (2016).

12. Shim, S., Strasfeld, D. B., Fulmer, E. C. & Zanni, M. T. Femtosecond pulse shaping directly in the mid-IR using acousto-optic modulation. *Opt. Lett.* **31,** 838–840 (2006).

13. Shim, S.-H., Strasfeld, D. B., Ling, Y. L. & Zanni, M. T. Automated 2D IR spectroscopy using a mid-IR pulse shaper and application of this technology to the human islet amyloid polypeptide. *Proc. Natl. Acad. Sci. U. S. A.* **104,** 14197–14202 (2007).

14. Golonzka, O. & Tokmakoff, A. Polarization-selective third-order spectroscopy of coupled vibronic states. *J. Chem. Phys.* **115,** 297–309 (2001).

15. Woutersen, S. & Hamm, P. Structure determination of trialanine in water using polarization sensitive two-dimensional vibrational spectroscopy. *J. Phys. Condens. Matter* **104,** 11316–11320 (2000).

16. Zanni, M. T., Gnanakaran, S., Stenger, J. & Hochstrasser, R. M. Heterodyned Two-Dimensional Infrared Spectroscopy of Solvent-Dependent Conformations. **105,** 6520–6535 (2001).

3. Impact of the double-single strand transition on vibrational coupling and spectral diffusion in an AT-15mer

This chapter contains results published in the following publication:

Hithell, G.; González-Jiménez, M.; Greetham, G. M.; Donaldson, P. M.; Towrie, M.; Parker, A. W.; Burley, G. A.; Hunt, N. T., *Ultrafast 2D-IR and Optical Kerr Effect Spectroscopy Reveal the Impact of Duplex Melting on the Structural Dynamics of DNA*, Phys. Chem. Chem. Phys., 19, 10333-10342 (2017)

3.1 Abstract

While the library of studies of DNA using 2D-IR spectroscopy continues to grow, only a very limited number of these studies have been focussed on the fundamental process of DNA melting. In this chapter, changes in the structural and solvation dynamics of a 15mer AT DNA duplex upon melting of the double-helix are observed by ultrafast two-dimensional infrared (2D-IR) spectroscopy. 2D-IR spectroscopy of the vibrational modes of the DNA bases reveal signature off-diagonal peaks arising from coupling and energy transfer across Watson-Crick paired bases that are unique to double-stranded DNA (ds-DNA). Spectral diffusion of specific base vibrational modes report on the solvation dynamics of the duplex and the DNA minor groove, which is predicted to contain a spine of hydration. Changes in these dynamics upon melting are assigned to increases in the degree of mobile solvent access to the bases in single-stranded DNA (ss-DNA) relative to the duplex.

3.2 Introduction

One of the first steps in using 2D-IR spectroscopy to study DNA is having a clear interpretation and assignment of the features observed in the spectra. However, it is clear that great care must be taken when assigning observed spectral features that may not be as simple as relying on previous assignments of DNA vibrational modes made using FTIR spectroscopy due to the delocalisation effects reported.[1–5] While the first 2D-IR studies performed on DNA focussed on vibrational modes of the DNA bases for nucleic acid sequences containing only GC base pairs[6,7], a comparative study has not been performed for AT DNA. Furthermore, while the temporal resolution of 2D-IR spectroscopy allows observation of ultrafast dynamics which in the case of biological based systems such as DNA are thought to be crucial in underpinning biological function. A solid understanding of the basic spectroscopy of biological systems is required for these systems which for DNA is currently limited in terms of published studies. Understanding of the base spectroscopy will be vital in expanding 2D-IR to interrogate more complicated systems such as DNA binding interactions with small molecules that bind in the DNA minor groove or DNA-protein interactions in the DNA major groove. This chapter provides a detailed study of the impact of base-pairing on the vibrational modes of DNA bases in an all AT DNA 15mer sequence

(Figure 3.1). The results presented in this Chapter allow for careful assignment of 2D-IR spectral features based on the previous 2D-IR studies.

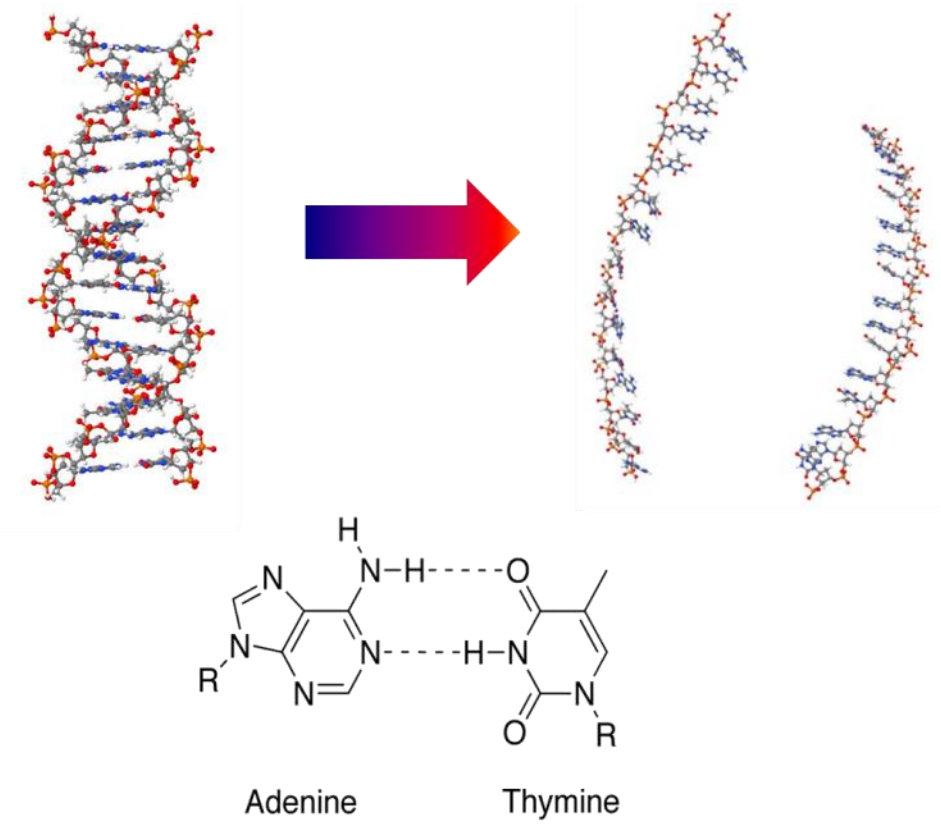

Figure 3.1 *– Schematic diagram illustrating the thermal denaturation transition of the AT-15mer DNA (top) and structure of A–T base pair highlighting Watson– Crick hydrogen bonding (bottom). (DNA images created in Jmol: an open – source Java viewer for chemical structures in 3D. http://www.jmol.org/).*

The recognition of base sequences is fundamental for replication and transcription; dictating the binding of proteins and small molecules with a high degree of specificity and selectivity. While there have been numerous studies of the molecular structure of DNA sequences, [8–12] a comprehensive understanding of the guiding principles for DNA-recognition and the conformational changes that occur upon binding remains to be established.[13] This shows that other factors need to be considered and we suggest that these include the action of molecular dynamics.[14]

An important factor in determining biomolecular dynamics in particular arises from the fact that, to a first approximation, biochemical processes take place in aqueous solutions and the unique nature of water is defined by hydrogen bonding. The lifetime of a hydrogen-

bond (H-bond) in water at room temperature is around a picosecond and the associated molecular motion imparts dynamics to any solute.[15,16] The H-bonds between bases in opposing DNA strands that are inherent in forming the secondary structure of nucleic acids will undergo similar dynamic motion, meaning that the molecule in solution inhabits a complex potential energy landscape featuring barriers that are often small in comparison to *kT*.[17] This potential surface means that the static structure is merely a time-averaged picture around which the molecule is in constant motion, but the role of this motion in initiating or directing processes such as excursions from duplex DNA to single stranded conformations, as might be implicated for example in formation of a 'bubble' in a DNA duplex, are not well understood.

The ultrafast temporal resolution of 2D-IR spectroscopy and sensitivity to localised changes in molecular structure means that it provides a valuable probe of DNA vibrational modes, in particular those located on the bases in a DNA sequence, and their interactions with both other bases and the solvent. 2D-IR spectroscopy is technique with a growing portfolio of studies that extract structural and dynamic information from biological systems.[18–20] While the greater portion of these studies have focused on protein and peptide based systems, a limited number of studies of nucleic acids with 2D-IR has already provided a number of interesting insights into their dynamic behaviour in solution.

The first 2D-IR studies of DNA focussed on separating interstrand base pairing from intrastrand base stacking effects in short-strand GC-containing DNA duplexes by observation of the carbonyl stretching and ring breathing vibrational modes of the DNA bases that are found in the 1500-1800 cm^{-1} spectral region.[6,7] Computational modelling has also been used to predict 2D-IR spectra for a number of DNA sequences and showed that the Watson– Crick hydrogen-bonding interaction induces significant vibrational coupling and delocalisation of these base vibrational modes across the base pair.[1–4] 2D-IR spectra recorded for the individual DNA bases extended this conclusion,[5] highlighting the delocalisation of vibrational modes of the DNA bases and the coupling that remains prevalent between these modes even for a single DNA base. A recent study has employed T-jump 2D-IR spectroscopy to study the dynamics of the ds-ss-DNA transition of mixed AT-GC sequences and has reported the occurrence of sequence specific melting behaviour such as strand fraying and 'unzipping'.[21] These initial studies of DNA using 2D-IR showcase

its sensitivity to the changes in nucleic acid conformation that occur in the dynamic process of dissociation of DNA strands.

In this Chapter, changes in 2D-IR spectral features which are correlated to the melting of the ds-DNA helix for an AT 15mer are observed and their temperature dependence is compared to those extracted from established methodologies. The features sensitive to oligomer conformation include specific off-diagonal peaks in the 2D-IR spectra, attributable to interbase coupling and vibrational energy transfer arising from Watson–Crick H-bonding. 2D-IR spectral diffusion measurements on base vibrational modes also provide insight into the structural dynamics and solvation of the duplex. Changes observed in these dynamics upon melting are largely attributed to increases in solvent access to the bases.

3.3 Experimental

3.3.1 Absorption Spectroscopy

The standard method for characterising the melting temperature ™ is via UV-visible absorption spectroscopy. This experimental technique is sensitive to the loss of base stacking between the DNA bases upon dissociation of the component strands which manifests itself hyperchromic effect on the absorption band of DNA located at around 260 nm. To allow comparison of new results with established methods, UV-visible spectra were measured using the same temperature controlled sample cell already described in Chapter 2 for FTIR spectroscopy.

DNA oligomers containing 15 A and T bases with the sequence 5'–ATTATTATTATATTA–3' plus complementary oligomer, were procured from Eurofins Genomics Ltd. And used without further purification. This particular sequence was chosen to reduce the number of base pairing conformations available to the oligomers. DNA oligomers containing only Adenine and another containing only Thymine leaves a possibility of 'slippage' between the DNA bases meaning a chance of unpaired bases even at room temperature. Oligomers were dissolved in a deuterated phosphate buffer (100mM) at pD 7 containing 100mM NaCl to a final duplex concentration of 5mM. 20ul of this sample solution was then placed between two CaF_2 windows with a 6 um polytetrafluoroethylene (PTFE) spacer. Spectra were then recorded between 200 and 500 nm using a WinCary Lambda 25 UV-Vis spectrometer.

Spectra were recorded at a range of temperatures between 293 K and 353 K controlled by a Harrick temperature control unit.

All FTIR spectra were recorded using the same sample conditions used in the UV-visible spectroscopy measurements with the exception of the use of a thicker 25 um PTFE spacer used in the sample cell. FTIR spectra were recorded using a Bruker 70 FTIR spectrometer with a resolution of 2 cm^{-1}. As in the UV-visible measurements, spectra were recorded at a range of temperatures from 293 K and 353 K.

3.3.2 2D-IR Spectroscopy

2D-IR spectra were recorded using the ULTRA laser system[22,23] as described in Chapter 2. A set of spectra were recorded at a range of temperatures between 293 K and 353 K with a fixed waiting time of 250 fs, although the temperature interval between spectra was larger than in the linear spectra due to the significantly longer timescale needed to acquire a 2D-IR spectrum (around one minute for an FTIR spectrum compared to 45 minutes for a 2D-IR spectrum). Further spectra were required at the extremes of the temperature range (293 K and 353 K) this time at a series of waiting times in order to extract solvation dynamics from the base modes. The experiments employed an all-parallel (ZZZZ) pulse polarisation geometry.

3.4 Results

3.4.1 Absorption Spectroscopy

In order to study establish the spectroscopy of ds-DNA and ss-DNA using 2D-IR spectroscopy, some preliminary information on the melting behaviour of the chose DNA sequence must first be obtained in order to gain some insight into its melting behaviour and establish temperature ranges where the sequence can be can considered to be wither ds- or ss-DNA. The most widely used method for studying DNA melting is UV-Visible absorption spectroscopy. Analysis of the changes of the features in these spectra allows for quantification of the DNA melting process by extraction of a T_m for a given sequence.

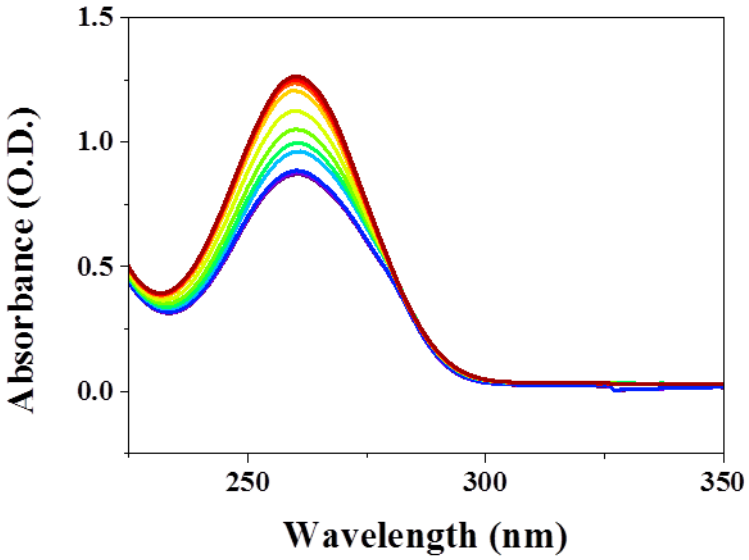

Figure 3.2 *– UV-Visible absorption spectrum of the AT-15mer recorded at a range of temperatures from 293 K (purple trace) to 353 K (red). Spectral region focussed between 225-350 nm where the only feature in the spectrum is observed.*

From the UV-Visible spectra obtained, Figure 3.2, it can be seen that there is an increase in intensity of the absorption band centred at 260 nm as the sample is heated from 293 K (blue trace) to 353 K (red trace). Following the intensity of this band as a function of temperature allows extraction of a 'melting curve' for the AT-15mer. This melting curve, shown in Figure 3.3 below, highlights the transition from double stranded- (ds-) to single stranded-DNA.

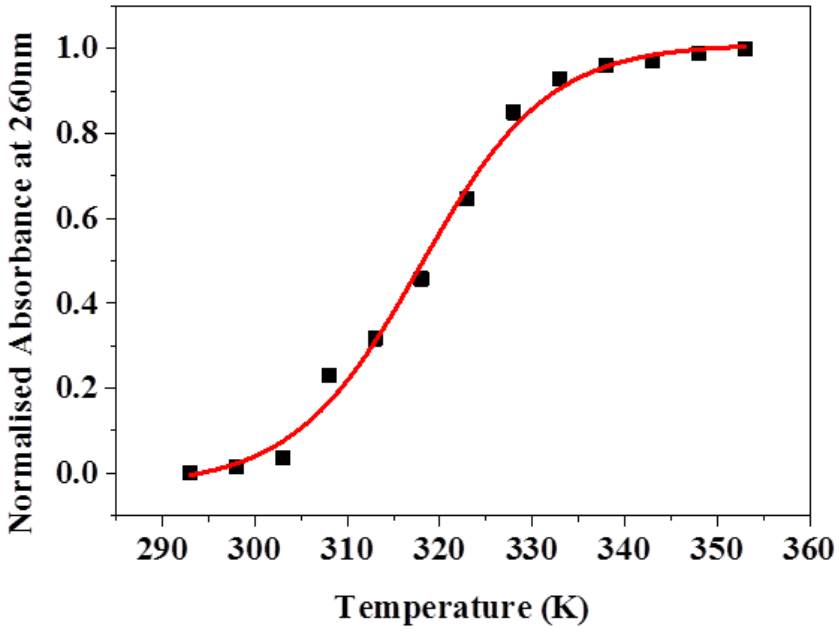

Figure 3.3 *– Normalised absorption measured at 260 nm as a function of sample temperature for the AT-15-mer duplex.*

The melting curve shown in Figure 3.3 has been fit with a sigmoid function which models a two-state transition in order to extract a midpoint of the transition ™. The data has been fitted with a Boltzmann Sigmoid function of the form:

$$A = \frac{A2+(A1-A2)}{1+e^{\frac{t-tm}{dt}}} \tag{3.1}$$

Where A is absorbance, $A1$ is the minimum value of absorbance, $A2$ is the maximum value of absorbance, t is temperature and T_m is the midpoint of the transition taken as the melting temperature. The fitting result yields a melting temperature of 318±2 K for the AT-15mer sequence. This temperature will act as a reference point for the IR spectroscopy measurements that follow in order to determine whether the temperature dependence of the changes observed in the IR spectra upon melting of the duplex correlate with those using the established methodology. It should also be noted that the theoretical T_m value for this DNA sequence provided by the supplier is 319 K ('atdbio Oligo Calculator' using the nearest neighbour method). This theoretical value compares very well with the Tm values for the sequence obtained throughout these experiments.

Following quantification of the melting behaviour of the DNA sequence chosen for these experiments, the focus is shifted from UV-Visible spectroscopy to FTIR spectroscopy. FTIR

spectroscopy has been shown to be sensitive to changes in DNA conformation[12] and determining the number of features that will be expected in the 2D-IR spectra of this spectral region along with how these features change will be important for interpreting the 2D-IR data to follow.

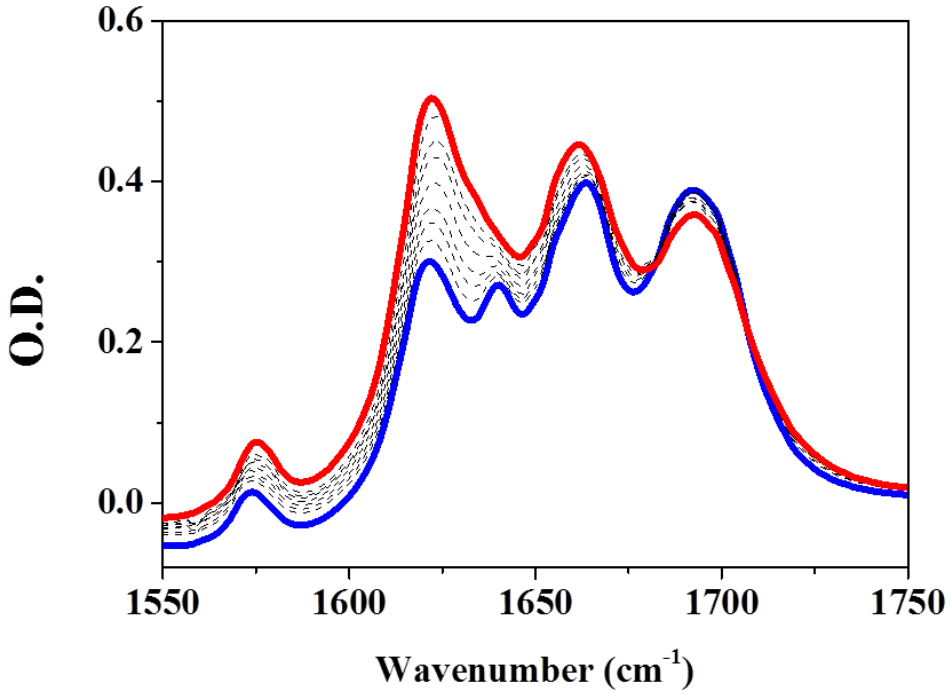

Figure 3.4 *– FTIR spectra of AT-15mer DNA at a range of temperatures from 293 K (blue) to 353 K (red) with intermediate temperatures shown as dashed lines.*

FTIR spectra for the AT-15mer have been recorded at a range of temperatures. DNA base modes found in the 1550-1700 cm^{-1} spectral window have been shown to be sensitive to DNA melting. In the spectra recorded there are five bands observed at 293 K (Figure 3.4 blue trace) with frequencies 1575 cm^{-1}, 1622 cm^{-1}, 1643 cm^{-1}, 1663 cm^{-1} and 1692 cm^{-1}. Previously these features have been assigned to C=C ring vibration of adenine, C=C/C=N ring vibration of Adenine, ring vibration of Thymine, T_4 carbonyl stretching and T_2 carbonyl stretching modes, respectively, using FTIR spectroscopy.[12] Upon heating to 353 K (Figure 3.4 red trace) an increase in intensity of the band at 1622 cm^{-1} is observed, partially obscuring any changes undergone by the band at 1643 cm^{-1} however a clear shoulder remains on the high frequency side of the band at 1622 cm^{-1}. An increase in intensity is also observed in the band at 1663 cm^{-1} while a slight decrease in the intensity in the band at 1692 cm^{-1} can also be seen. These changes also agree well with those seen in previous FTIR studies of DNA melting.[12]

Quantification of the duplex melting process and subsequent extraction of a T_m from the FTIR data proved somewhat more difficult than in the UV-Visible data. In previous FTIR studies, the melting transition was quantified by following peak amplitudes as a function of temperature.[12] However, due to the congestion in this spectra region, results of this form of analysis proved unreliable, as fitting of a series of Gaussian linshapes to extract the peak amplitudes as a function of temperature resulted in inclusion of features either too broad to fit the spectra obtained or too narrow to represent real IR lineshapes in the final fitting result. A more reliable method for extracting melting behaviour in the FTIR spectra was found in the form of Principal Component Analysis (PCA).[24] PCA is a multivariate analysis method which is able to extract elements of variance from a given data set by loading the dataset of variables into a matrix, calculating the weighting of each of the variables and reconstructing them as vectors of the matrix then calculating their variance across the data set.

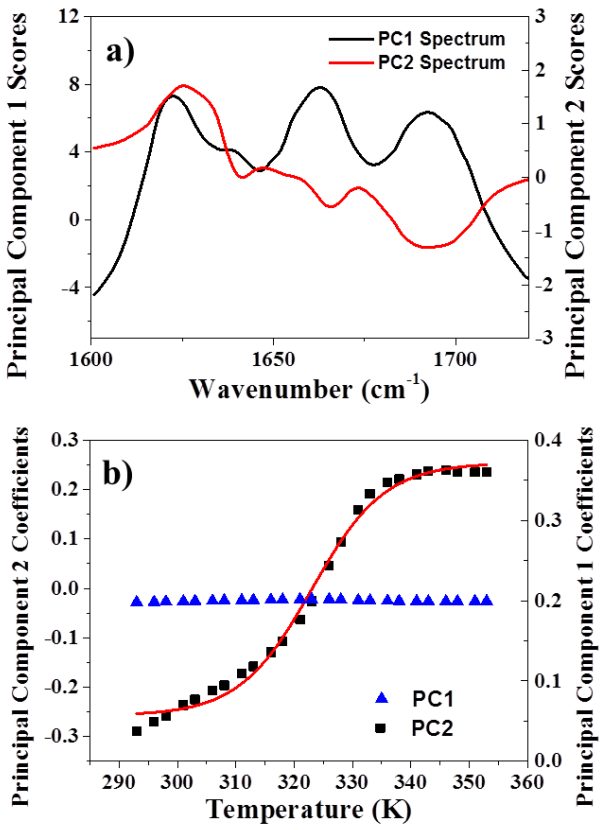

Figure 3.5 *– a) Spectra of the contributions of PC1 and PC2 to the PCA analysis. By adding varying amounts of PC2 to PC1 (amounts shown in b)) each of the individual spectra at each temperature can be reconstructed. b) Coefficients of PC1 and PC2 as a function of temperature*.

In order to extract a melting curve from the FTIR data, spectra recorded at each temperature is loaded into the pre-programmed PCA function of Origin 9.0 software. This then returns the number of Principal components that describe the variations in the dataset as a function of temperature and the principal components used to describe the variation in the data. Further to this, the relative weight of each principal component that is present in each of the original spectra is returned. PCA determined that the majority of the variations in the spectra (99.9%) can be adequately described by two principal components. The first principal component (PC1) is an average of the FTIR spectra and describes 98.2% of the variation in the spectra (black trace Figure 3.5a). As PC1 reflects the average of the spectra, the contribution of PC1 to each individual spectrum remains invariant with temperature (blue triangles Figure 3.5b). The second principal component (PC2) reflects 1.8% of the variance in the spectra and directly represents the changes undergone by each of the modes (red trace Figure 3.5a). By adding a weighted amount of PC2 to the 'average spectrum' (PC1), each of the input spectra can be reconstructed. For example, the result of the PCA suggests that the real FTIR spectrum recorded at 293 K can be represented by a weighted combination of PC1 and PC2, in this case the relative weights are 0.198xPC1 and 0.289xPC2 (y values of the first blue triangle and black square at a temperature of 293 K in Figure 3.5b). A reconstructed spectrum for these values is shown in Figure 3.6 below and compared directly with the real FTIR spectrum.

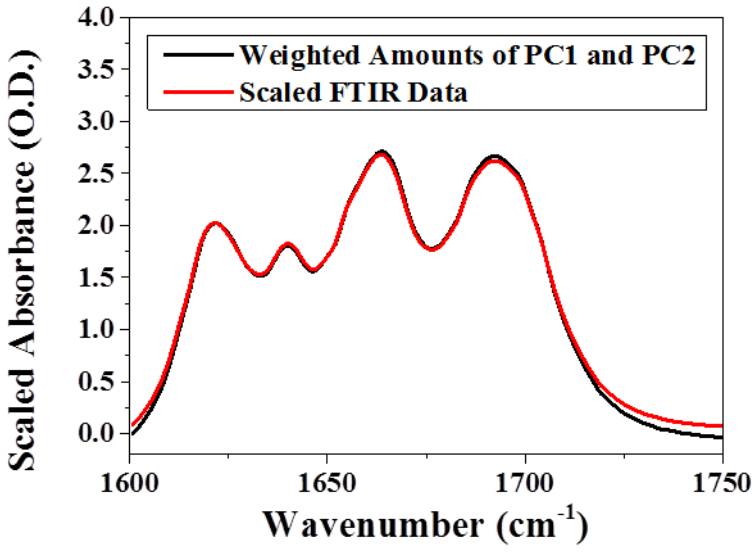

Figure 3.6 *– Comparison of scaled real FTIR Data (red trace) with reconstructed spectrum using weighted amounts of PC1 and PC2 (black trace).*

As can be seen from Figure 3.6 above, the red and black traces (representing the scaled real FTIR spectrum and the reconstructed PCA spectrum) compare very well, with all of the main features in the spectrum being well represented in the reconstructed spectrum. Each of the real FTIR spectra can be reconstructed in the same manner using the varying weighted amounts of PC2 as returned by the PCA. The variance of the weighted amount of PC2 can therefore be taken to represent the changes in the FTIR spectrum upon melting and as such plotting the weighted amount of PC2 as a function of temperature yields the temperature profile for the FTIR spectra and is shown in Figure 3.5b) (black squares). As was the case for the UV-Visible data, the melting curve obtained is fitted with a Boltzmann sigmoid (equation 3.1) in order to extract a T_m for the transition. The plot of PC2 against temperature fitted with a Boltzmann sigmoid (red trace Figure 3.5b) yields a T_m of 323±2 K and compares well the melting temperature obtained from the UV-vis data.

Now that the melting behaviour of the AT-15mer sequence has been established using accepted methodologies, this information will be used as a guide to study this process in the 2D-IR data.

3.4.2 2D-IR Spectroscopy

In order understand the information obtained by studying the melting of DNA with 2D-IR spectroscopy, assignment of the spectral features observed must be performed. As mentioned earlier, previous 2D-IR studies (both experimental and computational) of DNA point to the need to move away from traditional assignment of IR spectral features due to delocalisation of the vibrational mode across the base pairs. As such this section begins by presenting representative spectra of the AT-15mer at both 293 K and 353 K which correspond to the sequence being in ds- and ss- conformations respectively based on the UV-Visible and FTIR data. Assignment of the spectral features is presented and this is followed by the discussion of changes in the 2D-IR spectrum induced by DNA melting.

2D-IR spectra have been recorded at a range of temperatures and the 2D-IR spectrum at the two temperature extremes are shown in Figure 3.7b) and c) along with the corresponding FTIR spectra (Figure 3.7a). Figure 3.7b) shows the 2D-IR spectrum of the AT-15mer recorded at 293K and a population time of 250fs. By measuring spectra at very short waiting-times means that off-diagonal features will be due to coupling of vibrational modes as insufficient time has passed to allow energy transfer processes to occur. Along the

diagonal of the spectrum are five negative features (black crosses Figure 3.7b), each corresponding to the υ=0- 1 transition of the five modes found in the FTIR spectrum (dotted guidelines indicate the correlation of FTIR bands with the circled 2D-IR features in Figure 3.7). Each of these negative features is paired with an anharmonically shifted positive feature corresponding to the υ=1- 2 transition for each of the five modes (pink circles Figure 3.7b). In the off-diagonal regions of the spectrum, cross-peak features connecting each of the diagonal modes to one another can be observed. These are most prominent in the lower right portion of the spectrum where the negative bleach features of the cross-peaks are predominant (red boxed area Figure 3.7b). The presence of these cross peaks in the spectrum is indicative of interactions between the vibrational modes that can be either through coupling or energy transfer. Heating the sample to 353 K induces a number of changes in the 2D-IR spectrum. Changes in the intensities of the on-diagonal features that correspond to those seen in the FTIR spectra are observed as well as significant changes in the off-diagonal features, the significance of which will be discussed further below.

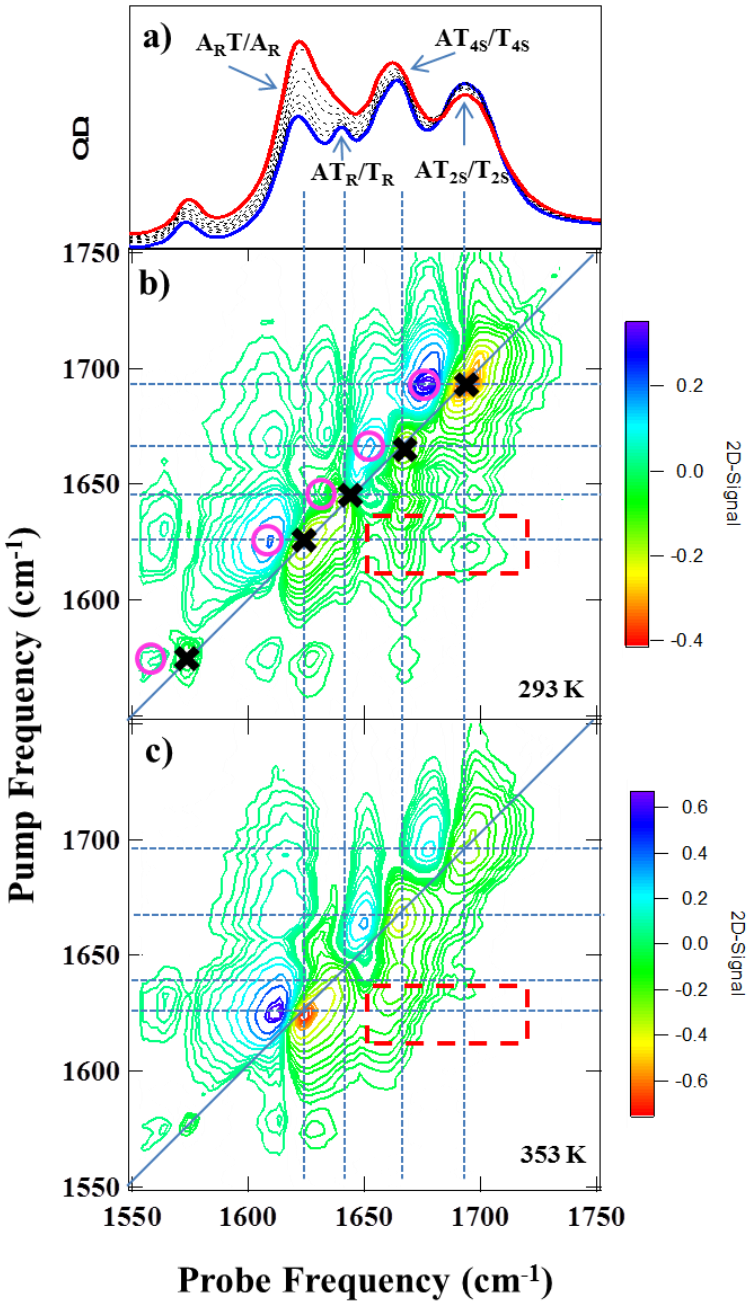

Figure 3.7 *– a) FTIR spectra of AT 15mer duplex recorded at a range of temperatures between 293 K (blue) and 353 K (red), assignments of bands are discussed in the text. B) 2D-IR spectrum of AT 15mer at 293 K, T_w = 250 fs. c) 2D-IR spectrum of AT 15mer at 353 K T_w = 250 fs. Colour scale runs from red (negative) to blue (positive) with contours at 10% intervals. On-diagonal features in the 2D-IR spectrum are 293 K are highlighted for each of the υ=0- 1 features (black crosses) and υ=1- 2 features (pink circles) of the base vibrational modes. Key off-diagonal features assigned to DNA melting are highlighted in the red boxes at low and high temperatures. These features are discussed further in the text.*

An assignment of the 2D-IR spectral features was performed using the computational studies performed by Cho et al. as a guide[1–4] instead of resorting to the classical local mode assignments used in FTIR studies. In order to help facilitate this assignment, 2D-IR spectra of individual adenosine monophosphate (AMP) and thymidine monophosphate (TMP) have also been measured under the same sample conditions (albeit at higher sample concentrations to increase the size of the absorption bands) as the AT-15mer duplex. These spectra and comparisons to the duplex spectra at low and high temperatures are shown in Figure 3.8.

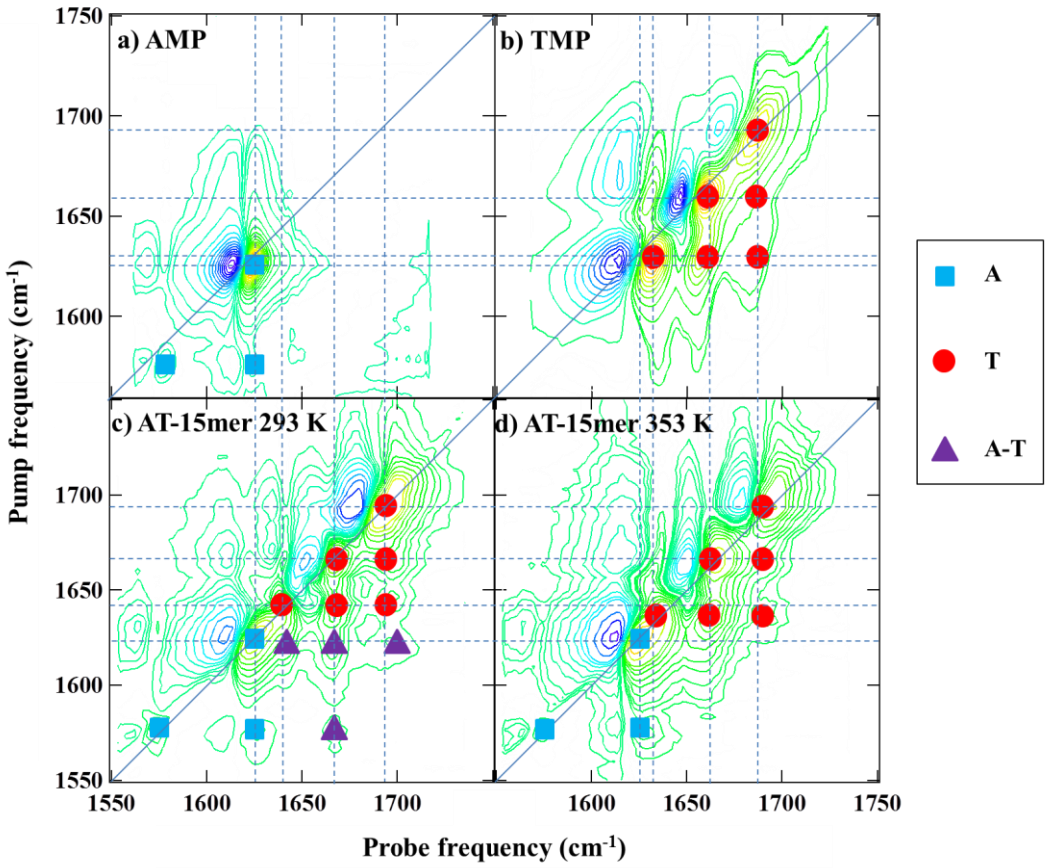

Figure 3.8 *– 2D-IR spectra of a) AMP b) TMP and ds- AT 15mer at c) 293 K and d) 353 K. Coloured symbols indicate the assignment of peaks visible in the AT 15mer spectra (c,d) based on the mononucleotide spectra (a,b).*

These AMP and TMP spectra are in good agreement with previous work[5] and show two adenosine modes in the AMP spectrum at 1575 cm^{-1} and 1627 cm^{-1} (blue squares Figure 3.8a) and in the TMP spectrum thymidine features at 1630 cm^{-1}, 1663 cm^{-1} and 1692 cm^{-1} (red circles Figure 3.8b) . Each of the on-diagonal modes in the AMP spectrum displays

evidence of intra-base coupling between the modes. This is also true for the vibrational modes observed in the TMP spectrum where coupling between each of the three modes is also observed. A linear superposition of the measured AMP and TMP spectra results in a spectrum with strong similarities, with some variations in intensity ratios, to the AT-15mer spectrum at high temperature. This then allows assignment of the high temperature AT-15mer spectrum or single strand DNA (ss-DNA) spectrum in accordance with previous assignments made for the AMP and TMP spectra. Measurement of one of the two ss-DNA strands that form the AT-15mer duplex has also been performed. While not shown here the spectrum is almost identical to that observed for the melted AT-15mer recorded at high temperature (Figure 3.8d) and further reinforces the assignments made here.It then follows that the features in Figure 3.8(d) at 1690cm^{-1}, 1660cm^{-1} and 1630cm^{-1} are due to the T_2, T_4 and T_R modes respectively while the lower frequency modes at 1627 cm^{-1} and 1578 cm^{-1} are adenine ring modes, A_{R1} and A_{R2} respectively. An illustration of these vibrational modes is depicted in Figure 3.9 below.

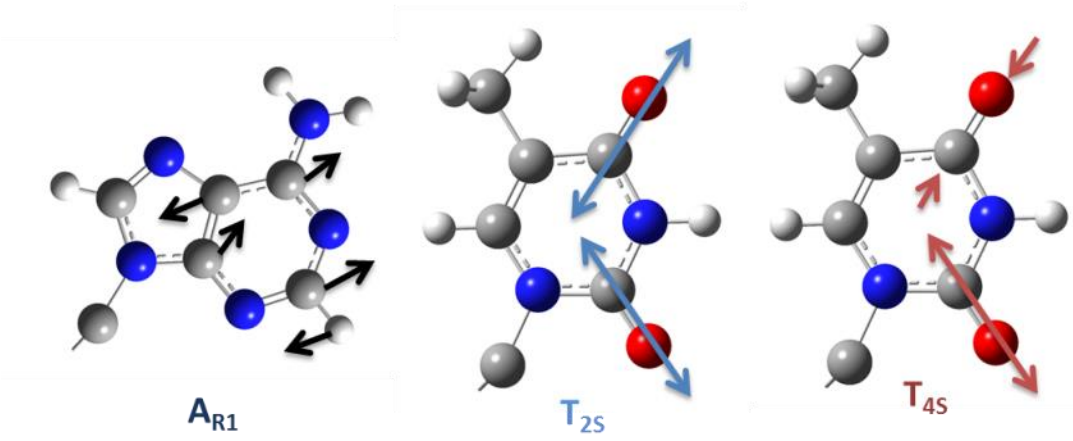

Figure 3.9 *– Schematic representation of vibrational modes of Adenine and Thymine bases.*

Following assignment of the ss-DNA spectrum, the low temperature duplex or double stranded DNA spectrum (ds-DNA) can be considered. The five vibrational modes identified in the AMP and TMP spectra are distinguishable on the diagonal of the ds-DNA spectrum, in particular the two modes that appear in the ss-DNA spectrum close to 1630cm^{-1} are now distinguishable as two separate modes. The two carbonyl modes from the thymine base and the lowest frequency adenine mode frequencies remain largely unchanged compared to their corresponding modes in the monophosphate spectra. In addition to the changes in the on-diagonal modes, the ds-DNA spectrum displays significant differences in the off-

diagonal region of the spectrum. These are denoted in Figure 3.8™ with purple triangles. These new features are present at frequencies that link the adenine mode located at 1622 cm^{-1} with each of the three thymine modes. Features between the lower frequency adenine mode at 1575 cm^{-1} and the three thymine modes are also observed, however, these are not clear in the 2D-spectrum and as such only one of these is denoted with the purple triangle. These features, however, are seen more clearly when looking at a horizontal slice through the 1575 cm^{-1} diagonal mode (Figure 3.10b) and zoomed in section of the 2D-IR spectrum (Figure 3.10c). The off-diagonal features are therefore characteristic of interaction between the adenine and thymine base modes that is facilitated by the W-C hydrogen bonding between the two DNA oligomers. Off-diagonal peaks in a 2D-IR spectrum can have one of three-origins: vibrational coupling of two vibrational modes, energy transfer between the modes during the waiting time, or chemical exchange.[25] Chemical exchange is not applicable in the experiments performed here as the core DNA molecular structure is not varying during the measurements, which leaves coupling and energy transfer as possible explanations of how the base vibrational mode are interacting with one another. The low temperature spectrum is in good agreement with that predicted by computational simulations[1,2] and so supports the assignment proposed by designating the vibrational modes in the ds-DNA spectrum as AT_{2S}, AT_{4S} and AT_{R}, $A_{R1}T$ and $A_{R2}T$ (1692, 1663, 1643, 1622 and 1578 cm^{-1} respectively) to reflect the coupling-induced delocalisation occurring across the base pair. While the features are at very similar frequencies to their counterparts in the ss-DNA spectra, the presence of the off-diagonal peaks indicates that the modes are spread across the base pair. A schematic of the base paired vibrational modes is shown in Figure 3.11.

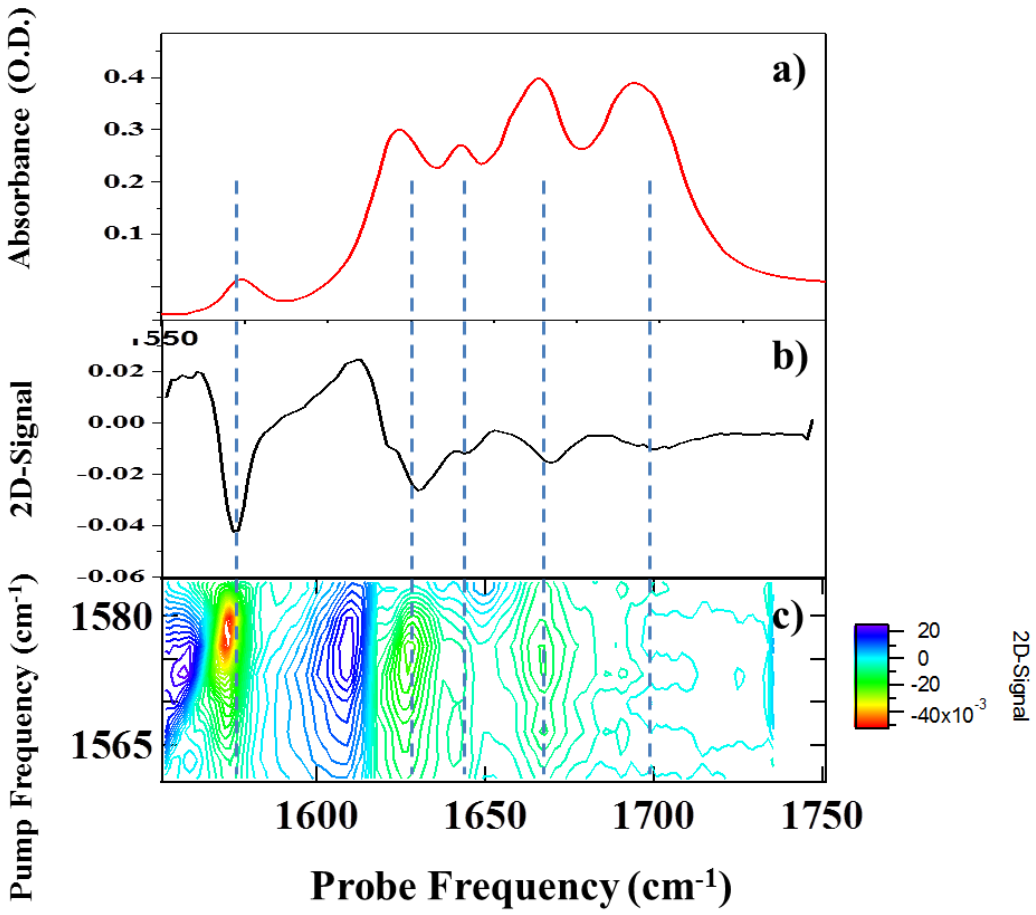

Figure 3.10 *– a) FTIR spectrum of the AT-15mer at 293 K. b) Pump slice (horizontal slice) extracted from 2D-IR spectrum of AT-15mer at 293K and a waiting time of 250 fs. c) Expansion of 2D-IR spectrum of AT-15mer at 293 K from which the trace in b) was extracted.*

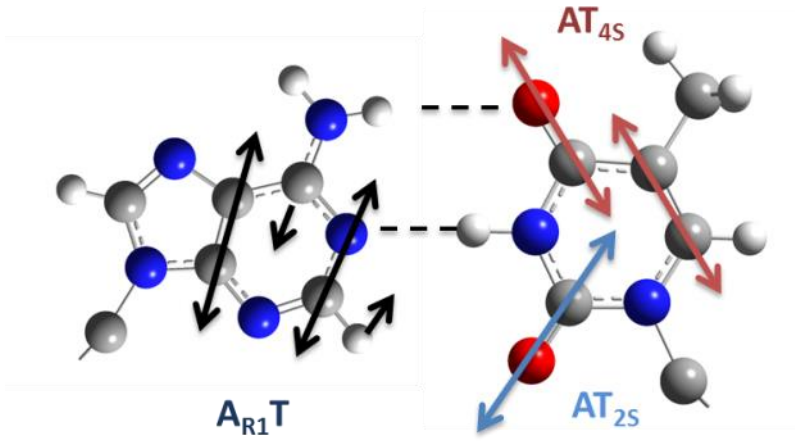

Figure 3.11 *– Schematic representation of vibrational modes of the W-C AT base pair.*

The large number of on-diagonal as well as off-diagonal features in the 2D-IR spectra and the overlapping of these features in this congested spectral region make fitting of peaks to quantify changes in the spectra upon heating difficult and results returned were unreliable. As such PCA has again been used to extract a melting temperature from the data. From the 2D-IR data recorded at a series of temperatures loaded into the PCA function, two principal components again were required to reflect the variance in the spectra with temperature. As in the PCA performed on the FTIR spectra, PC1 was once more a reflection of the average 2D spectrum and represented 94.9% of the variance but its contribution to the melt was largely invariant with temperature as seen in Figure 3.12 (blue triangles). The second component PC2 represented 4.8% of the variance in the spectra and represents the spectral changes induced upon heating the sample which causes the DNA duplex to unwind as is seen in the established UV-Visible spectroscopy data. Plotting the relative coefficients of PC2 against temperature (Figure 3.12 black squares) and fitting the resulting profile with Boltzmann sigmoidal fit (Figure 3.12 red trace) yields a T_m of 319±2 K, in good agreement with the UV-vis and FTIR data.

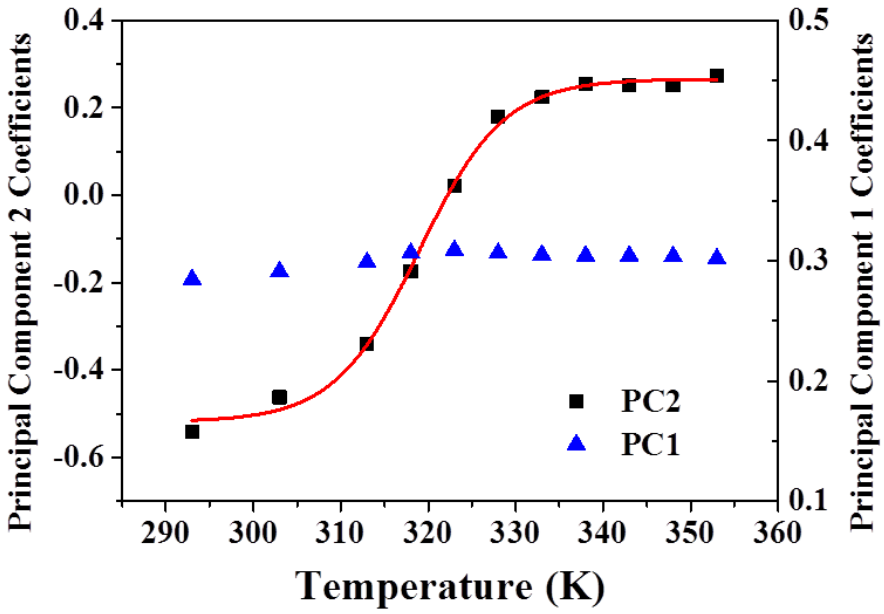

Figure 3.12 *– PCA analysis for AT-15mer 2D-IR spectra. PC2 reflects changes in the 2D-IR spectrum as a whole upon heating, Boltzmann sigmoidal fitting yields a T_m of 319±2 K.*

Details of the spectral features in PC2 are shown in Figure 3.13b) and four key features have been highlighted in green boxes. Overall the PC2 2D spectrum qualitatively has the appearance of a difference spectrum where the highest temperature 2D-IR spectrum

recorded is subtracted from the lowest temperature spectrum. The first key feature noted from the PC2 spectrum is the sign of the on-diagonal features for the AT_{2S}/T_{2S} mode (green box 1 Figure 3.13b). In all the 2D spectra presented here, positive features are denoted with blue colouring while negative features are denoted in red. In the PC2 spectrum the sign of the AT_{2S}/T_{2S} feature is opposite to what is observed in the experimental spectra. Figure 3.13a) shows the same 2D-IR spectrum shown in Figure 3.7b) however this is plotted in a different format to highlight changes picked out in the PCA. In the experimental data v=0-1 features are indicated by red colouring and v=1-2 features are shown in blue. In the PC2 spectrum generated from PCA (Figure 3.13b) a feature that is the opposite colour as the corresponding feature in the experimental data indicates that the overall amplitude of that feature is decreasing with increasing temperature. This behaviour is observed for the AT_{2S}/T_{2S} features by the PCA and this is consistent with the behaviour of this mode in the FTIR spectra. The second noted feature is similar to the first; the sign of the $A_{R1}T/A_{R1}$ diagonal features have retained the same colour (sign) as observed in the experimental spectra (green box 2 Figure 3.13b). In contrast to the AT_{2S}/T_{2S} mode this is indicative of an increase in amplitude with temperature and again is consistent with behaviour observed in the FTIR spectra.

The third and fourth features highlighted in Figure 3.13 (green boxes 3 and 4 Figure 3.13b) pertain to changes in the off-diagonal portions of the spectrum. Feature three reports on the behaviour of the AT_R/T_R mode upon melting. The blue feature highlighted in green box 3 (Figure 3.13b) indicated a loss of intensity of the cross peak centred at a pump frequency of 1643 cm^{-1} and a subsequent gain in intensity at a pump frequency of 1630 cm^{-1}. This clearly shows that upon denaturation of the duplex the T_R mode shifts to lower frequency, a feature not entirely clear in the FTIR spectra due to the close proximity of the adenine and thymine ring modes in this region. The final noted feature relates to the off-diagonal peaks between the adenine and thymine modes which have been identified as features specific to ds-DNA. In the PC2 spectrum the sign of the cross peaks has been inverted, indicative of a decrease in their intensity upon melting and further confirming their characterisation as duplex specific spectral features.

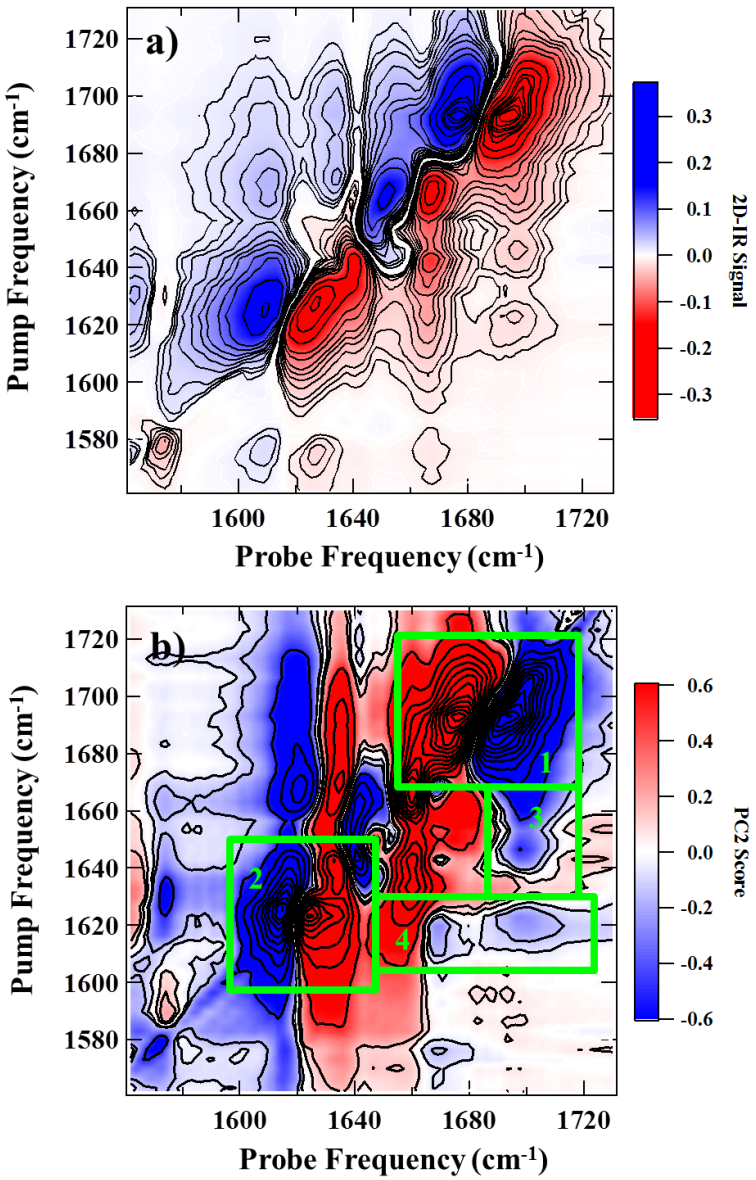

Figure 3.13 *– a) 2D-IR spectrum of AT-15mer at 293 K plotted in an alternate format to match PCA plot and give context to PCA results, b) PC2 spectrum from PCA of AT-15mer melting. 4 key features are highlighted in the green boxes and are discussed in the text.*

3.4.3 Pump-Probe Data

Pump-probe measurements have been performed on the AT-15mer sample in order to obtain the vibrational lifetime for each of the base modes. Pump-probe signals were recorded at a series of delay times out to a maximum of 10 ps at both 293 K and 353 K to observe if vibrational lifetimes are affected by DNA strand conformation. Examples of signals obtained at both temperatures are shown below in Figure 3.14.

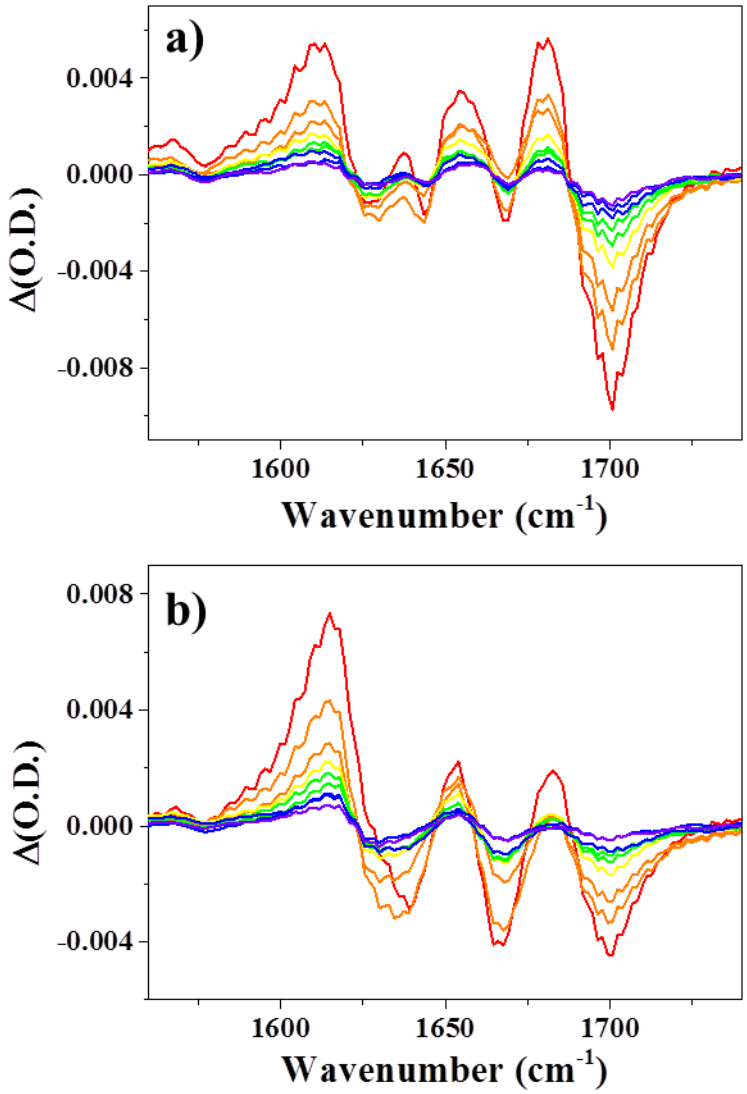

Figure 3.14 *– Pump-probe traces recorded for the AT-15mer at 293 K (a) and 353 K (b). Data is shown at a number of delay times between 0.1 (red) and 2 ps (purple).*

Pump-probe signals obtained for the AT-15mer in the double-stranded conformation at 293 K are shown in for a series of waiting times in Figure 3.14a). At a short waiting time of 0.1 ps (red trace Figure 3.14a) four negative features are observed at frequencies of 1625, 1645, 1667 and 1700 cm^{-1}, corresponding to the v=0-1 transitions of the $A_{R1}T$, AT_R, AT_{4S} and AT_{2S} modes, respectively. Of these features, the negative feature from the AT_{2S} modes is the most prominent as the other features are subject to overlapping of a number of positive and negative features that are not well separated, resulting in an overall reduced intensity of signals located in the middle of the spectral region shown in Figure 3.14a). A positive

feature accompanies each of these negative features which correspond to the v=1-2 transitions of each of the four respective base modes mentioned.

Figure 3.14b) shows pump-probe spectra obtained following heating of the AT-15mer sample to 353 K and so corresponds to the AT-15mer in single stranded conformation. Only three pairs of positive and negative features are observed which is consistent with the behaviour of the diagonal features in the 2D-IR data due to melting. The features corresponding to the T_R mode are not well resolved in the 2D-IR spectra and this is also the case in the pump-probe data as the A_{R1} and T_R modes overlap. As a result, only features from the A_{R1}, T_{4S} and T_{2S} are well resolved in the single strand data.

As the waiting time is increased, the amplitude of each of the features decreases (see purple traces in Figures 3.14a) and 3.14b) which show pump-probe spectra at a waiting time of 2ps). This decrease is a result of the probability of the population state created by the pump excitation in the molecular ensemble spontaneously relaxing also increasing with increasing waiting time. By extracting the amplitude of each of the features in the pump probe spectra as a function of waiting time allows measurement of the vibrational lifetime from the data as the amplitude decays exponentially with increasing waiting time by fitting the kinetic plots of amplitude against waiting time. An example of the kinetic traces obtained from the pump-probe data for the AT_{2S} features is shown in Figure 3.15.

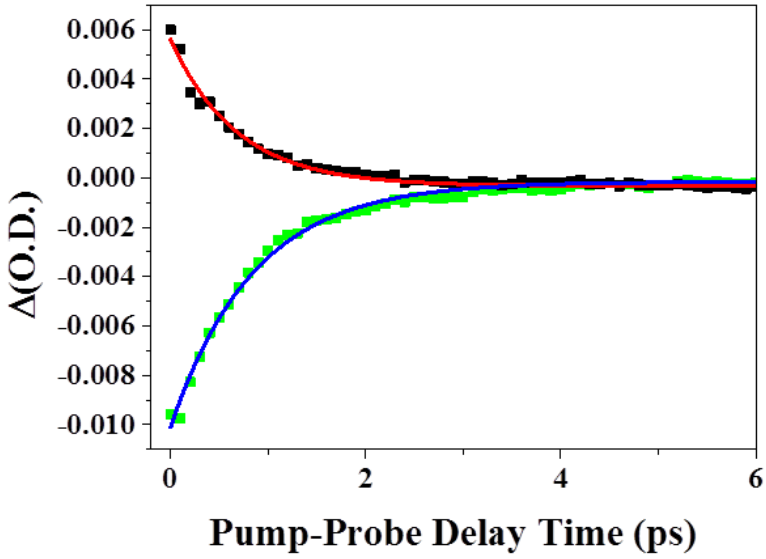

Figure 3.15 *– Pump-probe kinetics for the v=0-1 (green trace) and v=1-2 (black trace) features of the AT_{2S} mode at 293 K. Data fitted with single exponentials (blue and red traces) and the average of the two decay constants is taken as the vibrational life time of the mode.*

Vibrational lifetimes are extracted from the kinetic plots as shown in Figure 3.15 via fitting of single exponential decays to the data using the equation:

$$y = y_0 + A_1 * exp\left(\frac{-t}{\tau}\right) \tag{3.2}$$

Where y_0 is the value of any offset in the amplitude y at long values of waiting time t, A_1 is an amplitude scaling factor and τ is the decay constant which corresponds to the vibrational lifetime T_1. In general the pump-probe signals obtained are all well described by fitting single exponential decay functions and yielded vibrational lifetimes on the order of 850 fs (shown in Table 3.1 below). Upon heating of the sample, while the shape of the pump-probe signals changed in correspondence with melting of the duplex, the vibrational lifetime of the vibrational modes upon melting (single strand data) remained largely comparable to the modes observed in the DNA duplex data albeit slightly faster in the single strand data. Pump probe measurements have also been formed on a single strand of DNA and subsequent lifetimes obtained are listed in Table 3.2.

Temperature (K)	Mode Frequency (cm^{-1})	Assignment	Vibrational Lifetime (fs)	FFCF (fs)
293	1692	AT_{2S}	770	-
	1663	AT_{4S}	1030	-
	1643	AT_R	930	-
	1622	$A_{R1}T$	860	-
353	1692	T_{2S}	800	570 ± 50
	1661	T_{4S}	760	-
	1630	T_R	-	-
	1626	A_{R1}	650	1060 ± 520

Table 3.1 *– Mode assignments and extracted dynamic parameters from ds-AT-15mer 2D-IR spectra.*

3.4.4 Time Resolved 2D-IR Data

2D-IR results presented to this point have focused on 2D-IR spectra at a range of temperatures showing changes in spectra that pertain to structural changes upon melting. However, one of the key advantages presented by 2D-IR spectroscopy is its high time resolution and ability to extract dynamic information from a system. As such, time-resolved spectra have also been a measured at a series of waiting times for both AT-15mer DNA at low temperature, where the oligomers are in the duplex conformation, and also high temperature when the duplex has been denatured into component single strands. This allows observation of lineshape evolution of 2D-IR spectral features under both ds- and ss-conditions. Extracting the temporal-dependence of this change of lineshape reports on the local molecular dynamics influencing the transition frequency, the FFCF, as described in Chapter 1.[25–30] Due to the congested nature of this spectral region, with four modes found on the diagonal, reliable dynamical timescales were only extracted from the AT_{2S}/T_{2S} and $A_{R1}T/A_{R1}$ modes at low and high temperatures respectively. Qualitatively the AT_{4S}/T_{4S} does exhibit evidence of spectral diffusion while the relative size of the AT_R/T_R mode compared to the other modes in this region coupled with the spectral overlap with these neighbouring modes made spectral diffusion analysis impossible.

Figure 3.16 demonstrates a set of example spectra focussed on the spectral feature of the AT_{2S} and T_{2S} mode at a number of waiting times. At the earliest waiting times recorded both spectral features are clearly elongated along the diagonal (Figure 3.16 a, b, c) and in the higher temperature spectra (ss-DNA) the lineshapes can be seen to become increasingly

more circular at later waiting times (Figure 3.16 d, e, f), indicative of the mode undergoing spectral diffusion.

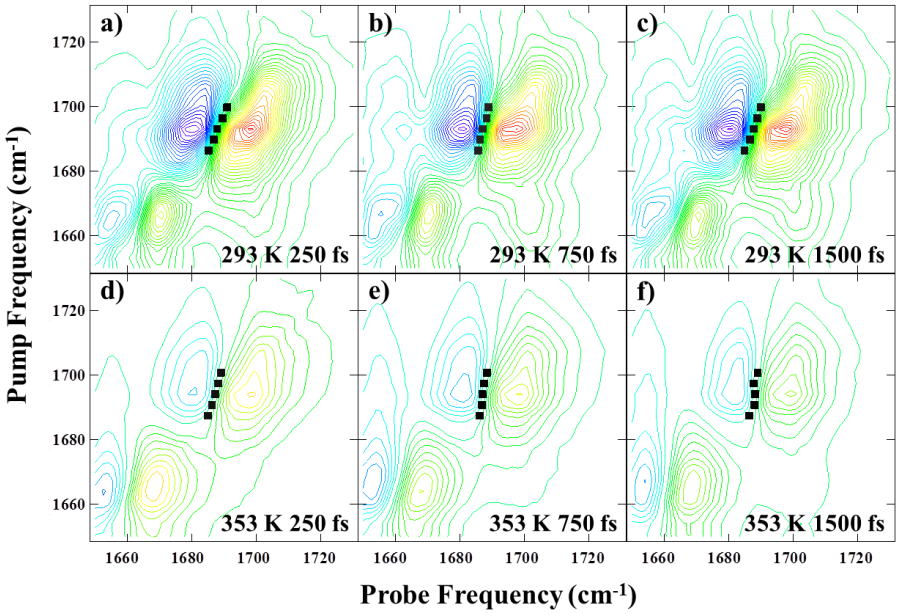

Figure 3.16 *– 2D-IR spectra of the AT_{2S}/T_{2S} mode of the AT 15mer obtained as a function of waiting time and temperature. (a-c) show T_w = 250, 750 and 1500 fs at 293 K. (d-f) shows the same waiting times at 353 K. The black symbols show the results of a nodal line slope (NLS) analysis of the line shapes.*

A combination of methods has been used to extract the frequency-frequency correlation function from the AT_{2S}/T_{2S} and $A_{R1}T/A_{R1}$ modes. The three methods used were – Centre Line Slope analysis (CLS),[31] Nodal Line Slope analysis (NLS)[32,33] and 2D-Gaussian fitting.[34] Each of these methods used for extraction of the FFCF was discussed in Chapter (1) and are accepted in the literature as methods for extracting solvation dynamics from 2D-IR spectra. The three methods returned individually similar results[35] and the average of these analyses is taken as the most reliable reporter of the spectral diffusion of the modes.

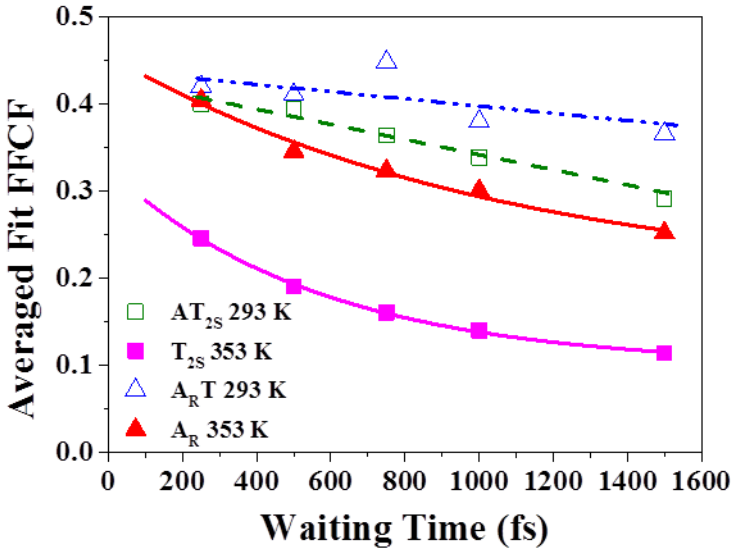

Figure 3.17 *– Average FFCF dynamics as a function of T_W for the T_{2S} and A_{R1} modes of the AT 15mer DNA in ds and ss conformations (see legend).*

Figure 3.17 shows the results of the spectral diffusion analysis. At 293 K, when DNA is in the double stranded configuration both the $A_{R1}T$ and AT_{2S} modes (blue and green traces Figure 3.17) exhibit very little spectral diffusion on the timescale of the data recorded, indicating that any dynamics are occurring on a longer timescale than 1500 fs. However, it is noteworthy that the initial value of the FFCF found at 250 fs is reduced from unity, indicating a potential contribution of dynamics that occur on a sub 200 fs timescale. This is faster than the temporal resolution of the laser system dictated by the duration of the laser pulses used in the experiment.

Upon heating the sample to 353 K, at which point the DNA sequence has melted into its constituent DNA single strands. The initial value of the FFCF is still reduced from unity, indicating that fast dynamics are still present. However this is now accompanied by clear exponential decays in the FFCF for both modes (red and pink traces Figure 3.17). Spectral diffusion of the T_{2S} mode decays on a timescale of 570 ± 50 fs while the A_{R1} mode decay occurs on a longer timescale of 1060 ± 520 fs. The result for the A_{R1} mode is less well defined due to the very fast vibrational relaxation of the diagonal modes (~850 fs). Dynamic parameters recorded for the experiment are summarised in Table 1.

In order to establish whether changes observed in the solvation dynamics of the ds- AT 15mer are induced by melting of the duplex structure or by effects caused by interaction

with a heated solvent environment the time-resolved experiments were repeated using only one of the two oligomers that make up the 15mer duplex. FFCF parameters were also extracted from the ss-DNA data. In this data set, the T_{2S} mode exhibited exponential decays in the FFCF at both 293 K and 353 K with respective decay constants of 350 ± 120 fs and 760 ± 140 fs obtained. However, the A_{R1} mode behaves similarly to that in the ds-DNA data, at 293 K little to no spectral diffusion is observed while at 353 K a decay is once more obtained on a timescale of 610 ± 530 fs. FFCF curves obtained for the ss-DNA data are shown in Figure 3.18 and accompanying dynamic parameters in Table 2 below.

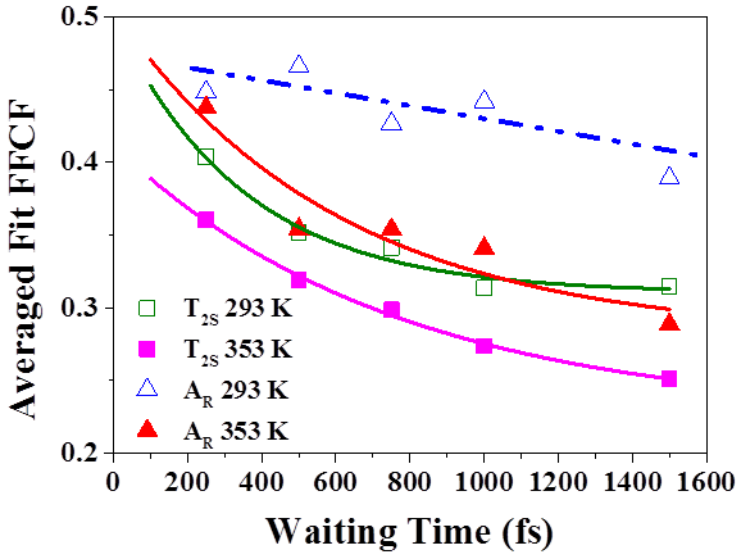

Figure 3.18 *– Average FFCF dynamics as a function of T_W for the T_{2S} and A_{R1} modes of the AT 15mer DNA single strand.*

Temperature (K)	Mode Frequency (cm^{-1})	Assignment	Vibrational Lifetime (fs)	FFCF (fs)
293	1692	T_{2S}	990	350 ± 120
	1661	T_{4S}	1020	-
	1632	T_R	-	-
	1622	A_{R1}	790	-
353	1692	T_{2S}	860	760 ± 140
	1661	T_{4S}	1080	-
	1632	T_R	-	-
	1622	A_{R1}	750	610 ± 530

Table 3.2 *– Mode assignments and extracted dynamic parameters from ss-AT-15mer 2D-IR spectra.*

3.5 Discussion

3.5.1 Impact of Duplex Formation on the Spectroscopy of DNA

2D-IR has the combination of structural sensitivity and temporal resolution to investigate ultrafast dynamics that underpin biological processes. One of the initial stages in biological processes involving DNA is unwinding of the DNA duplex and therefore understanding the changes in 2D-IR spectral features and identifying markers characteristic of DNA conformation are of great importance for furthering this technique to investigate more complex systems. The results presented here of the temperature-dependent 2D-IR spectra identify features which enable the determination of the conformation of DNA oligomers in solution. In addition to changes in the on-diagonal features that reflect the same changes observed in linear spectroscopic studies, changes in off-diagonal peaks that show they are dependent on the conformation of the DNA oligomers are also observed. It has been shown previously that the vibrational modes of the single DNA bases are significantly delocalised[5] while studies of DNA duplexes containing on only GC base pairs show signs of interbase coupling.[7] The differences between the ss- and ds-AT 15mer spectra show clearly that a similar situation is present here in ds-AT DNA and that Watson-Crick base pairing induces significant delocalisation of the base vibrational modes. This effect manifests itself by the presence of off-diagonal peaks linking the A_{R1} vibrational mode of the Adenine base to the three vibrational modes (T_R, T_{4S} and T_{2S}) of the Thymine base which are lost upon melting of the duplex.

For the first time a combination of 2D-IR spectroscopy and PCA has been used to quantify the DNA melting process for an AT-15mer DNA sequence. This highlights the ability of 2D-IR to be used as a tool for investigating fundamental structural dynamics in biological processes. A T_m value of 319 ± 2 K extracted from the temperature dependent 2D-IR data compared favourably with that extracted from the UV-Visible data (318 ± 2 K). As UV-Visible spectroscopy is widely recognised as the established technique for determining DNA melting information, then this result points to the reliability of 2D-IR to extract the similar information while also offering the time resolution that allows the denaturing of W-C base pairs in real time.[21]

3.5.2 Signatures of Coupling and Energy Transfer

Vibrational coupling of the modes is certainly present, as off-diagonal features in the 2D-IR spectrum are present from the earliest waiting times recorded. Vibrational coupling constants between the base modes of around 4-10 cm^{-1} have been predicted by computational simulation,[3] which translate to values for off-diagonal anharmonicities of around 1 cm^{-1} which can be calculated from the following equation:[25]

$$\Delta_{12} = -4\Delta \frac{\beta_{12}^2}{(\hbar\omega_2 - \hbar\omega_1)^2} \tag{3.3}$$

Where Δ_{12} is the off-diagonal anharmonicity, Δ is the diagonal anharmonicty, β_{12} is the coupling constant between the two modes and $(\hbar\omega_2 - \hbar\omega_1)$ is the frequency sepearation of the two coupled modes. Features in the lower right corner of the ds-DNA spectra recorded here appear to have off-diagonal anharmonicities of a similar order to that predicted by equation (3.3), while the positive and negative features are not clearly resolvable (Figure 3.19a), clearer separation of positive and negative contributions to the off-diagonal would be expected for large values of the off-diagonal anharmonicity. The off-diagonal features also decay at the same rate as their corresponding on-diagonal features which is consistent with coupling behaviour (Figure 3.20).

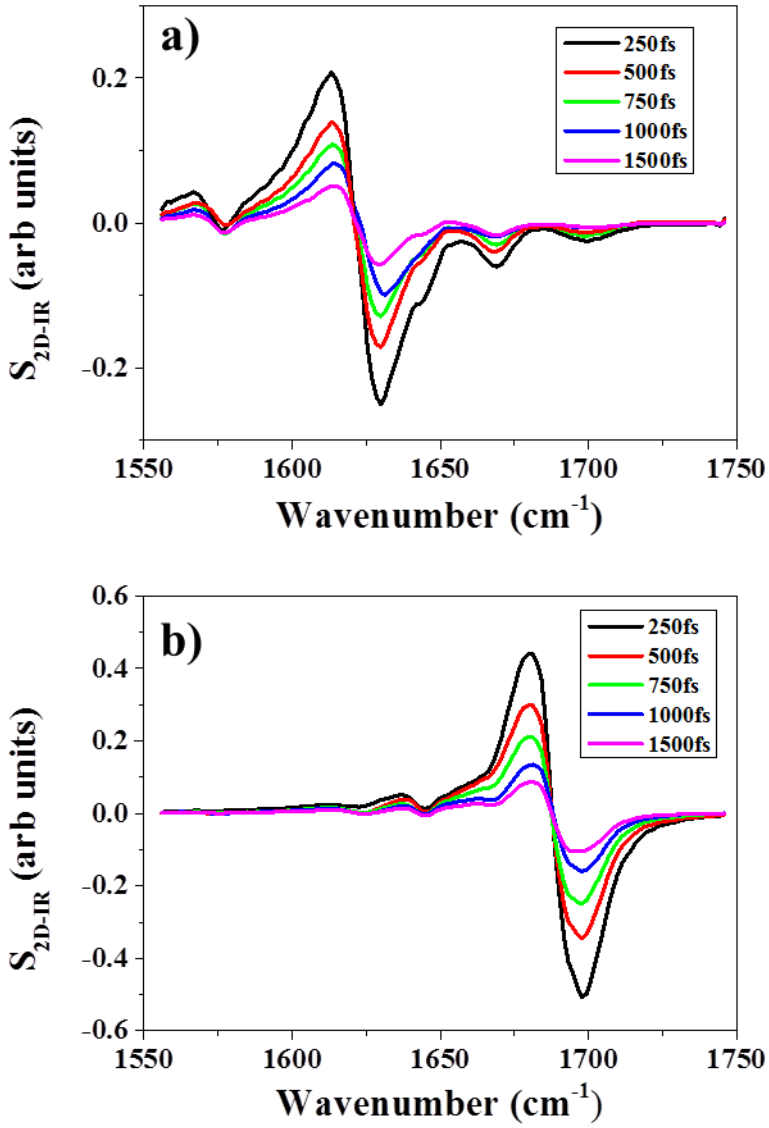

Figure 3.19 *– Slices through the 2D-IR spectra of ds-AT-15mer at a series of waiting times, taken at pump frequencies of a) 1622cm^{-1} and b) 1693cm^{-1}.*

It is also reasonable to expect a degree of energy transfer as well as coupling to be present among the vibrational modes. Evidence of this is found in the off-diagonal features in the upper left quadrant of the 2D-IR spectra. A slice through the spectrum at a pump frequency of 1693 cm^{-1} is shown in Figure 3.19b). Peak shapes in this slice differ to that observed in the lower right quadrant as positive and negative components can be more readily distinguished, indicative of off-diagonal anharmonicities that are comparable to the diagonal anharmonicities of the base vibrational modes which are all around 5-10 cm^{-1}.[5] This highlights the transfer of population from one diagonal mode to another. The relative

amplitude of the on and off-diagonal features in this region also differs to those in the lower right quadrant. Rather than decaying at a constant rate, the relative amplitude of the on and off diagonals decreases over time on a timescale of 850 fs which compares well with the vibrational relaxation time of the diagonal modes (Figure 3.20). This behaviour is consistent with downhill energy transfer.

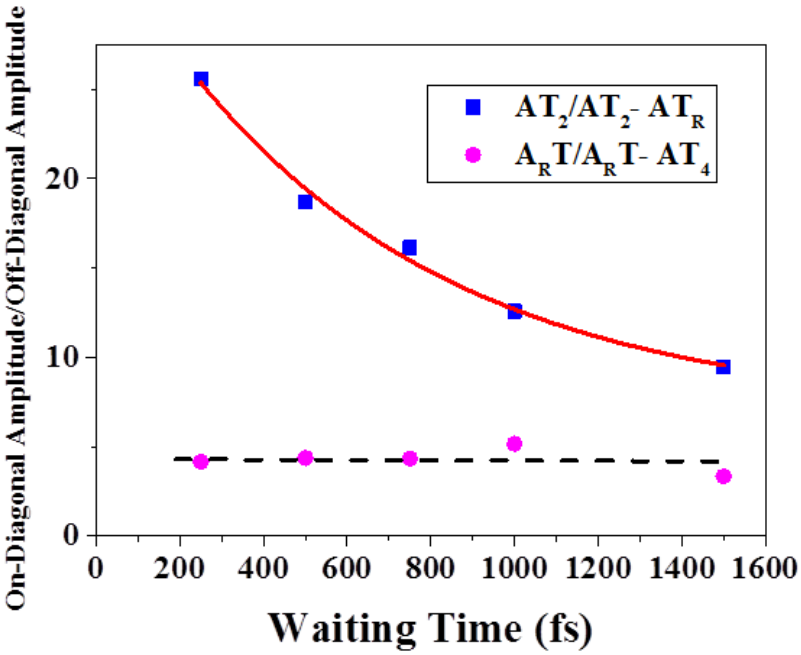

Figure 3.20 *– Relative signal sizes of on and off-diagonal features in the 2D-IR spectrum of the AT-15mer recorded at 293 K. The amplitude ratio of the respective on diagonal to the off-diagonal peak between the A_RT and AT_{4S} modes in the lower right quadrant, denoted A_RT /A_RT-AT_{4S} shows behaviour consistent with coupling with the relative signal sizes between on and off-diagonal signals remaining constant with T_w (circles).The amplitude ratio of the respective on-diagonal mode to the off-diagonal feature between the AT_{2S} diagonal and the AT_R modes in the upper left quadrant of the spectrum, denoted AT_{2S}/AT_{2S}-AT_R, shows behaviour characteristic of energy transfer with a decay of the on-diagonal/off-diagonal peak amplitude ratio of 650±150 fs (squares).The line indicates the results of fitting to an exponential decay function.*

3.5.3 Conformation-dependent Solvation Dynamics

Spectral diffusion analysis of the A_R and T_{2S} modes showed significant differences between DNA in ds- conformation (293 K) and that in ss- conformation (353 K). Throughout the

analysis, indications of fast contributions to the dynamics are present but in general the ds-DNA shows little evidence of spectral diffusion on the timescale measured, while heating the sample and melting the duplex allowed for exponential decay behaviour to be recovered. This observation is consistent with those observed for spectral diffusion of a nitrile vibrational probe group in a 'villin headpiece' protein system which showed an increase in spectral diffusion upon unfolding of the protein, allowing greater exposure of the probe to the solvent environment.[30]

Understanding the nature of the vibrational modes investigated by spectral diffusion analysis is important. In ss-DNA, the T_{2S} mode is predominantly a C=O stretching vibration whereas the A_R mode is predominantly a ring vibration with a degree of NH_2 bending.[5,36] When the ds-DNA duplex is formed these modes exhibit coupling and form the A_RT and AT_{2S} modes and so the similar behaviour of the two coupled modes is consistent with a 'base paired' environment within the double helix structure whereby little interaction with solvent molecules is possible, which is typically required for sub-ps dynamics.[33,37] The lack of spectral diffusion in ds-DNA is also consistent with a previous study which shows that the principal method of interaction between DNA and its solvent environment is through the phosphate groups.[38]

Melting of the helix resulted in a marked difference of the spectral solvation dynamics for the A_R and T_{2S} modes which now exhibited sub-ps spectral diffusion as a result of the change of conformation allowing increased solvent access to the bases. In the double-helix conformation, the C=O group of the AT_{2S} mode is directed into the minor groove of DNA. Bound, ice-like water molecules are thought to be located in the DNA minor groove forming a so called 'spine of hydration'.[39] Therefore the AT_{2S} mode while likely to interact with water molecules, this will not be a comparable interaction to that with bulk water and so fast spectral diffusion would not be expected. Thus it could be concluded that the AT_{2S} mode is a viable probe of water dynamics within the minor groove of DNA. However, it is not possible to confirm the water interaction solely via 2D-IR measurements. The indication these results are that if the T_{2S} carbonyl is interacting with the water in the groove, then the timescale of the dynamics observed for the this 'spine of hydration' is consistent with a heavily dynamically restricted picture of water molecules.[40,41]

Upon melting of the DNA duplex the minor groove is disrupted and the T_{2S} mode becomes more accessible to bulk solvent molecules and spectral diffusion is observed as has been

observed for other systems where carbonyl groups are exposed to bulk water.[17,42,43] Timescales of the spectral diffusion are consistent with solvation dynamics in water, although noticeably slower than that observed for the spectral diffusion of the phosphate groups (300 fs).[38] This behaviour is consistent with preferential solvation through the phosphate groups instead of the more hydrophobic bases. The longer spectral diffusion timescale of the A_R mode compared to the T_{2S} mode suggests further differential solvation between the Adenine and Thymine bases where Thymine contains hydrophilic C=O units.

Spectral diffusion of the single DNA strand had some differences to that of the duplex data. The A_R mode behaved similarly to the comparable mode in the duplex data. At low temperatures no decay was observed however this was recovered upon heating of the sample to higher temperature. The timescale of the decay recovered at high temperature however was slightly faster than observed in the duplex data. The T_{2S} mode however behaves differently in the single strand sample. At both low and high temperatures, exponential decays in the FFCF is observed with the decay at lower temperatures being slightly faster than that observed at higher temperature. As a single DNA strand, which is not self-complementary, does not have a complementary strand to base pair with, it would be reasonable to consider that a single DNA strand would behave similarly at low and high temperatures as no duplex formation is expected. However the spectral diffusion analysis shown here does not invite the conclusion that the A_R mode is interacting with comparable solvent environments at both low and high temperatures in the single strand sample. The T_{2S} mode does seem to follow this behaviour as spectral diffusion is observed at both low and high temperatures, consistent with the T_2 carbonyl group being much more solvent accessible at low temperatures as opposed to being in the compact environment of the minor groove of a duplex. The A_R mode however behaves differently to the T_{2S} mode and a change in FFCF dynamics is observed upon heating of the single strand. This indicates that the single DNA strand possesses some more ordered structure instead of randomly coiled. This structure is likely facilitated by hydrophobic interactions between the bases at low temperatures. Adenine base stacking interactions has been shown to be particularly stable and the results presented here suggest that these interactions may exert considerable influence even over single strands of DNA in solution.[44]

3.6 Conclusions

2D-IR spectroscopy has revealed conformation-dependent coupling patterns and dynamics of an AT-15mer DNA duplex under solution phase conditions. 2D-IR spectroscopy has probed the vibrational modes of the DNA bases and revealed off-diagonal peaks attributed to coupling and energy transfer across the DNA bases which is facilitated by the formation of Watson-Crick base pairs. Temperature-dependent melting behaviour obtained also compares well with that obtained from accepted methods underlining the viability of 2D-IR as a method for studying dynamic biological process involving DNA. Melting the DNA duplex induced an increase in spectral diffusion of the base vibrational modes which is consistent with increased solvent access to the individual DNA strands. Spectral diffusion results for the AT_{2S} mode in ds-DNA supports the idea that water bound in the DNA minor groove is dynamically restricted compared to bulk water and suggests the potential of the T_2 carbonyl group as a probe of solvation dynamics in the minor groove of DNA. These features requires further studies to allow a clear link to be established to the biological function of DNA, for example probing the NH stretching modes of the DNA bases or the vibrational responses of the solvent environment which may provide new insights.[36,45] A clear message from the results obtained is that a range of dynamic behaviour must be considered when trying to understand the behaviour of DNA in solution.

3.7 References

1. Lee, C., Park, K.-H., Kim, J.-A., Hahn, S. & Cho, M. Vibrational dynamics of DNA. III. Molecular dynamics simulations of DNA in water and theoretical calculations of the two-dimensional vibrational spectra. *J. Chem. Phys.* **125,** 114510 (2006).

2. Lee, C., Park, K.-H. & Cho, M. Vibrational dynamics of DNA. I. Vibrational basis modes and couplings. *J. Chem. Phys.* **125,** 114508 (2006).

3. Lee, C. & Cho, M. Vibrational dynamics of DNA. II. Deuterium exchange effects and simulated IR absorption spectra. *J. Chem. Phys.* **125,** 114509 (2006).

4. Lee, C. & Cho, M. Vibrational dynamics of DNA: IV. Vibrational spectroscopic characteristics of A-, B-, and Z-form DNA's. *J. Chem. Phys.* **126,** 145102 (2007).

5. Peng, C. S., Jones, K. C. & Tokmakoff, A. Anharmonic vibrational modes of nucleic acid bases revealed by 2D IR spectroscopy. *J. Am. Chem. Soc.* **133,** 15650–15660 (2011).

6. Krummel, A. T., Mukherjee, P. & Zanni, M. T. Inter and Intrastrand Vibrational Coupling in DNA Studied with Heterodyned 2D-IR Spectroscopy. *J. Phys. Chem. B* **107,** 9165–9169 (2003).

7. Krummel, A. T. & Zanni, M. T. DNA vibrational coupling revealed with two-dimensional infrared spectroscopy: insight into why vibrational spectroscopy is sensitive to DNA structure. *J. Phys. Chem. B* **110,** 13991–14000 (2006).

8. Wüthrich, K. NMR - This Other Method for Protein and Nucleic Acid Structure Determination. *ACTA Crystallogr. Sect. D-BIOLOGICAL Crystallogr.* **51,** 249–270 (1995).

9. Doty, P., Boedtker, H., Fresco, J. R., Hall, B. D. & Haselkorn, R. Configurational Studies of Polynucleotides and Ribonucleic Acid. *Ann. NEW YORK Acad. Sci.* **81,** 693–708 (1959).

10. Tsuboi, M. Application of Infrared Spectroscopy to Structure Studies of Nucleic Acids. *Appl. Spectrosc. Rev.* **3,** 45–90 (1969).

11. Taillandier, E. & Liquier, J. Infrared Spectroscopy of DNA. *Methods Enzymol.* **211,** 307–335 (1992).

12. Banyay, M., Sarkar, M. & Graslund, A. A library of IR bands of nucleic acids in solution. *Biophys. Chem.* **104,** 477–488 (2003).

13. Bostock-Smith, C. E., Harris, S. A., Laughton, C. A. & Searle, M. A. Induced fit DNA recognition by a minor groove binding analogue of Hoechst 33258: fluctuations in DNA A tract structure investigated by NMR and molecular dynamics simulations. *Nucleic Acids Res.* **29,** 693–702 (2001).

14. Mittag, T., Kay, L. E. & Forman-Kaya, J. D. Protein dynamics and conformational disorder in molecular recognition. *J. Mol. Recognit.* **23,** 105–116 (2010).

15. Eaves, J. D. *et al.* Hydrogen bonds in liquid water are broken only fleetingly. *Proc.*

Natl. Acad. Sci. U. S. A. **102,** 13019–13022 (2005).

16. Kraemer, D. *et al.* Temperature dependence of the two-dimensional infrared spectrum of liquid H2O. *Proc. Natl. Acad. Sci. U. S. A.* **105,** 437–442 (2008).

17. Ishikawa, H. *et al.* Neuroglobin dynamics observed with ultrafast 2D-IR vibrational echo spectroscopy. *Proc. Natl. Acad. Sci. U. S. A.* **104,** 16116–16121 (2007).

18. Bredenbeck, J. & Hamm, P. Peptide structure determination by two-dimensional infrared spectroscopy in the presence of homogeneous and inhomogeneous broadening. *J. Chem. Phys.* **119,** 1569–1578 (2003).

19. Ghosh, A., Ostrander, J. S. & Zanni, M. T. Watching Proteins Wiggle: Mapping Structures with Two-Dimensional Infrared Spectroscopy. *Chem. Rev.* **117,** 10726–10759 (2017).

20. Chung, J. K., Thielges, M. C. & Fayer, M. D. Conformational dynamics and stability of HP35 studied with 2D IR vibrational echoes. *J. Am. Chem. Soc.* **134,** 12118–12124 (2012).

21. Sanstead, P. J., Stevenson, P. & Tokmakoff, A. Sequence-Dependent Mechanism of DNA Oligonucleotide Dehybridization Resolved through Infrared Spectroscopy. *J. Am. Chem. Soc.* **138,** 11792–11801 (2016).

22. Greetham, G. M. *et al.* ULTRA laser system: a new dual-output 10 kHz Ti:Sapphire amplifier with UV–IR generation for time-resolved spectroscopy. *Cent. Laser Facil. Annu. Rep.* 249–250 (2008).

23. Greetham, G. M. *et al.* ULTRA : A Unique Instrument for Time-Resolved Spectroscopy. *Appl. Spectrosc.* **64,** 1311–1319 (2010).

24. Bro, R. & Smilde, A. K. Principal component analysis. *Anal. Methods* **6,** 2812–2831 (2014).

25. Hamm, P. & Zanni, M. T. *Concepts and Methods of 2D Infrared Spectroscopy*. (Cambridge University Press: Cambridge, 2011).

26. Hunt, N. T. 2D-IR spectroscopy: ultrafast insights into biomolecule structure and function. *Chem. Soc. Rev.* **38,** 1837–1848 (2009).

27. Adamczyk, K. *et al.* Measuring protein dynamics with ultrafast two-dimensional infrared spectroscopy. *Meas. Sci. Technol.* **23,** 62001 (2012).

28. Finkelstein, I. J. *et al.* Ultrafast dynamics of myoglobin without the distal histidine: Stimulated vibrational echo experiments and molecular dynamics simulations. *J. Phys. Chem. B* **109,** 16959–16966 (2005).

29. Simpson, N. *et al.* The effect on structural and solvent water molecules of substrate binding to ferric horseradish peroxidase. *Faraday Discuss.* **177,** 163–179 (2015).

30. Chung, J. K., Thielges, M. C. & Fayer, M. D. Dynamics of the folded and unfolded villin headpiece (HP35) measured with ultrafast 2D IR vibrational echo spectroscopy. *Proc. Natl. Acad. Sci. U. S. A.* **108,** 3578–3583 (2011).

31. Kwak, K., Park, S., Finkelstein, I. J. & Fayer, M. D. Frequency-frequency correlation functions and apodization in two-dimensional infrared vibrational echo spectroscopy: A new approach. *J. Chem. Phys.* **127,** 124503 (2007).

32. Kwac, K. & Cho, M. Molecular dynamics simulation study of N-methylacetamide in water. II. Two-dimensional infrared pump-probe spectra. *J. Chem. Phys.* **119,** 2256–2263 (2003).

33. Ghosh, A. & Hochstrasser, R. M. A peptide's perspective of water dynamics. *Chem. Phys.* **390,** 1–13 (2011).

34. Adamczyk, K. *et al.* The effect of point mutation on the equilibrium structural fluctuations of ferric Myoglobin. *Phys. Chem. Chem. Phys.* **14,** 7411–7419 (2012).

35. Guo, Q., Pagano, P., Li, Y.-L., Kohen, A. & Cheatum, C. M. Line shape analysis of two-dimensional infrared spectra. *J. Chem. Phys.* **142,** 212427 (2015).

36. Greve, C. *et al.* N-H stretching excitations in adenosine-thymidine base pairs in solution: Pair geometries, infrared line shapes, and ultrafast vibrational dynamics. *J. Phys. Chem. A* **117,** 594–606 (2013).

37. Park, S., Kwak, K. & Fayer, M. D. Ultrafast 2D-IR vibrational echo spectroscopy: A probe of molecular dynamics. *Laser Phys. Lett.* **4,** 704–718 (2007).

38. Siebert, T., Guchhait, B., Liu, Y., Costard, R. & Elsaesser, T. Anharmonic Backbone

Vibrations in Ultrafast Processes at the DNA–Water Interface. *J. Phys. Chem. B* **119,** 9670–9677 (2015).

39. Haq, I. Thermodynamics of drug-DNA interactions. *Arch. Biochem. Biophys.* **403,** 1–15 (2002).

40. Drew, H. R. & Dickerson, R. E. Structure of a B-DNA Dodecamer 3. Geometry of Hydration. *J. Mol. Biol.* **151,** 535–556 (1981).

41. Kopka, M. L., Fratini, A. V, Drew, H. R. & Dickerson, R. E. Ordered water structure around a B-DNA dodecamer: A quantitative study. *J. Mol. Biol.* **163,** 129–146 (1983).

42. Thielges, M. C., Chung, J. K. & Fayer, M. D. Protein dynamics in cytochrome P450 molecular recognition and substrate specificity using 2D IR vibrational echo spectroscopy. *J. Am. Chem. Soc.* **133,** 3995–4004 (2011).

43. Feng, C.-J. & Tokmakoff, A. The dynamics of peptide-water interactions in dialanine: An ultrafast amide I 2D IR and computational spectroscopy study. *J. Chem. Phys.* **147,** 85101 (2017).

44. Guckian, K. M. *et al.* Factors contributing to aromatic stacking in water: Evaluation in the context of DNA. *J. Am. Chem. Soc.* **122,** 2213–2222 (2000).

45. Greve, C. & Elsaesser, T. Ultrafast Two-Dimensional Infrared Spectroscopy of Guanine − Cytosine Base Pairs in DNA Oligomers. *J. Phys. Chem. B* **117,** 14009–14017 (2013).

4. Long-Range Vibrational Dynamics Are Directed by Watson–Crick Base Pairing in Duplex DNA

This chapter contains results published in the following publication:

Hithell, G.; Shaw, D.; Donaldson, P. M.; Greetham, G. M.; Towrie, M.; Burley, G. A.; Parker, A. W.; Hunt, N. T., *Long-Range Vibrational Dynamics Are Directed by Watson–Crick Base Pairing in Duplex DNA*, J. Phys Chem. B, **120**, 4009–4018 (2016)

4.1 Abstract

In the previous chapter, the thermal denaturation of an AT-15mer DNA sequence was studied by monitoring changes in off-diagonal coupling patterns as well as solvation dynamics using 2D-IR spectroscopy. The data presented along with literature using 2D-IR to study DNA points to significant delocalisation of the vibrational modes when part of a larger biomacromolecule. The evidence of delocalisation presents the question of how far this delocalisation extends through DNA oligomers and whether coupling or energy transfer interaction can be observed between the different components of DNA's building blocks.

In this chapter, two-colour 2D-IR spectroscopy has been used to excite the base vibrational modes of the same AT-15mer sequence used in the previous chapter and subsequently probe not only those base modes but also vibrational modes of the sugar-phosphate backbone of DNA located in a lower frequency spectral window. This allows for observation of features located in a far off-diagonal spectral region that links the two sets of vibrational modes. This allows observation of the pathways of vibrational relaxation from the excited base modes to those located on the DNA backbone. Possible mechanisms through which this relaxation is facilitated and the dependence on DNA strand conformation is discussed.

4.2 Introduction

Despite considerable efforts since the structure of the double helix was first determined in 1953,[1] questions regarding the relationship between the solution phase molecular physics of DNA and its biological function remain unanswered. For example, the manner in which disparate aspects of the DNA structure (base pairing and stacking; deoxyribose rings; phosphodiester groups) combine cooperatively to stabilize double-helical DNA or contribute to duplex unwinding in transcription and replication are not clear. These inter- and intramolecular interactions also influence the dynamic landscape of DNA, and variations in molecular dynamics with base sequence are believed to underpin fundamental biological processes such as protein−DNA interactions and the recognition of damaged DNA bases. This is manifest in the action of antisense therapeutics where the subtle interplay of backbone and base influence efficacy through control of solvation and binding strength, respectively.[2]

The dynamics of vibrational relaxation, relating to mode−mode energy migration and efficient energy dissipation, are linked to the naturally short nonradiative lifetimes of DNA excited states and may contribute to the prevention of extensive DNA damage following electronic excitation and relaxation.[3–5]Ultrafast spectroscopy has provided considerable insights into the dynamics of electronically excited DNA,[6–11] including investigations using time-resolved IR spectroscopy on adenine and thymine systems,[5,12] but the precise relaxation pathways remain to be clearly elucidated.

2D-IR spectroscopy has been used to observe ground state dynamics and has highlighted the role of delocalised phenomena particularly with regards to base vibrational modes. Studies of GC DNA sequences identified the importance of coupling across DNA base pairs versus coupling that occurs through-strand stacking interactions.[13,14] These studies encouraged computational studies of the base vibrational modes which were found to form delocalised modes across the DNA pairs on duplex formation and have been discussed at length in Chapter (3).[15–18] Delocalisation of vibrational modes have also been shown to be prominent in single DNA bases[19] and studies of the N-H stretching modes of DNA have been shown to be sensitive to vibrational coupling and indeed that they are able to relax into lower frequency base modes.[20–29]

Recently, 2D-IR studies have been carried out on the spectral region wherein features of the vibrational modes of the sugar-phosphate backbone are observed. [30,31] These studies revealed that the vibrational modes located in this region of the phosphate and phosphodiester moieties are coupled and that the primary method of energy dissipation in DNA is through the interaction of the phosphate groups with the solvent environment.

2D-IR studies have shown that coupling and delocalisation of vibrational modes applies to multiple features in different spectral regions. However, it remains unclear if this delocalisation extends to link the base modes with the sugar ring modes.[32,33] A link between the base and sugar modes would appear to have significant importance when considering a potential pathway for energy transfer through the DNA molecule.

In this study, two-colour 2D-IR spectroscopy is used to study the interaction between the base and backbone vibrational modes for both double-stranded and single-stranded DNA oligomers. The results presented here show that despite significant spatial separation, these two moieties are dynamically linked and as such a mechanism is proposed through

which energy absorbed by the bases can be dissipated through the DNA molecule into the solvent environment.

4.3 Experimental

4.3.1 Absorption Spectroscopy

The sample consisted of a 15 base pair oligomer 5'- ATTATTATTATATTA-3' and its complementary sequence (purchased from Eurofins Genomics) dissolved, without further purification, to a concentration of 10 mM in deuterated Tris buffer (100 mM, pD7.4) containing 100 mM NaCl. UV–visible and FT-IR absorption spectroscopy has been carried out on this sample as in the previous Chapter. Repetition of this step is necessary due to the change in buffer system used, changing from phosphate buffer to Tris buffer. This change of buffer system was necessitated due to the aim to observe features due to phosphate vibrations of the DNA backbone which could be complicated by the presence of phosphate ions in the buffer solution.

For all measurements, the sample was held between two CaF_2 windows separated by a 6 um spacer for UV-visible spectroscopy and 25 µm thick polytetrafluoroethylene spacer for FTIR and 2D-IR spectroscopy. Samples were housed in a thermostatically controlled mount, allowing the temperature to be varied between 293 and 353 K, accurate to ±1 K. UV-Vis spectra were recorded on a Win Cary Lambda 25 UV-Vis spectrometer with a resolution of 1nm. FTIR spectra were recorded on a Bruker Vertex 70 FTIR spectrometer and acquired with a resolution of 1 cm^{-1}.

4.3.2 2D-IR Spectroscopy

Fourier-transform ultrafast 2D-IR spectra were obtained using the pump–probe geometry method[34,35] with the LIFEtime spectrometer[36] as described in Chapter 2. The dual probe OPA system allowed for simultaneous probing of two different spectral regions while the increased repetition rate of the laser compared to the UTLRA laser system allowed for much faster data acquisition without sacrificing signal to noise quality. OPA1 provided the 2D-IR excitation pulses centred near 1650 cm^{-1}, resonant with the base carbonyl/ring stretching modes. OPA2 provided probe pulses also centred on these base modes (1650 cm^{-1}) for single-color "base" 2D-IR experiments while OPA3 was used in two-colour

"backbone" 2D-IR experiments to probe the phosphate backbone region of the spectrum near 1070 cm^{-1}. The probe pulse durations produced by the OPAs were ~200 fs while the pump pulse duration was ~300 fs, which limits the experimental time resolution. 2D-IR signals were measured using phase cycling, and 2D-IR data sets were obtained by scanning τ for a fixed waiting time. Spectra were obtained by Fourier transform along τ. Data were collected in both ZZZZ and ZZYY polarisation geometries though all data shown in this chapter is from ZZYY as this data offered the better signal to noise quality.

4.4 Results

4.4.1 Absorption Spectroscopy

As in the previous chapter, understanding the melting behaviour of the AT-15mer is required for this study. As the buffer system used for these experiments differs to those in Chapter 3, then this step must be repeated in order to confirm the temperatures at which the DNA sample can be considered to be either double (ds-) or single-stranded (ss-). Once again UV-Visible absorption spectroscopy has been used to extract the melting temperature of the AT-15mer DNA sequence in Tris buffer via measurement of the increase in intensity of the absorption band at 260 nm that accompanies unstacking of the bases as the double helix is denatured. The change in absorbance observed at a wavelength of 260 nm has been normalised and shown in Figure 4.1 below.

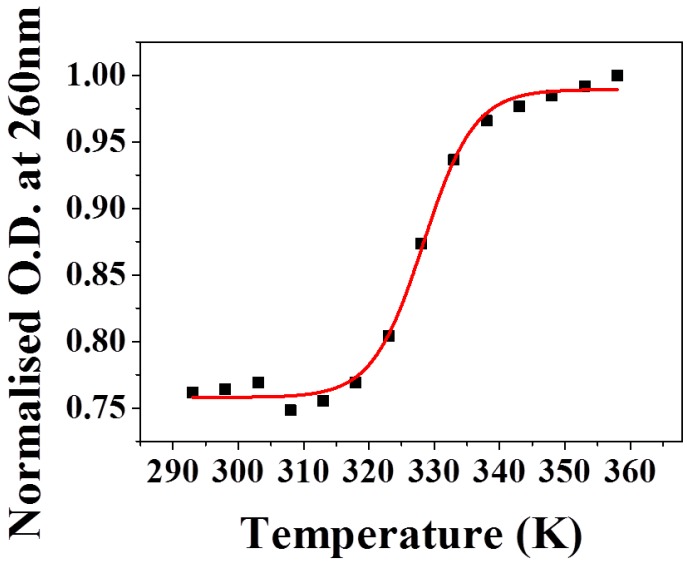

Figure 4.1 *– Melting curve of AT 15mer DNA sequence derived from UV-Visible spectroscopy as a function of temperature from 293 K to 353 K. Black squares represent measurements of absorbance at 260nm by DNA duplex; red line represents Boltzmann sigmoidal fit used to extract melting temperature ™ for the sequence.*

Fitting the normalised absorbance as a function of temperature with a Boltmann sigmoid function as in the previous chapter allows extraction of a value for the T_m taken as the midpoint of the transition in the sigmoid. A T_m value of 328 ± 2 K was extracted from the data. This value is slightly higher than observed in the Chapter 3.4.1 (318 ± 2 K) and is attributed to the use of an alternative buffer solution. The experiments in this Chapter are performed using a Tris buffer instead of the phosphate buffer used in Chapter 3. This was to avoid convolution of the absorption bands due to the phosphate groups in the DNA with phosphate ions in solution. From the UV-vis data it can be observed that at 293 K the DNA is in the ds- conformation while at 353 K the DNA has completely denatured into its component single strand.

FTIR spectra in the base vibration region, explored in the previous chapter, recorded for between 293 and 353 K are shown in Figure 4.2a) below.

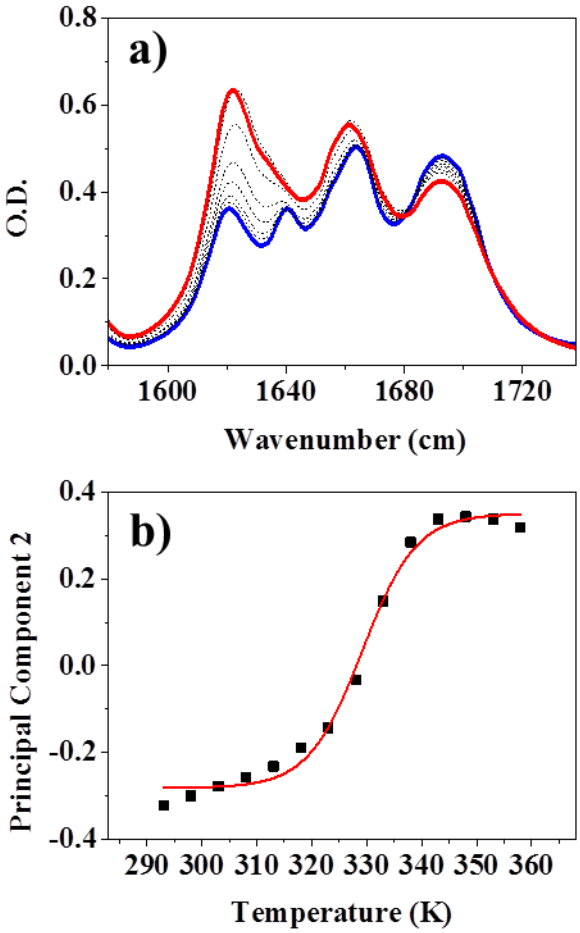

Figure 4.2 *– a) FTIR spectra in the base region recorded for the AT 15mer DNA sequence recorded at a range of temperatures between 293 K (blue trace) and 353 K (red trace). b) PCA results, principal component 2 plotted as a function of temperature and fitted with a Boltzmann sigmoid to extract a value of the* T_m.

Upon melting of the DNA duplex, the FTIR spectral features for the AT-15mer sequence displays similar behaviour as in Chapter 3.4.1. At low temperature, the same four absorption bands previously observed for the sample are observed in the 1600-1700 cm^{-1} spectral window. Features are found at frequencies 1622, 1643, 1666 and 1693 cm^{-1} and these are once again assigned to the $A_{R1}T$, AT_R, AT_{4S} and AT_{2S} modes respectively.

Upon heating of the sample the double helix is thermally denatured and induces changes in the spectrum that are in agreement with those observed in the previous chapter. There is a decrease in amplitude of the T_{2S} mode while the amplitude of the A_{R1} and T_{4S} modes increases upon melting. There is also a shift of the T_R mode to lower frequency such that it

appears as a shoulder on the high frequency side of the A_{R1} absorption band. Melting of the DNA duplex was quantified as in Chapter 3.4.1 using principal component analysis (PCA). Principal component 2 (PC2) contains information on the variance in the spectrum upon heating and the relative amount of PC2 added to PC1, which is essentially an average of the spectra recorded, to reconstruct each spectrum at each temperature. PC2 is plotted as a function of temperature in Figure 4.2b), fitting this plot with a Boltzmann sigmoid allows extraction of the melting temperature. A melting temperature of 329 ± 2 K was extracted from the data which is in good agreement with that yielded from the UV-Vis data.

For the two-colour 2D-IR experiments performed in this study, both the base and backbone regions must be considered. Melting of the DNA double helix induces a number of changes in the backbone absorption bands in the FTIR spectra that occur in the 1020-1150 cm^{-1} region, these are shown in Figure 4.3a).

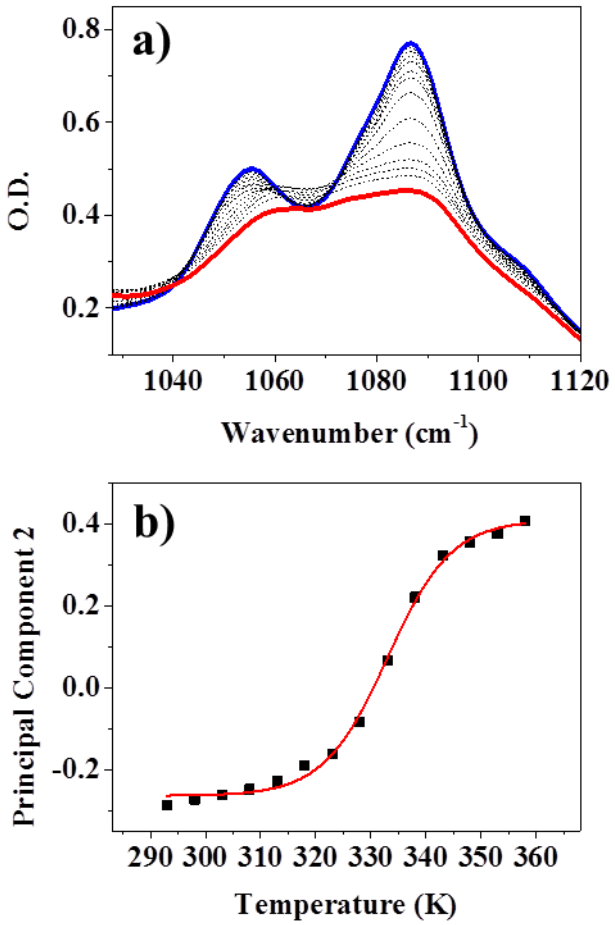

Figure 4.3 *– a) FTIR spectra in the backbone region recorded for the AT 15mer DNA sequence recorded at a range of temperatures between 293 K (blue trace) and 353 K (red trace). b) PCA results, principal component 2 plotted as a function of temperature and fitted with a Boltzmann sigmoid to extract a value of the* T_m.

At low temperature (293 K) in Figure 4.3a), three bands are observed. These have been previously assigned to the symmetric stretch of the phosphate group (P_2) found at 1086 cm^{-1} and two modes of the phosphodiester linkages assigned L_1 and L_2, found at frequencies 1075 cm^{-1} and 1055 cm^{-1} respectively[30] and these assignments are used to identify the features in the spectra presented here. A further mode of the DNA backbone, the asymmetric stretch of the phosphate group (P_1) is typically found at a slightly higher frequency of 1230 cm^{-1} however in the samples measured this feature is obscured by a large D_2O solvent absorption band. An additional low intensity feature is observed at a frequency if 1105 cm^{-1} which is assigned to a vibrational mode of the deoxyribose ring.[32,37]

Upon heating of the sample, a marked reduction in the intensity of the P_2 band is observed, this is also accompanied by a slight drop in amplitude and a blue-shift of the L_2 mode to a slightly higher frequency. The changes in this spectral region were also quantified in the same manner as the base region using PCA (Figure 4.3b). A plot of PC2 versus temperature again allows extraction of the T_m by fitting with a Boltzmann sigmoid. A T_m value of 333 ± 2 K was found for the changes in this spectral region. This compares well with that extracted from the base region albeit when the relative error in each value is taken into account.

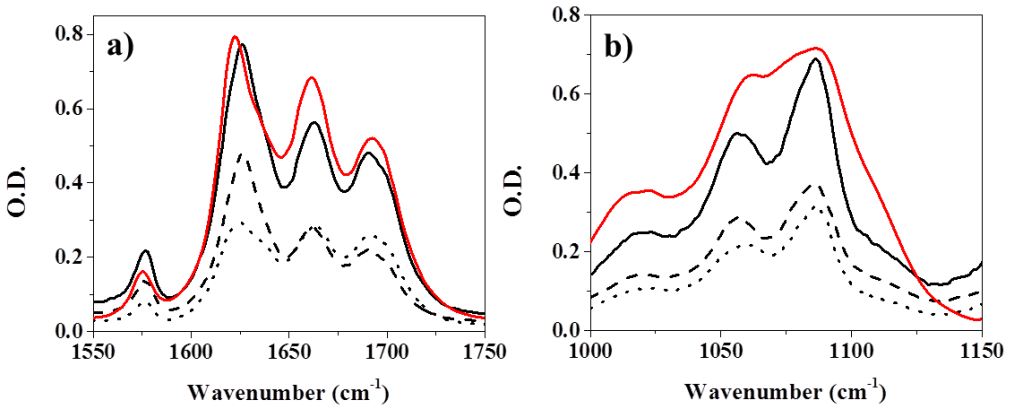

Figure 4.4 *– Comparisons of the base (a) and backbone (b) regions of the FT-IR spectra of the two component ss-DNA strands Oligomer 1 (sequence –* 5'-ATTATTATTATATTA-3') *(dotted) and Oligomer 2 (sequence -* 5'-TAATATAATAATAAT-3') *(dashed) alongside the sum of these spectra (solid black line) and the melted duplex (red) spectra.*

In order to ensure that studying of the melted DNA duplex at 353 K is an adequate method for studying ss-DNA dynamics, the individual single strands have been measured at low temperature in order to compare with the melted duplex spectrum. Figure 4.4 shows the comparison of the FTIR spectra of the component single strands that make up the DNA duplex (dashed and dotted lines). Summation of the two component single strand spectra (black trace) at low temperature is compared to the spectrum of the melted duplex (red) in both the base and backbone regions. In both cases the sum of spectra of the individual strands compares well with the melted duplex spectrum, apart from the effects of some broadening of the modes in the backbone spectra that occurs in the melted duplex spectrum at high temperatures.

4.4.2 Base Region 2D-IR Spectroscopy

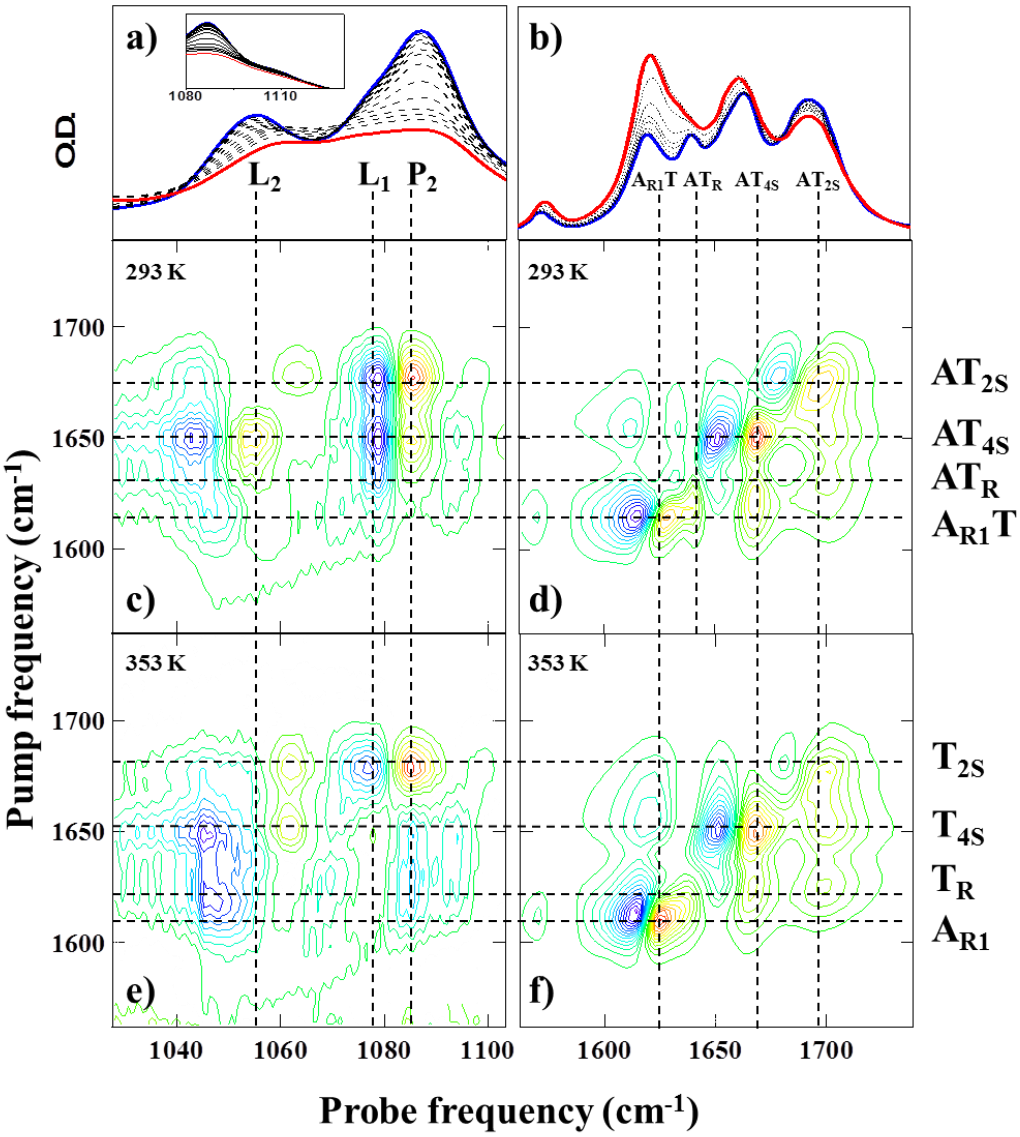

Figure 4.5 *- (a) IR absorption spectra of AT 15-mer in the backbone stretching region of the spectrum at a range of temperatures from 239 K (blue) to 353 K (red). (b) IR absorption spectra showing vibrational modes of the bases as a function of temperature. (c–f) 2D- IR spectra showing results of one-colour (d, f) and two-colour (c, e) experiments at 293 K (c, d) and 353 K (e, f). Colour scale of the 2D-IR spectra runs from red (negative) to blue (positive).*

Representative spectra measured by one colour (base region) and two-colour (backbone region) 2D-IR spectra are shown in Figure 4.5 accompanied by linear FTIR spectra linking the features in the 2D spectra to the vibrational modes found in the linear spectra. Figure 4.5d) shows the 2D-IR spectrum recorded for the sample at 293 K at a waiting time of 250 fs. This

is comparable to the parameters used when acquiring the same spectrum on the ULTRA laser system in the previous chapter. Features observed in this spectrum compare well with those seen in the ULTRA data. Four pairs of peaks are found along the spectrum diagonal. Red features for the v=0-1 transition of each of the four vibrational modes in the linear spectrum. Each of this is accompanied by a blue feature corresponding to the v=1-2 transition of each of these modes, shifted to a lower probe frequency by the diagonal anharmonicity of the mode. As in the previous chapter a number of off-diagonal features are observed indicating that there modes in this region are coupled to one another.

Figure 4.5f) shows the base region spectrum acquired at an elevated temperature of 353 K where the DNA duplex has melted into its constituent single strands. Changes in the spectrum upon melting of the double helix also compared favourably with those observed in the previous chapter. There is a drop in intensity of the T_{2S} diagonal features accompanied by a concurrent increase in amplitude of the A_{R1} diagonal features. The T_R mode shifts to lower frequency and finally coupling between the A_{R1} mode and each of the thymine base modes are lost upon denaturation of the duplex.

2D-IR spectra were recorded at a series of waiting times at both low and high temperatures. This allowed for the extraction of vibrational relaxation times by fitting the diagonal features to Gaussian lineshapes (Figure 4.6a). Amplitudes of the fitted Gaussians were plotted as a function of waiting time and the result could be well represented by fitting with a single exponential decay function (Figure 4.6b). The decay constant used to fit the amplitude as a function of waiting time is taken to be the vibrational relaxation time (T_1). Vibrational relaxation times extracted from the fits are listed in Table 4.1.

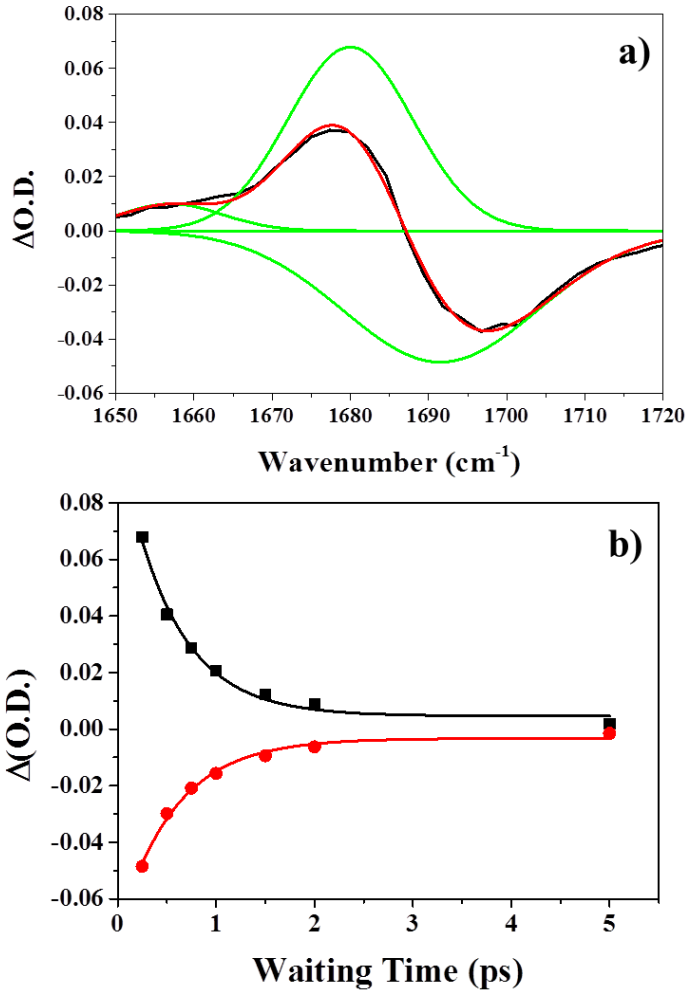

Figure 4.6 *– a) Example of fitting Gaussian lineshapes to pump slices of 2D-IR spectrum to extract vibrational relaxation kinetics. Gaussian lineshapes (green traces) are added together (red trace) to model the experimental data (black trace). b) Kinetics extracted from Gaussian fitting, timescales extracted via fitting of single exponential decay.*

T (K)	Excited Mode	T_1 (fs)
293	AT_{2S}	550
	AT_{4S}	850
	AT_R	900
	$A_{R1}T$	850
353	T_{2S}	700
	T_{4S}	850
	T_R	-
	A_{R1}	800

Table 4.1 *– Results of fitting to extract vibrational relaxation times of diagonal modes in AT-15mer 2D-IR spectra.*

The v=0-1 and v=1-2 features showed consistent temporal behaviour and compare favourably with vibrational lifetimes measured on the ULTRA laser system in the previous chapter.

4.4.3 Backbone Region 2D-IR Spectroscopy

The dual-probe OPA system of LIFEtime allowed for simultaneous measurement of 'two-colour' 2D-IR spectra of the backbone region along with the base region spectra. Figure 4.5c) shows the off-diagonal spectrum for the AT 15mer sequence under double stranded conditions. In this spectrum, features linking each of the four base modes with the P_2 mode of the phosphate group and the phosphodiester L_2 mode are observed. Data were recorded under both parallel (ZZZZ) and perpendicular (ZZYY) conditions. Changes in amplitude but not peak positions were observed between the two polarisation geometries. ZZYY offered the best signal to noise ratio between the two data sets and as such it is only ZZYY data that is presented and discussed here.

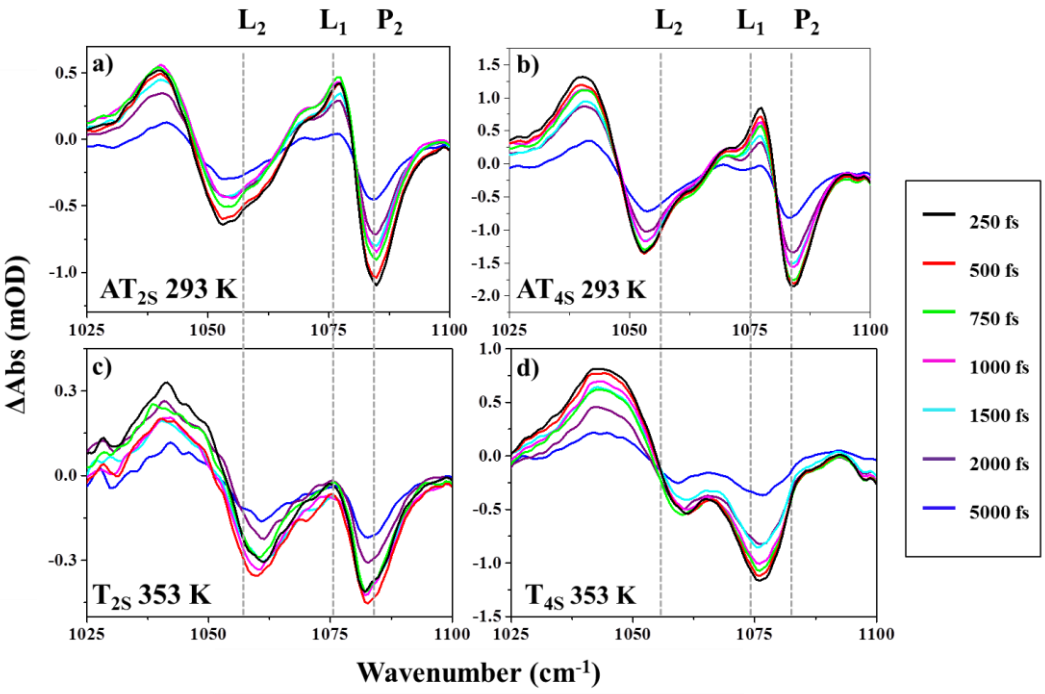

***Figure 4.7** – Slices taken through backbone off-diagonal 2D-IR spectra at a series of waiting times.*

Figure 4.7 shows a series of cross sections taken through 2D-IR at both low and high temperatures. Gaussian lineshapes were fitted to the cross sections in order to extract dynamic information from the off-diagonal spectra. Cross sections were well represented

by fitting Gaussians that linked the base modes to not only the P_2 and L_2 modes but also the L_1 phosphodiester mode. However with the exception of slices at a pump frequency concurrent with AT_{2S} mode, the L_1 peaks are largely obscured by the much larger L_2 and P_2 features. An example of fitting the 2D-IR slices is shown in Figure 4.8 below.

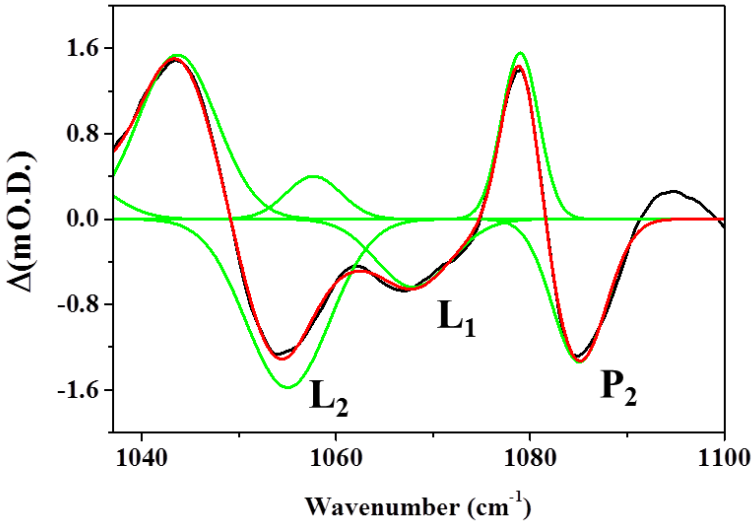

Figure 4.8 *– Example of fitting peaks in backbone 2D-IR spectra to Gaussian lineshape functions (green) to extract dynamic information. The sum of the fitted Gaussian lineshapes is indicated in red. Black line indicates experimental data obtained at an excitation frequency matching the AT_{4S} mode in the ds-DNA sample with a waiting time of 0 fs.*

Temporal dynamics of the backbone modes are yielded from the fitting of the slices. Peaks were found to be present from the earliest waiting times recorded. The off-diagonal features linking the L_2 mode to the base modes all displayed an initial rise in amplitude. The timescale of this rise (τ_r) was found to be mode dependent. Rise times of the order 650 ± 100 fs were found at excitation frequencies corresponding to the AT_R and $A_{R1}T$ modes while the of the τ_r of the AT_{4S}-L_2 mode was found to be noticeably longer. Following the initial increase in these features, the amplitudes decayed on a long timescale that was not easily defined by the timescale of the experiments performed but appear to be on the order of around 10 ps. Extraction of dynamic information from L_1 features proved to be difficult due to the congestion in this spectral region. 2D-IR spectra of the ds-DNA sequence recorded at a series of waiting times is shown in Figure 4.9 and dynamic parameters extracted from both ds- and ss-DNA are listed in Table 4.2.

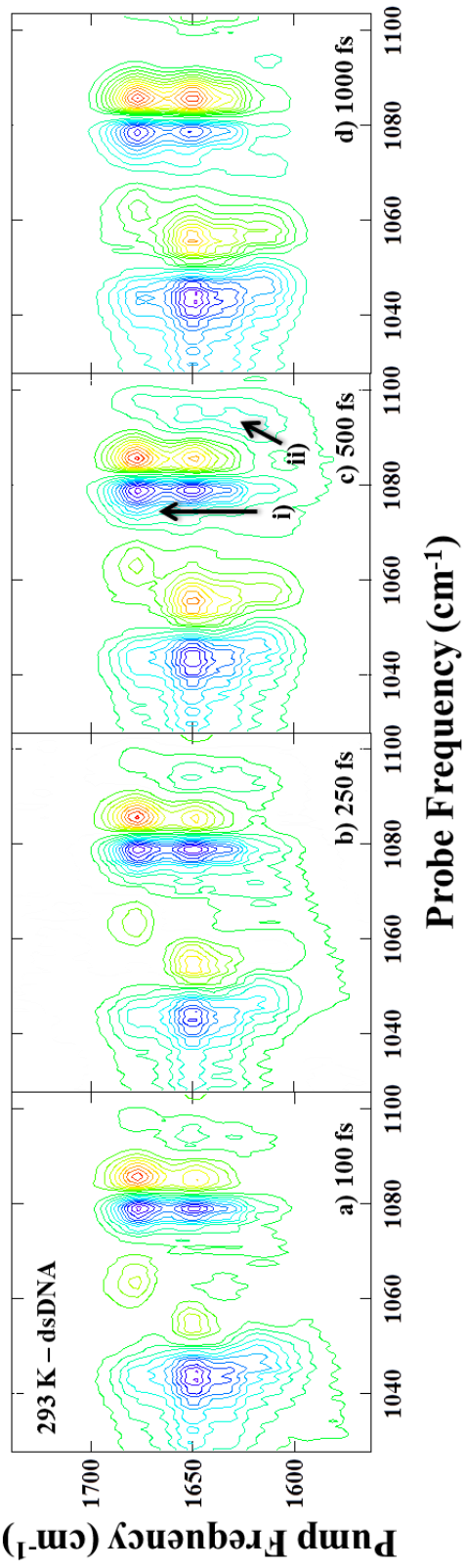

Figure 4.9 *– Backbone 2D-IR spectra obtained at a range of waiting times for the ds-DNA sample at 293 K.*

Temperature (K)	Excited Mode	T_1 (fs)	τ_r (fs)	
			P_2	L_2
293	AT_{2S}	550	700	-
	AT_{4S}	850	700	1550
	AT_R	900	750	700
	$A_{R1}T$	850	1900	600
353	T_{2S}	700	350	-
	T_{4S}	850	-	600
	T_R	-	-	700
	A_{R1}	800	-	-

Table 4.2 *– Results of fitting to extract dynamic timescales from 2D-IR spectra.*

The temporal dynamics of the off-diagonal features between the base modes and the P_2 mode were found to be more complex than the other features measured. The shape of these off-diagonal features was observed to evolve over time. An example of this is shown in Figure 4.10a), depicting a slices through the P_2 mode at a pump frequency corresponding to the AT_{4S} base mode at a series of waiting times. This figure is representative of all the P_2 off-diagonal features. The negative feature in Figure 4.10a), highlighted with the blue arrow, displays dynamics similar to that observed for the L_2 modes. A rise time of 700 ± 150 fs is observed for the majority of these features. The corresponding positive feature is more complex, containing two components. At early waiting times, a narrow feature found at a frequency corresponding to a peak separation of positive and negative components of 5 cm^{-1} (red arrow Figure 4.10a) is the predominant feature observed. As the waiting time is increased, the amplitude of this narrow features decays and a broader feature grows into the spectrum (black arrow Figure 4.10a) centred at a frequency corresponding to a peak separation of positive and negative components of 12-15 cm^{-1} with respect to the negative feature. This effect is most prevalent when comparing slices at the earliest waiting time (0 fs) and latest waiting time (1500 fs) but the effect can also be observed in the 2D-IR spectra (labelled ‘i’ in Figure 4.9).

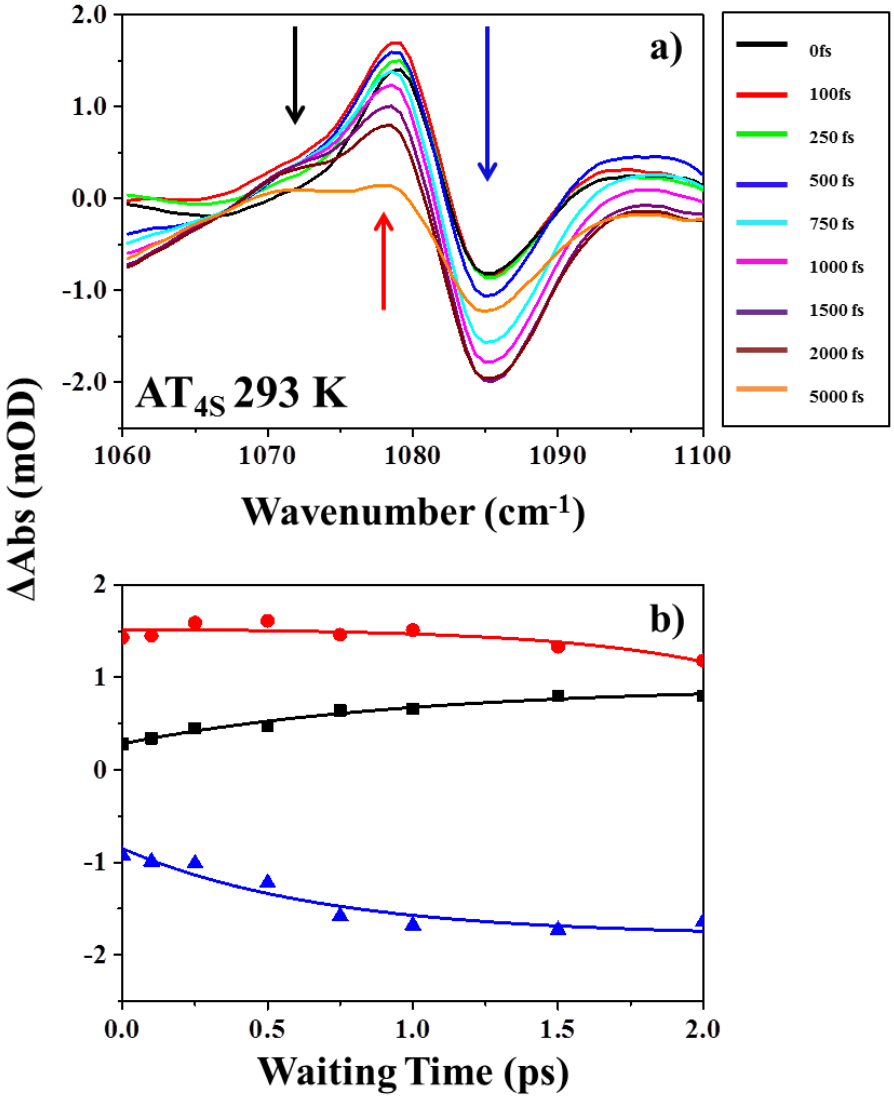

Figure 4.10 *– (a) Slices through two-colour 2D-IR spectra as a function of waiting time showing the peak shape evolution of the off-diagonal peaks to the P2 mode. (b) shows the early time dynamics of the three components identified by arrows in a).*

The early time dynamics extracted from the fitting of the data is shown in Figure 4.10b). Two time scales were observed for the P_2 off-diagonal features. The negative (blue) and broad positive feature (black) features typically shared a 700 ± 150 fs rise time while the narrow positive feature (red arrow) displayed a very slight initial increase; however, placing a timescale for this is not possible as it lies well within the pulse duration used in the experiments. As such it is only reasonable to state that the feature is present at the earliest measured waiting times. All P_2 features then exhibit a long decay similar to the L_2 off-diagonals.

At the high frequency edge of the 2D-IR spectra at a probe frequency just above 1090 cm^{-1}, another positive feature is observed (labelled 'ii' in Figure 4.9), although it is noted that this feature is partially obscured by the larger P_2 off-diagonals. This feature exhibited temporal dynamics that reached maximum amplitude at around 500 fs and had decayed by 1500 fs.

Denaturing the DNA duplex by heating the sample to 353 K resulted in a number of changes in the spectroscopy observed in the backbone region. This indicates that there has been a significant change in the fundamental nature of the base-backbone interaction. Spectra recorded for the melted DNA strands at 353 K are shown in Figure 4.11 for a series of waiting times. In all ss-DNA off-diagonal spectra, features linking each of the base modes to the L_2 backbone mode are still visible. However a large change is observed in the P_2 off-diagonal features as all but those that link the P_2 mode to the T_{2S} base mode are no longer present. As a consequence of this, features that link the base modes to L_1 modes become clearer. The changes are more obvious when looking at cross-sectional slices through the data at pump frequencies corresponding to the T_{2S} and T_{4S} modes (Figure 4.7c, d). Figure 4.7c) shows a clear feature linking the T_{2S} and P_2 modes while Figure 4.7d) shows a shift in the highest frequency negative features from a detection frequency corresponding to the P_2 mode, to a lower frequency in line with the L_1 mode centre frequency.

Temporal dynamics of the off-diagonal features in ss-DNA are also observable in the spectra shown in Figure 4.11. As in the 293 K spectra, all features were found to be present at the earliest waiting times, albeit some of these at low intensities (Figure 4.11a). For L_2 off-diagonal features (labelled 'i' in Figure 4.11), dynamics extracted in the same manner as the low temperature spectra were similar to those observed for ds-DNA. This consisted of an increase in amplitude on a timescale of ~650 fs followed by a long decay on the order of ~10ps.

Dynamics of the remaining P_2 off-diagonal features (labelled 'ii' in Figure 4.11) were notably different in ss-DNA compared to those observed in ds-DNA. Evolution of the peak shape in the positive features observed in the ds-DNA spectra is no longer present in the ss-DNA data (Figure 4.7c) and dynamics for these features behaved similarly to the L_2 off-diagonals with an initial rise in amplitude followed by a long decay. The rise time for the P_2 feature in ss-DNA was slightly faster than the other features with a rise time of 350 fs extracted from the data.

As in the ds-DNA spectra, extracting reliable dynamics for the L_1 off-diagonals proved difficult due to overlapping of neighbouring peaks. In addition, the positive feature observed near 1090 cm^{-1} in the ds-DNA data is also present in the ss-DNA spectra (labelled 'iii' in Figure 4.11). Dynamics for this feature are in good agreement with the low temperature data displaying a fast rise in amplitude that peaked around 500 fs and had decayed almost entirely by 1500 fs.

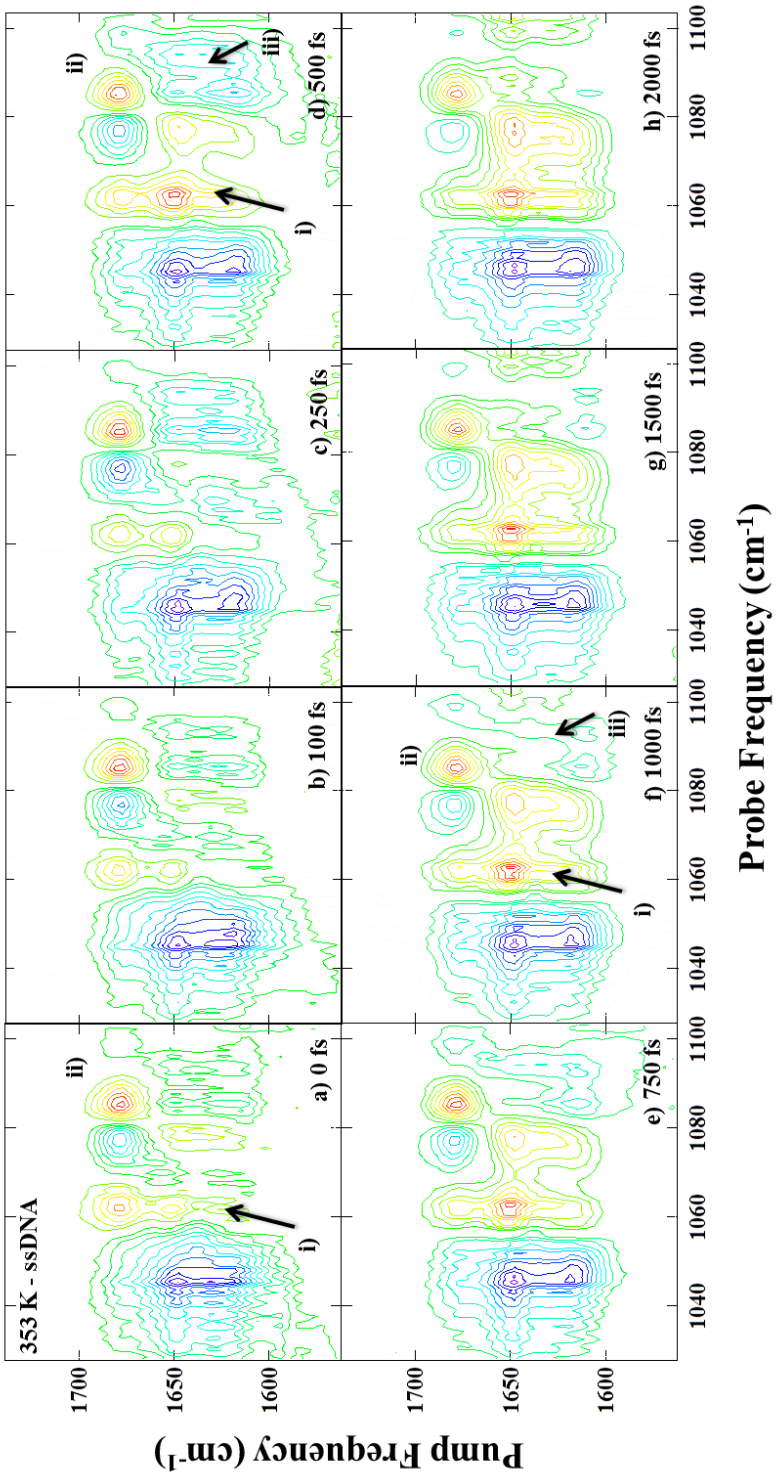

Figure 4.11 *– Two-colour 2D-IR spectra as a function of waiting time obtained for the ss-DNA sample at 353 K.*

4.5 Discussion

Three main points of discussion have arisen from the results presented in this chapter. Firstly the assignment of off-diagonal features in the backbone 2D-IR spectra which appear to be sensitive to DNA oligomer conformation. Secondly, comparison of dynamics observed between the ds-DNA and ss-DNA spectra. Finally, the differences in the dynamic behaviour observed for the off-diagonal features to the P_2 mode under both ds- and ss- DNA conditions.

4.5.1 Off-diagonal Peak Assignments: Coupling

As discussed in the previous chapter, off-diagonal features in 2D-IR spectra can have one of three possible origins.[38] As before, elimination of chemical exchange leaves two-possibilities for the origins of the backbone off-diagonal features: coupling of the base modes with the backbone modes and/or energy transfer.

In the case where off-diagonal features arise from vibrational coupling, one would expect to observe features from the earliest waiting times as the influence of one mode oscillating on a coupled mode is near-instantaneous. Further to this, the separation of the v=0-1 and v=1-2 features would be characterised by the off-diagonal anharmhonicity of the coupled modes (Δ_{ij}, the shift in energy of the combination band relative to the sum of the energies of the two v=0-1 transitions).[39] For weak couplings, this results in an amplitude reduction of the two components of opposing sign which are overlapping. In terms of temporal dynamics, off-diagonal features that result from coupling would be expected to decay with the lifetime of the excited mode. For off-diagonal features that arise from energy transfer, the off-diagonal anharmonicity reflects the diagonal anharmonicty of the mode that is the recipient of the energy transfer. Amplitudes of off-diagonal features of this nature typically follow a rise and decay profile associated with a relaxation pathway.[40]

Off-diagonal features observed in the backbone 2D-IR spectra presented in this chapter (Figures 4.5, 4.9 and 4.11) are present from the earliest waiting times. This tempts an assignment of these features to vibrational coupling. However the amplitude of these features display an amplitude <5% of the corresponding diagonal features, despite similar transition dipole strengths, suggesting that this effect is likely to be very weak ($\Delta_{ij} \leq 1$ cm^{-1}). Furthermore, the off-diagonal features observed decay over a much longer timescale than

the relaxation time of the DNA base modes (~750 fs). Vibrational coupling also reduces sharply with distance between oscillators and frequency separation between modes. As such direct coupling between the base and backbone modes seems unlikely without a large delocalised vibrational mode structure or spatial proximity of the base and backbone moieties.[40] It is also plausible that the fast relaxation of the base modes and the 300 fs duration of the pulses employed in these experiments could combine to result in small signals due to energy transfer without vibrational coupling of the modes.

The data presented in this chapter provides some evidence for assigning the majority of off-diagonal features, in particular those features linking the base vibrational modes to the L_1 and L_2 modes, in the spectra to direct vibrational coupling however this is not conclusive. It may be considered that the DNA double helix may give rise to the long range effects that could enable coupling between the base and backbone modes, as is seen for the examples of carbonyl vibrations in an α-helix.[41] However, the L_1 and L_2 features persist at high temperatures where the duplex has been denatured which is not consistent with this hypothesis. Conversely, a number of changes in the P_2 off-diagonal features in the spectra measured accompany the transition from ds- to ss-DNA. This indicates that the ordered structure of ds-DNA does have a direct effect on the coupling between the base and backbone vibrational modes.

4.5.2 Off-diagonal Peak Assignments: Energy Transfer

The majority of off-diagonal features in backbone 2D-IR spectra recorded for AT DNA under both double- and single stranded conditions, with the exception of the narrow positive feature unique to the P_2 off-diagonals in ds-DNA, display temporal dynamics that rise to a maximum amplitude within 1-2 ps and subsequently decay. This behaviour suggests that an energy transfer mechanism is dominating the off-diagonal dynamics. The rise time for the majority of the off-diagonal features (~650 fs) compares well with T_1 relaxation times of the base modes, suggestive of a direct energy transfer pathway between the base and backbone modes. However the separation of v=0-1 and v=1-2 features in the 2D spectra presented here to do not exactly match diagonal anharmonicities as reported from a one-colour 2D-IR study of the DNA backbone region.[30] This observation is not consistent with a direct energy transfer mechanism. Furthermore, a mechanism of this type would require significant coupling of the vibrational modes or for the modes to be in close spatial proximity to one another which could act as a mechanism for energy conservation given

the large (~600 cm^{-1}) frequency separation of the base and backbone modes.[40] The vibrational lifetimes of the P_2, L_1 and L_2 modes have also been recently reported to be around 1200-2500 fs,[30] significantly shorter than the long decay times observed in the off-diagonal features observed in this data.

An alternative mechanism that could account for the temporal behaviour of the backbone off-diagonal features could involve an intermediate mode or modes into which the base modes initially relax via vibrational population transfer, if this intermediate is then coupled to the backbone modes this would give rise to off-diagonals with temporal dynamics in line with our experimental observations. Situations like this have been previously reported for large molecular systems using relaxation-assisted 2D-IR spectroscopy.[40,42,43] A mechanism of this sort would explain the correlation between the relaxation timescale of the base modes with the rise time of the off-diagonal features presented here without the need for a direct energy transfer mechanism. In this instance, the separation of positive and negative features in the off-diagonal region reflects the coupling of the intermediary and backbone modes, which would be expected to differ from the diagonal anharmonicity of the backbone modes. The indication here is that population transfer to the backbone modes then follows. The result of this is a slow decay time of the off-diagonal peaks as multiple energy transfer pathways through the DNA molecule extends the timescale for energy flow into the backbone modes with only the fastest of these pathways being clearly resolved in the off-diagonal peaks observed. It would be expected that the line shapes of the off-diagonal peaks would evolve over time as population transfer to the backbone modes occurs, though if diagonal and off-diagonal anhamonicites are comparable or multiple intermediate modes are involved, then this may obscure these line shape changes in the spectra.

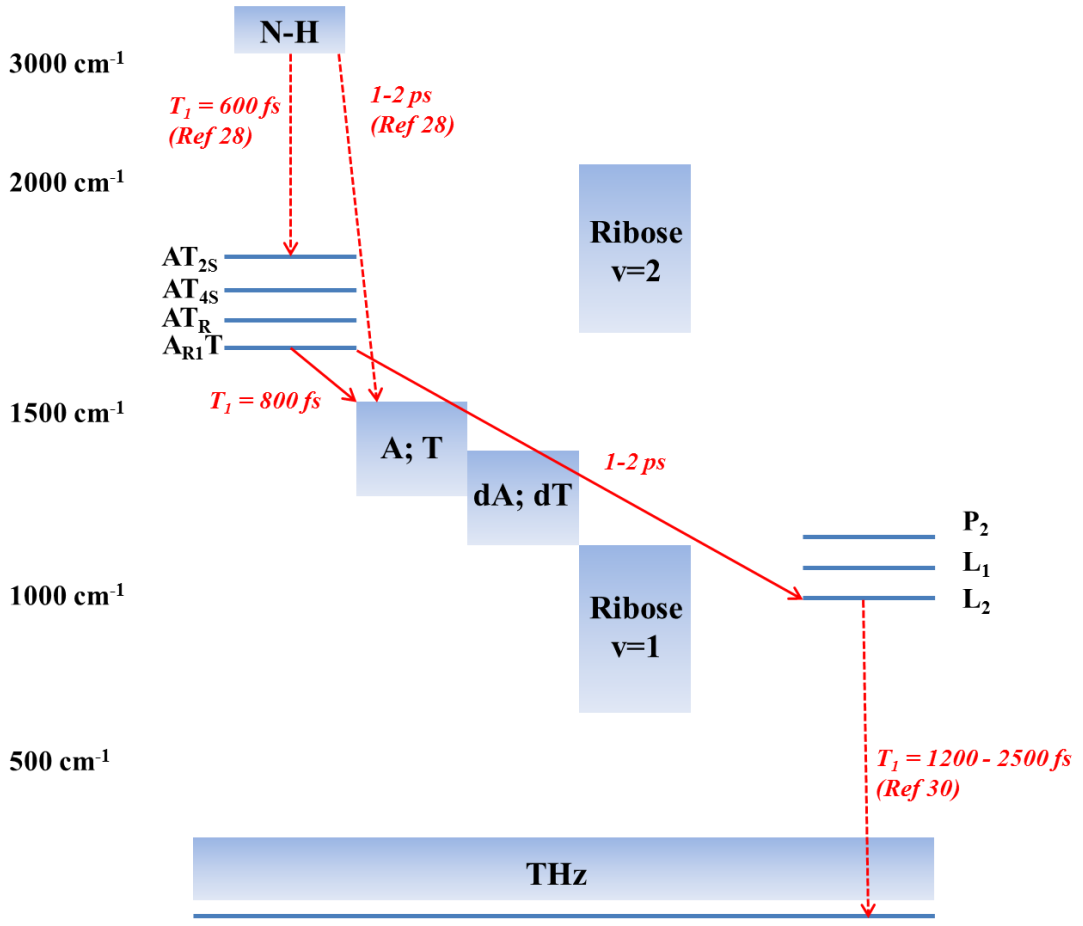

Figure 4.12 *– Schematic diagram showing relative frequencies of DNA vibrational modes. Assignments as per ref 37. Solid arrows show results from this work, and dashed arrows show results from prior publications.*

The various spectral regions that contain different vibrational modes of DNA are outlined in the schematic in Figure 4.12. There are a number of potential candidates that could act as intermediaries in the energy transfer pathway proposed that would be consistent with the temporal dynamics observed in the data, although no single route is suggested to be prominent. Structural inhomogeneity along the 15 base DNA strand may also have an influence over the observed dynamics.[37] Potential intermediate candidates include lower frequency (<1550 cm^{-1}) modes of the DNA bases and modes of the deoxyribose moiety. Coupling between low frequency and high frequency base modes has already been demonstrated[19] and coupling of base and sugar moieties has also been proposed in model systems.[32,33] It should be noted that the sugar moiety of DNA has vibrational modes that appear in the 800-900 cm^{-1} and have been described to be coupled to the phosphodiester modes.[37] The overtone (v=0-2 transition) of the sugar modes would there closely match the

frequency of the base modes and could provide an efficient route for relaxation. The previous reports of coupling of these modes to the phosphate modes also presents the sugar modes as viable candidates for an intermediary in the base-backbone energy transfer mechanism.

It is useful to consider the positive feature that appears at the high frequency edge of the off-diagonal spectra. This feature is found where the anharmonically shifted v=1-2 component of the deoxyribose mode located at 1105 cm^{-1} (labelled 'ii' in Figure 4.9 and 'iii' in Figure 4.11) would be expected. A comparison of the dynamics of this deoxyribose feature in both double and single stranded DNA with those of a neighbouring P_2 mode is shown in Figure 4.13. The fact that the deoxyribose feature peaks at earlier times than the P_2 and L_2 modes and then decays much faster is consistent with the picture of energy transfer from base to sugar and then subsequent transfer to the backbone. It also appears that the most prominent modes that link to this deoxyribose feature are the lower frequency base vibrations that are characterised by ring vibrations of the adenine and thymine bases. It would be expected that coupling between these base modes and the sugar modes would be enhanced due to the closer proximity of the two rings and a slightly smaller difference in frequency between the modes.[32,33] The temporal dynamics of this feature observed in the 2D-IR spectra help support the proposed energy transfer mechanism which allows relaxation of energy from the base modes through the sugar modes to the phosphate backbone.

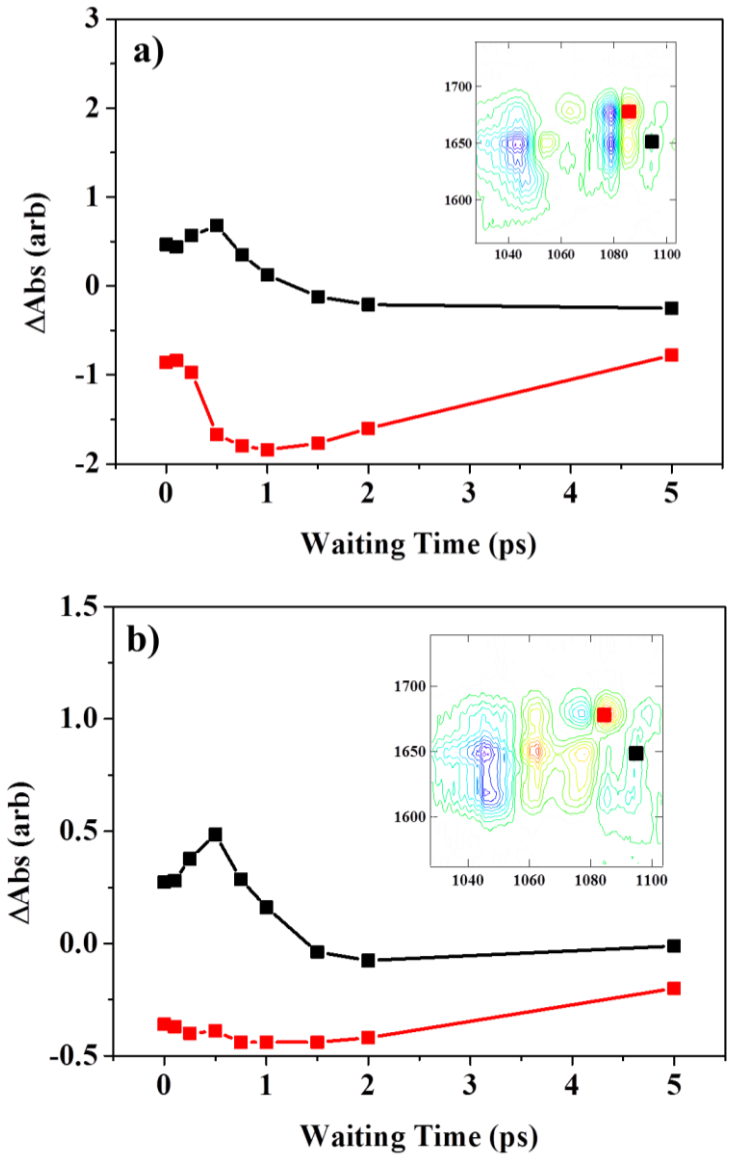

Figure 4.13 *– (a) Relative dynamics of P_2 off-diagonal feature (red) and peak assigned to v=1–2 transition of deoxyribose vibrational mode located at 1105 cm^{-1} (black) at 293 K (ds-DNA). The peak positions are marked on the 2D-IR spectra in the insets. Note the faster rise and decay of the black trace relative to the red. (b) As (a) but at 353 K (ss-DNA).*

The energy cascade model, depicted in Figure 4.12, involving energy transfer from the base through the sugar moiety is also consistent with IR pump-anti-Stokes probe studies performed on AT systems at 0% relative humidity. This study showed that N-H stretching modes relax by populating other base vibrational modes in the 1490-1660 cm^{-1} spectral region on a timescale of less than 1 ps and further to lower frequency modes around 1330 cm^{-1} on a 1-2 ps timescale which then decays over timescale of 5 ps.[28] This low frequency mode was not assigned but could be a low frequency mode of the DNA bases or indeed a

vibrational mode of the sugar moiety, either of which could be candidates as intermediate modes in the energy transfer model proposed.[37]

4.5.3 Conformation Dependence of Relaxation Dynamics

A clear conclusion from the dynamic data is that the relaxation processes in both double- and single-stranded DNA are very similar and therefore independent of DNA strand conformation.

The rise times of the L_2 mode as well as the broad features of the P_2 mode (indicated by blue and black arrows in Figure 4.10a) remain largely unchanged with DNA conformation which suggests that the dominant energy relaxation pathway is common to both ds- and ss-DNA and rules out direct involvement of a conformation-dependent pathway through solvent modes. As such it is concluded that the increase in solvent access to the bases, in particular the amino and carbonyl groups, upon melting is not a rate determining step in the overall relaxation mechanism. Overall the results presented here are in agreement with the 'downhill' transfer of energy toward the backbone of solvated DNA,[30] supporting the hypothesis that the fast energy dissipation mechanism acts to prevent damage in electronically excited DNA.

4.5.4 P_2 Off-Diagonal Dynamics

The final point of discussion arising from the data is the structure-dependent behaviour of the off-diagonal peaks that link the base modes to the P_2 mode. At low temperatures when DNA is in the double-stranded conformation, features linking each of the base modes to the P_2 mode are present while at high temperatures when DNA is single stranded only the feature linking the T_{2S} base mode to the P_2 mode is present. The features unique to ds-DNA show a complex peak-shape which evolves with waiting time, specifically a narrow component observed at short waiting times is joined by a broader, red-shifted peak at later times. This behaviour is consistent with evolution from behaviour that reflects coupling behaviour to reflecting energy transfer as the off-diagonal anharmonicity changes from smaller than the diagonal anharmonicty to comparable with the diagonal anharmonicity.[39,40] The broad positive feature of the P_2 mode (Figure 4.10 black arrow) displays dynamic behaviour consistent with the L_2 off-diagonal peaks which suggests that it is also attributable to the same energy transfer process from the base to backbone. While this broad feature has been assigned to the v=1-2 transition of the P_2 mode,[30] the

complexity of this spectral region is further highlighted by studies of the $H_2PO_4^-$ ion, which identifies a Fermi resonance with OPO bending vibration in the same spectral region.[44]

In contrast to the broad feature, the narrow component of the P_2 off-diagonal features (red arrow Figure 4.10a) displays markedly different behaviour which strongly suggests its origin lies in coupling interaction. The narrow component is present from the earliest waiting times and the smaller off-diagonal anharmonicity is consistent with coupling behaviour that arises from the formation of the DNA double helix that gives way to energy transfer features at longer waiting times. This suggests that the base modes are coupled to the phosphate group by the formation of the delocalised W-C modes, which extend over a greater spatial range than the modes of the individual DNA bases, leads to further delocalisation that facilitates interaction within the helix between the bases, sugar and backbone units. This agrees with, while significantly extending, predications of interactions between the base and deoxyribose ring vibrational modes[17,25] and points to the possibility of delocalised helix-specific modes.

In linear FTIR experiments, the P_2 mode exhibits a significant decrease in intensity upon melting of the DNA duplex (Figure 4.3a) that cannot be attributed to broadening due to increase in solvent temperature. One interpretation based on the 2D-IR results is that the loss of intensity stems from changes in the excitonic vibrational coupling of transition dipole moments as found for α-helix peptide units.[38] Computational predictions of the IR spectroscopy of B-Form AT sequences has shown that significant coupling between the T_{4S} and A_{R1} modes leads to spatially delocalised exciton states in double-stranded DNA.[18] In contrast to the α-helix case, the carbonyl modes of the W-C base pair align perpendicular to the axis of the double helix. As the P_2 transition dipole moments will align approximately parallel to the base pair axis, this would seem to favour an interaction of the base pair modes that could extend to coupling with the backbone modes. In support of this argument, the off-diagonal peak observed between the AT_{4S} mode (directly involved in W-C base pairing) and the P_2 mode is more intense than that linking to the AT_{2S} mode (not involved in base pairing) under ZZZZ (parallel) polarisation conditions. This is revered in the ZZYY (perpendicular) spectra indicating the alignment of base paired modes and phosphate modes in ds-DNA.

Overall, the indication of these observations is that a new set of couplings occurs in ds-DNA, which link the base modes and the P_2 mode of the phosphate group. This opens up a new

energy transfer pathway that did not exist in the ss-DNA sample, with the exception of the T_{2S} mode, and so augments the energy transfer process observed, particularly for the L_2 mode that is present in both ds- and ss-DNA. The differing structural arrangement of the bases, sugars, and backbone in the double helix thus opens up additional, though not apparently faster, routes for energy relaxation. This would correlate with the loss of other degrees of freedom associated with formation of the helix structure but implies that the rate-determining step is still the transfer of energy from the base modes to other, lower frequency base modes and the deoxyribose unit.

In considering the unusual behaviour of the T_{2S} mode, which retains an energy transfer interaction with the bases in ss-DNA (Figure 4.11, labelled ii), it is perhaps of relevance that this carbonyl does not engage in W–C H-bonding and, in the ds- DNA configuration, is protected from solvated water by projecting into the hydrophobic minor groove. This leads to a closer approach between the T_2 carbonyl and the phosphate backbone in the ds-DNA sample and the fact that the energy transfer process remains upon melting of the helix implies that there may be some element of this interaction, perhaps linked to persistent hydrophobic effects, that remains in the ss-DNA sample independent of the helix formation. Crucially, the aspect of the P_2 off-diagonal peaks assigned to helix-specific coupling is not seen in the ss-DNA sample.

4.6 Conclusions

For the first time, ultrafast energy transfer processes between the vibrational modes of the DNA bases and those of the phosphodiester backbone in both single- as well as double-stranded DNA have been observed using 2D-IR spectroscopy.

The results presented in this chapter show that vibrational energy dissipated from the DNA bases transfers to lower frequency modes via population relaxation, these modes inclusive of those located on the sugar moiety are in turn coupled to the phosphate backbone. The dynamics of this process has been found to be invariant upon melting of the DNA double helix, consistent with the hypothesis that the phosphate groups are the primary sink for dissipation of energy absorbed by the DNA bases to the solvent environment.

Formation of ds-DNA leads to changes in off-diagonal coupling patterns which link the base and backbone modes, specifically linking the bases to the symmetric stretch of the

phosphate moiety suggesting that the delocalisation of vibrational modes induced by W-C base pairing is extended in the double helix to the DNA backbone. The indication that these interactions are spanning the base and backbone groups raises questions of whether they are base or sequence specific and so could relate to long-range dynamic processes that play a role in recognition or excited state energy dissipation.

4.7 References

1. Watson, J. & Crick, F. Molecular structure of nucleic acids. *Nature* **171,** 737–738 (1953).

2. Krieg, A. M. *et al.* CpG Motifs in Bacterial DNA Trigger Direct B-cell Activation. *Nature* **374,** 546–549 (1995).

3. Kuimova, M. K. *et al.* Monitoring the effect of ultrafast deactivation of the electronic excited states of DNA bases and polynucleotides following 267 nm laser excitation using picosecond time-resolved infrared spectroscopy. *Chem. Commun.* 1182–1184 (2005).

4. Kuimova, M. K. *et al.* Monitoring the direct and indirect damage of DNA bases and polynucleotides by using time-resolved infrared spectroscopy. *Proc. Natl. Acad. Sci. U. S. A.* **103,** 2150–2153 (2006).

5. Towrie, M. *et al.* ps-TRIR covers all the bases – recent advances in the use of transient IR for the detection of short-lived species in nucleic acids. *Analyst* **134,** 1265–1273 (2009).

6. Middleton, C. T. *et al.* DNA Excited-State Dynamics: From Single Bases to the Double Helix. *Annu. Rev. Phys. Chem.* **60,** 217–239 (2009).

7. Schreier, W. J. *et al.* Thymine Dimerization in DNA Is an Ultrafast Photoreaction. *Science (80-.).* **315,** 625–629 (2007).

8. Perun, S., Sobolewski, A. L. & Domcke, W. Ab initio studies on the radiationless decay mechanisms of the lowest excited singlet states of 9H-adenine. *J. Am. Chem. Soc.* **127,** 6257–6265 (2005).

9. Kang, H. *et al.* Intrinsic Lifetimes of the Excited State of DNA and RNA Bases Intrinsic Lifetimes of the Excited State of DNA and RNA Bases. *J. Am. Chem. Soc.* **124,** 12958–12959 (2002).

10. Pecourt, J.-M. L., Peon, J. & Kohler, B. Ultrafast Internal Conversion of Electronically Excited RNA and DNA Nucleosides in Water [J. Am. Chem. Soc. 2000 , 122 , 9348−9349]. *J. Am. Chem. Soc.* **123,** 5166–5166 (2001).

11. Pecourt, J. M. L., Peon, J. & Kohler, B. DNA excited-state dynamics: Ultrafast internal conversion and vibrational cooling in a series of nucleosides. *J. Am. Chem. Soc.* **123,** 10370–10378 (2001).

12. Doorley, G. W. *et al.* Tracking DNA excited states by picosecond-time-resolved infrared spectroscopy: Signature band for a charge-transfer excited state in stacked adenine-thymine systems. *J. Phys. Chem. Lett.* **4,** 2739–2744 (2013).

13. Krummel, A. T., Mukherjee, P. & Zanni, M. T. Inter and Intrastrand Vibrational Coupling in DNA Studied with Heterodyned 2D-IR Spectroscopy. *J. Phys. Chem. B* **107,** 9165–9169 (2003).

14. Krummel, A. T. & Zanni, M. T. DNA vibrational coupling revealed with two-dimensional infrared spectroscopy: insight into why vibrational spectroscopy is sensitive to DNA structure. *J. Phys. Chem. B* **110,** 13991–14000 (2006).

15. Lee, C., Park, K.-H., Kim, J.-A., Hahn, S. & Cho, M. Vibrational dynamics of DNA. III. Molecular dynamics simulations of DNA in water and theoretical calculations of the two-dimensional vibrational spectra. *J. Chem. Phys.* **125,** 114510 (2006).

16. Lee, C., Park, K.-H. & Cho, M. Vibrational dynamics of DNA. I. Vibrational basis modes and couplings. *J. Chem. Phys.* **125,** 114508 (2006).

17. Lee, C. & Cho, M. Vibrational dynamics of DNA. II. Deuterium exchange effects and simulated IR absorption spectra. *J. Chem. Phys.* **125,** 114509 (2006).

18. Lee, C. & Cho, M. Vibrational dynamics of DNA: IV. Vibrational spectroscopic characteristics of A-, B-, and Z-form DNA's. *J. Chem. Phys.* **126,** 145102 (2007).

19. Peng, C. S., Jones, K. C. & Tokmakoff, A. Anharmonic vibrational modes of nucleic acid bases revealed by 2D IR spectroscopy. *J. Am. Chem. Soc.* **133,** 15650–15660 (2011).

20. Greve, C. *et al.* N-H stretching excitations in adenosine-thymidine base pairs in solution: pair geometries, infrared line shapes, and ultrafast vibrational dynamics. *J. Phys. Chem. A* **117,** 594–606 (2013).

21. Szyc, Ł., Yang, M., Nibbering, E. T. J. & Elsaesser, T. Ultrafast vibrational dynamics and local interactions of hvdrated DNA. *Angew. Chemie - Int. Ed.* **49,** 3598–3610 (2010).

22. Greve, C. *et al.* N-H stretching modes of adenosine monomer in solution studied by ultrafast nonlinear infrared spectroscopy and ab initio calculations. *J. Phys. Chem. A* **116,** 7636–7644 (2012).

23. Yang, M. *et al.* Dynamics and couplings of N-H stretching excitations of guanosine-cytidine base pairs in solution. *J. Phys. Chem. B* **115,** 5484–5492 (2011).

24. Yang, M., Szyc, Ł. & Elsaesser, T. Femtosecond two-dimensional infrared spectroscopy of adenine-thymine base pairs in DNA oligomers. *J. Phys. Chem. B* **115,** 1262–1267 (2011).

25. Yang, M., Szyc, Ł. & Elsaesser, T. Decelerated water dynamics and vibrational couplings of hydrated DNA mapped by two-dimensional infrared spectroscopy. *J. Phys. Chem. B* **115,** 13093–13100 (2011).

26. Szyc, Ł., Yang, M. & Elsaesser, T. Ultrafast Energy Exchange via Water-Phosphate Interactions in Hydrated DNA. *J. Phys. Chem. B* **114,** 7951–7957 (2010).

27. Szyc, Ł., Dwyer, J. R., Nibbering, E. T. J. & Elsaesser, T. Ultrafast dynamics of N-H and O-H stretching excitations in hydrated DNA oligomers. *Chem. Phys.* **357,** 36–44 (2009).

28. Kozich, V., Szyc, L., Nibbering, E. T. J., Werncke, W. & Elsaesser, T. Ultrafast redistribution of vibrational energy after excitation of NH stretching modes in DNA oligomers. *Chem. Phys. Lett.* **473,** 171–175 (2009).

29. Dwyer, J. R. *et al.* Ultrafast Vibrational Dynamics of Adenine-Thymine Base Pairs in DNA Oligomers Ultrafast Vibrational Dynamics of Adenine-Thymine Base Pairs in DNA Oligomers. *J. Phys. Chem. B Lett.* **112,** 11194–11197 (2008).

30. Siebert, T., Guchhait, B., Liu, Y., Costard, R. & Elsaesser, T. Anharmonic Backbone Vibrations in Ultrafast Processes at the DNA–Water Interface. *J. Phys. Chem. B* **119,** 9670–9677 (2015).

31. Guchhait, B., Liu, Y., Siebert, T. & Elsaesser, T. Ultrafast vibrational dynamics of the DNA backbone at different hydration levels mapped by two-dimensional infrared spectroscopy. *Struct. Dyn.* **3,** 43202 (2016).

32. Pelmenschikov, A., Hovorun, D. M., Shishkin, O. V. & Leszczynski, J. A density functional theory study of vibrational coupling between ribose and base rings of nucleic acids with ribosyl guanosine as a model system. *J. Chem. Phys.* **113,** 5986–5990 (2000).

33. Toyama, A., Takino, Y., Takeuchi, H. & Harada, I. Ultraviolet Resonance Raman Spectra of Ribosyl C(1')-Deuterated Purine Nucleosides: Evidence of Vibrational Coupling between Purine and Ribose Rings. *J. Am. Chem. Soc.* **115,** 11092–11098 (1993).

34. Deflores, L. P., Nicodemus, R. a & Tokmakoff, A. Two-dimensional Fourier transform spectroscopy in the pump-probe geometry. *Opt. Lett.* **32,** 2966–2968 (2007).

35. Shim, S.-H., Strasfeld, D. B., Ling, Y. L. & Zanni, M. T. Automated 2D IR spectroscopy using a mid-IR pulse shaper and application of this technology to the human islet amyloid polypeptide. *Proc. Natl. Acad. Sci. U. S. A.* **104,** 14197–14202 (2007).

36. Greetham, G. M. *et al.* A 100 kHz time-resolved multiple-probe femtosecond to second infrared absorption spectrometer. *Appl. Spectrosc.* **70,** 645–653 (2016).

37. Banyay, M., Sarkar, M. & Graslund, A. A library of IR bands of nucleic acids in solution. *Biophys. Chem.* **104,** 477–488 (2003).

38. Hamm, P. & Zanni, M. T. *Concepts and Methods of 2D Infrared Spectroscopy*. (Cambridge University Press: Cambridge, 2011).

39. Rubtsov, I. V & Hochstrasser, R. M. Vibrational Dynamics, Mode Coupling, and Structural Constraints for Acetylproline-NH2. *J. Phys. Chem. B* **106,** 9165–9171 (2002).

40. Rubtsova, N. I. & Rubtsov, I. V. Vibrational Energy Transport in Molecules Studied by Relaxation-Assisted Two-Dimensional Infrared Spectroscopy. *Annu. Rev. Phys. Chem.* **66,** 717–738 (2015).

41. Fang, C. *et al.* Two-dimensional infrared spectroscopy of isotopomers of an alanine rich Alpha-helix. *J. Phys. Chem. B* **108,** 10415–10427 (2004).

42. Naraharisetty, S. R. G., Kasyanenko, V. M. & Rubtsov, I. V. Bond connectivity measured via relaxation-assisted two-dimensional infrared spectroscopy. *J. Chem. Phys.* **128,** 104502 (2008).

43. Kurochkin, D. V, Naraharisetty, S. R. G. & Rubtsov, I. V. A relaxation-assisted 2D IR spectroscopy method. *Proc. Natl. Acad. Sci. USA* **104,** 14209–14214 (2007).

44. Costard, R., Tyborski, T. & Fingerhut, B. P. Anharmonicities and coherent vibrational dynamics of phosphate ions in bulk H $_2$ O. *Phys. Chem. Chem. Phys.* **17,** 29906–29917 (2015).

5. Effect of Oligomer Length on Vibrational Coupling and Energy Transfer in Double-Stranded DNA

This chapter contains results to be published in the following publication:

Gordon Hithell, Paul M. Donaldson, Gregory M. Greetham, Michael Towrie, Glenn A. Burley, Anthony W. Parker and Neil T. Hunt, Effect of Oligomer Length on Vibrational Coupling and Energy Transfer in Double-Stranded DNA, *Chemical Physics*, Available Online

5.1 Abstract

The effects of sequence length on the long-range vibrational energy pathways in AT DNA oligomers has been investigated using ultrafast two-dimensional infrared spectroscopy (2D-IR). Structure-dependent coupling was observed for sequences between 6 and 15 bases pairs in length, with a reduced amount of this coupling observed in a DNA sequence 4 bases long. This result indicates that the minimum number of bases required to form a double helix structure is 6. Dynamic information from the sequences indicated that the length of the DNA oligomers used did not impact the timescale of energy transfer processes that occurs between the base and backbone vibrational modes. Expansion of the detection window compared to the experiments in the previous chapter allowed for further exploration into the nature of the exact pathway that facilitates this energy transfer process.

5.2 Introduction

At the core of all processes in Eukaryotic cells lies the genetic information stored within the base sequence of DNA.[1] While the structure of the DNA double helix was first realised from x-ray crystallographic measurements,[2] this static picture lacks insight into the highly dynamic processes of replication and transcription. These processes are vital in providing mechanisms for passing on genetic information as well as providing templates for constructing the biological machinery which carry out cellular function. Damage to this crucial piece of biological equipment can therefore have disastrous consequences on cellular lifetime.[3] One of the most prominent causes of DNA damage is absorption of excess energy through ultraviolet (UV) radiation.[4] While nature has developed repair mechanisms to fix damaged sequences, understanding the impact of how energy flows through DNA is an issue of significant importance.

Recent advances in experimental methodologies have allowed observation of fast dynamics of DNA based systems in solution, thus allowing observation of structural dynamics[5] as well as excited state relaxation dynamics.[6,7] In particular, two-dimensional infrared spectroscopy (2D-IR) is becoming a promising method for solution phase studies of biomolecules. While this has primarily been applied to protein based systems,[8–11] this technique is increasingly applied to study nucleic acid based systems. Initial experimental studies[12,13] and subsequent

computational studies[14–17] focused on the spectral region containing absorption features due to carbonyl stretching modes of the DNA bases. These early studies have since allowed recent studies into DNA melting[18,19] as well as small molecule binding interactions.[20]

Studies have also been performed that show the delocalised nature of base vibrational modes in individual nucleic acids bases.[21] This has been supported by studies on the N-H stretching modes of DNA that indicate coupling having a similar effect on these modes and also reports the relaxation of these higher frequency modes into lower frequency base modes.[22–30]

2D-IR spectroscopy has also been used to observe dynamics of the sugar-phosphate backbone under controlled hydration conditions.[31,32] Coupling between the backbone modes in this spectral region was observed and dynamic information pointed to the phosphate group as the primary dissipation method for transferring energy from DNA to the solvent environment. Following on from these experiments, the work presented in the previous chapter was carried out of a 'two-colour' 2D-IR study of an AT 15mer DNA sequence to examine the long-range interaction between the base modes and those due to the phosphate backbone.[33] Dynamic data from these experiments revealed an energy transfer pathway from the base to the backbone modes with indications that this pathway is possibly facilitated by modes from the deoxyribose moiety. Further observations have been made that highlight 'whole molecule' phenomena, a study using optical Kerr effect (OKE) spectroscopy demonstrated that low-frequency (GHz-THz) delocalised phonon-like modes are present in DNA and are sensitive to DNA strand conformation,[34] further highlighting the delocalisation effects present in DNA duplexes. While evidence is mounting of these whole molecule phenomena, some questions remain regarding their fundamental nature.

Observations made in Chapter (4) were made for a single DNA sequence and it was noted that off-diagonal spectral features linking the base modes with the phosphate vibrational mode were found to have conformational dependence. Whether these long-range interactions between base and backbone moieties are generic for DNA strands of any length or sequence content to this point is unclear. Furthermore, as only one DNA sequence has thus far been observed to exhibit these long range interactions, the question remains if the relaxation mechanism proposed in the experiments in the previous chapter is affected by varying DNA strand length. Is the mechanism only achievable by DNA strands of

a minimum length, such as those long enough to form a double helix or indeed do the roots of this mechanism reside in the individual building blocks that are at the foundation of DNA structure.

In this chapter, work presented in the previous chapter is expanded upon by observing how the effects of sequence length impact the timescale of the energy transfer dynamics. A number of sequences are measured ranging from a single nucleotide monophosphate unit (structure shown in Figure 5.1a) to the 15mer duplex (structure shown in Figure 5.1c) measured in the previous work and the data presented here shows how a single mononucleotide building block appears to display the traits of a fundamental energy transfer pathway for DNA duplexes. In addition to measuring a number of different sequences of varying length, the spectral detection window has been increased in order to better resolve high frequency modes in the backbone vibration region that were previously on the edge of the detection window. The extra information gained from these high frequency features helps shed light on the nature of the interactions in the base-sugar-phosphate relationship.

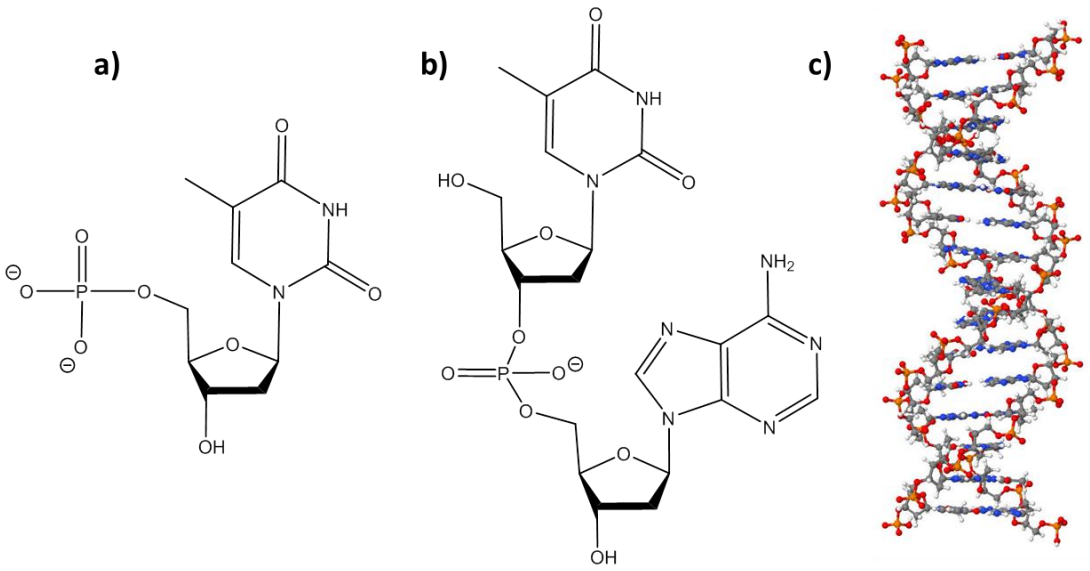

Figure 5.1 *– a) Thymidine Monophosphate structure b) AT 2mer structure c) AT 15mer duplex (AT 15mer duplex image created in Jmol: an open – source Java viewer for chemical structures in 3D. http://www.jmol.org/).*

5.3 Experimental

5.3.1 IR Absorption Spectroscopy

A series of DNA oligomers have been measured in this work containing only Adenine and Thymine bases. Sequences measured are listed in Table 5.1. Oligomers used were procured from Eurofins Genomics (AT 15mer, AT 10mer, and AT 6mer), Eurogentec (AT 4mer and AT 2mer) and Sigma-Aldrich (TMP). All samples were used without further purification.

Sequence Name	Sequence (5'->3')	T_m (K)
15mer	ATTATTATTATATTA (plus complimentary oligomer)	328 ± 2
10mer	ATTATTATTA (plus complimentary oligomer)	309 ± 2
6mer	ATTATT (plus complimentary oligomer)	290 ± 5
4mer	AATT	-
2mer	AT	-
TMP	T	-

***Table 5.1** – DNA sequences used in the present study. T_m values obtained from UV-Visible measurements not presented in this Chapter.*

All samples were dissolved in a D_2O Tris buffer (100 mM Tris, 100 mM NaCl, pD7.4). FTIR spectra were recorded on a Bruker Vertex 70 FTIR spectrometer. Samples were held between two CaF_2 windows separated by a 25 µm thick polytetrafluoroethylene spacer and housed in a thermostatically controlled mount, allowing the temperature to be varied between 293 and 353 K, accurate to ±1 K. Spectra were acquired with a resolution of 1 cm^{-1}.

5.3.2 2D-IR Spectroscopy

Fourier-transform ultrafast 2D-IR spectra were obtained using the co-linear pump-probe geometry method[35,36] with the LIFEtime spectrometer as described in Chapter (2).[37] OPA2 again provided probe pulses also centred on these base modes (1650 cm^{-1}) for single colour 2D-IR experiments while OPA3 was used in two-colour 2D-IR experiments to probe the phosphate backbone region of the spectrum centred at a slightly higher frequency than in the Chapter (4) near 1090 cm^{-1}. A diffraction grating with less dispersion than in the

experiments presented in Chapter (4) was used to direct the signals generated in the two-colour experiments onto the MCT detector. This allowed for an extended probe window, allowing resolution of higher frequency backbone modes. All spectra presented in this Chapter were collected using the parallel (ZZZZ) polarisation geometry.

5.4 Results

5.4.1 IR Absorption Spectroscopy

IR absorption spectra have been recorded for each of the 6 DNA sequences used in the study. Figures 5.2 and 5.3 show the DNA base (1550-1750 cm^{-1}) and backbone (1000-1200 cm^{-1}) vibration spectral regions respectively, highlighting the impact of heating the sample from 293 K (solid lines Figures 5.2 and 5.3) to 353 K (dashed lines Figures 5.2 and 5.3) on the spectrum of each sequence.

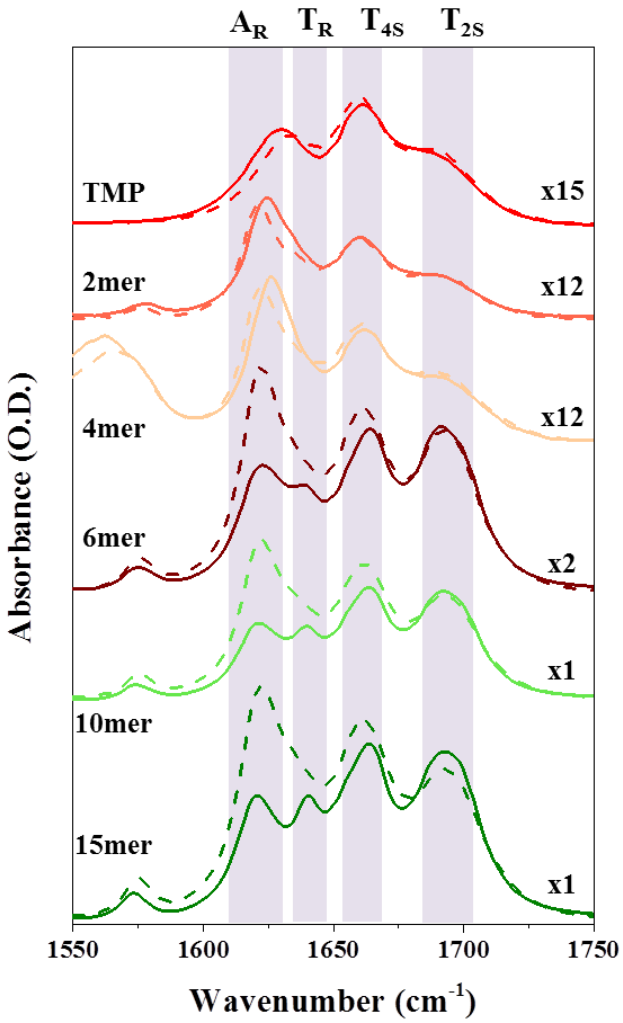

Figure 5.2 *– Base region FTIR spectra for each of the 6 DNA sequences measured at 293 K (solid lines) and 353 K (dashed lines). Relative signal sizes are indicated by a scaling factor on the right side which takes into account concentration relative to the 15mer concentration (10 mM) and scaling factor applied to the spectra for comparison purposes.*

The base region spectra are considered here first. It is clear from Figure 5.2 that the sequences can be divided into two distinct groups. Those that undergo significant spectral changes upon heating of the sample and those that only show minor spectral changes. The AT 15mer, AT 10mer and AT 6mer sequences fall into the former of these two categories while the AT 4mer, AT 2mer and TMP samples fall into the latter. For the sequences equal to or greater than six bases in length, four bands are observed in the base region of the FTIR spectrum (highlighted in purple shaded boxes in Figure 5.2) at 293 K at frequencies of 1622, 1640, 1663, 1693 cm^{-1} respectively. These are assigned to the A_RT, AT_R, AT_{4S} and AT_{2S} modes

which is the same assignment used in Chapters (3) and (4) for the AT 15mer sequence. Upon heating of the samples to 353 K, each of these three sequences exhibited changes in the base region FTIR spectra, namely and increase in intensity of the A_RT and AT_{4S} modes while the intensity of the AT_{2S} mode decreases. The AT_R mode also shifts down in frequency and appears as a shoulder on the high frequency side of the A_RT band.

The second group of sequences is those less than or equal to 4 bases in length. Features in these base region spectra are notably more similar to those observed in spectra for the single strands of longer sequences. As such these spectra have been assigned using the non-base paired nomenclature of four vibrational modes previously reported in this region for individual mononucleotides[21] and for single strand spectra in Chapters (3) and (4). These are the T_{2S} mode appearing at 1692 cm^{-1}, T_{4S} mode appearing at 1661 cm^{-1}, T_R mode appearing at 1633 cm^{-1} and the A_R mode appearing at 1625 cm^{-1}. A full list of the assignments for the six sequences at 293 K is presented in Table 5.2.

Sequence	Mode Frequency (cm^{-1})	Assignment
AT 15mer	1693	AT_{2S}
	1663	AT_{4S}
	1640	AT_R
	1622	A_RT
AT 10mer	1693	AT_{2S}
	1663	AT_{4S}
	1640	AT_R
	1622	A_RT
AT 6mer	1692	AT_{2S}
	1663	AT_{4S}
	1639	AT_R
	1622	A_RT
AT 4mer	1689	T_{2S}
	1661	T_{4S}
	1634	T_R
	1625	A_R
AT 2mer	1690	T_{2S}
	1660	T_{4S}
	1633	T_R
	1623	A_R
TMP	1687	T_{2S}
	1661	T_{4S}
	1630	T_R

Table 5.2 *– DNA Base Mode Assignments for FTIR spectra of the 6 AT DNA sequences used in this study at 293 K.*

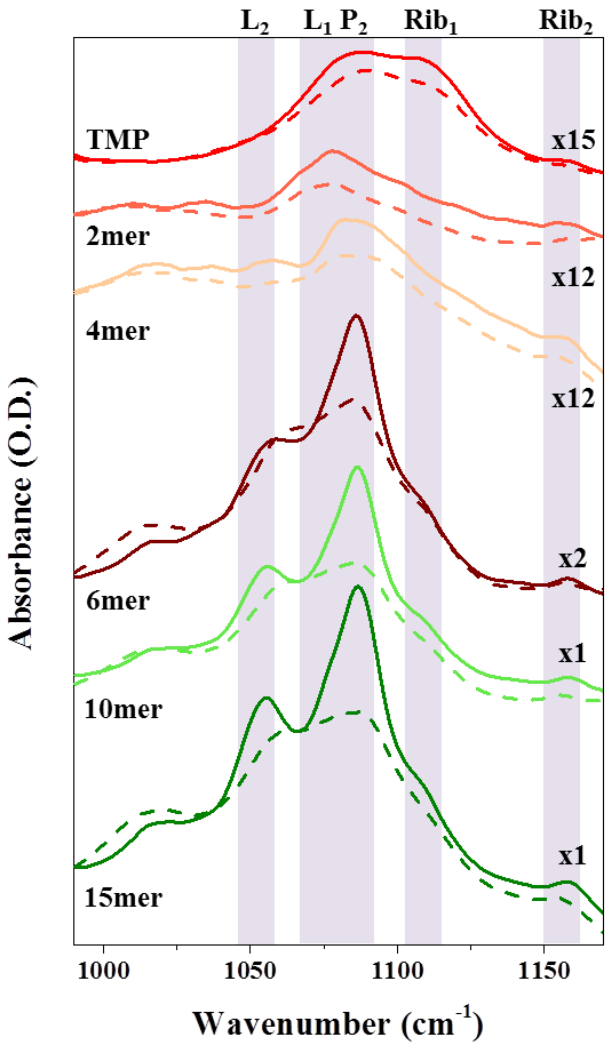

Figure 5.3 *– Phosphate region FTIR spectra for each of the 6 DNA sequences measured at 293 K (solid lines) and 353 K (dashed lines). Relative signal sizes are indicated by scaling factor on the right side which takes into account concentration relative to the 15mer concentration (10 mM) and scaling factor applied to the spectra for comparison purposes.*

Figure 5.3 focuses on the backbone spectral region of the six sequences and has highlighted five features of interest (purple shaded areas). The three lower frequency features are assigned to modes observed in the previous chapter and in the work by Siebert et al.[31] The features at 1050 cm^{-1} and 1075 cm^{-1} are assigned to a vibrational modes of the phosphodiester linkages (L_2 and L_1) while the band at 1087 cm^{-1} is assigned to the symmetric phosphate stretching mode (P_2). The two higher frequency bands at 1108 cm^{-1} and 1158 cm^{-1} are more difficult to assign. Previous work has assigned a ribose mode at 1108 cm^{-1} [38] however there is no current literature assignment for the band at 1158 cm^{-1}. In

order to aid this assignment we have measured the FTIR spectrum of the Thymine base on its own to try and eliminate the possibility of the mode at 1158 cm^{-1} being a low frequency base mode (spectra shown in Figure 5.4). Thymine has a relatively low solubility in water when not conjugated to the sugar-phosphate moiety. The mode at 1158 cm^{-1} does not appear in the Thymine spectrum and therefore must be due to the sugar-phosphate backbone unit. The increased intensity at frequencies higher than 1100 cm^{-1} are subject to a baseline effect due to a solvent band of the D_2O buffer that is present at a frequency of 1200 cm^{-1}. The 1108 cm^{-1} and 1158 cm^{-1} spectral features in the AT DNA and TMP spectra are therefore both assigned to vibrations of the deoxyribose moiety of the backbone which we will refer to as Rib_1 and Rib_2 modes respectively. It should also be noted that low frequency modes of Thymine are observed in (Figure 5.4a) at frequencies of 1070 and 1115 cm^{-1}. While these features would be expected to lie close to the L_1 and Rib_1 features in the FTIR spectrum of the DNA sequences, they appear to have no impact on the spectral features as neither are observed TMP FTIR spectrum where they would be likely to be most prominent. Assignments for the features observed in each of the backbone region spectra at 293 K are listed in Table 5.3.

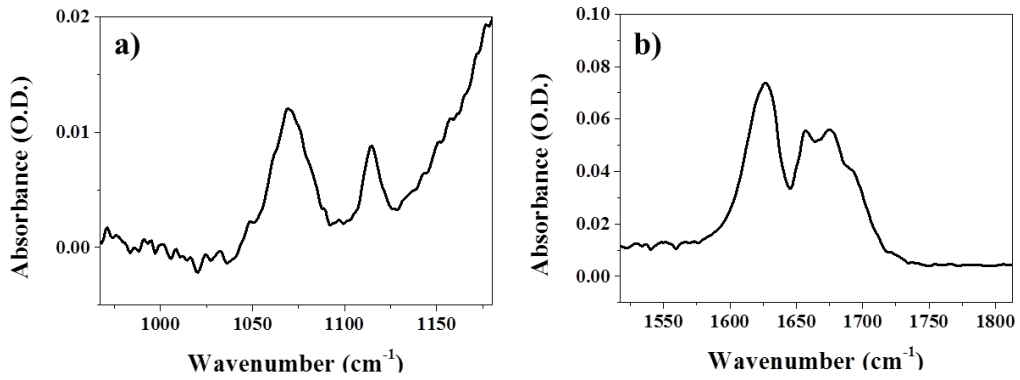

Figure 5.4 *– Backbone region (a) and base region (b) FTIR spectrum of Thymine DNA base dissolved in D_2O buffer. Despite features in the base region having intensities comparable to the other DNA sequences used in this study, no features are observed at 1158 cm^{-1}. The rise in the baseline at frequencies above 1100 cm^{-1} is due to the presence of a D_2O solvent band that appears at 1200 cm^{-1} which effects solvent subtraction.*

As for the base region spectra, it is clear that the backbone FTIR spectra can also be split into two groups defined by the amount of changes induced by heating of the respective samples. The AT 15mer, AT 10mer and AT 6mer sequences each display intense P_2

absorption bands that drop in intensity upon heating to 353 K. The P_2 bands appear to display significant enhancement when the DNA strands are in the duplex conformation. The AT 4mer, AT 2mer and TMP spectra do not exhibit the same changes in the P_2 band upon heating of the sample. It should also be noted that for this group of shorter sequences, the relative intensity of the features in this region are much smaller than observed in the longer sequences, despite the corresponding base regions displaying similar orders of intensity. In order to compare the spectra in Figures 5.2 and 5.3 a scaling factor is indicated for each sequence which denotes the relative intensity of each of the sequences based on the sample concentration compared to the AT 15mer sample and also if the spectrum has been further scaled when plotted. For sequence longer than six bases in length the features in the backbone region are of largely comparable size while for the shorter sequences these features are markedly lower in intensity despite increased sample concentrations and scaling of the spectra.

Sequence	Mode Frequency (cm^{-1})	Assignment
AT 15mer	1158	Rib_2
	1108	Rib_1
	1087	P_2
	1075	L_1
	1055	L_2
AT 10mer	1158	Rib_2
	1108	Rib_1
	1085	P_2
	1075	L_1
	1055	L_2
AT 6mer	1158	Rib_2
	1108	Rib_1
	1085	P_2
	1077	L_1
	1056	L_2
AT 4mer	1158	Rib_2
	1108	Rib_1
	1085	P_2
	1077	L_1
	1057	L_2
AT 2mer	1156	Rib_2
	1106	Rib_1
	1078	P_2
TMP	1156	Rib_2
	1108	Rib_1
	1086	P_2

Table 5.3 *– DNA Backbone Mode Assignments for FTIR spectra of the 6 AT DNA sequences used in this study at 293 K.*

Using the same method of PCA as in the Chapters (3) and (4), the melting behaviour of the FTIR spectra for each of the six sequences used in this study was quantified and melting temperatures extracted. In all cases 2 principal components were used to describe the

spectral changes upon heating. The weighted amounts of PC2 obtained for each of the three sequences is plotted as a function of temperature to yield the melting curve of their respective transitions from which the T_m is extracted from each sequence by fitting with a Boltzmann sigmoidal fit. The melting profiles are shown in Figure 5.5.

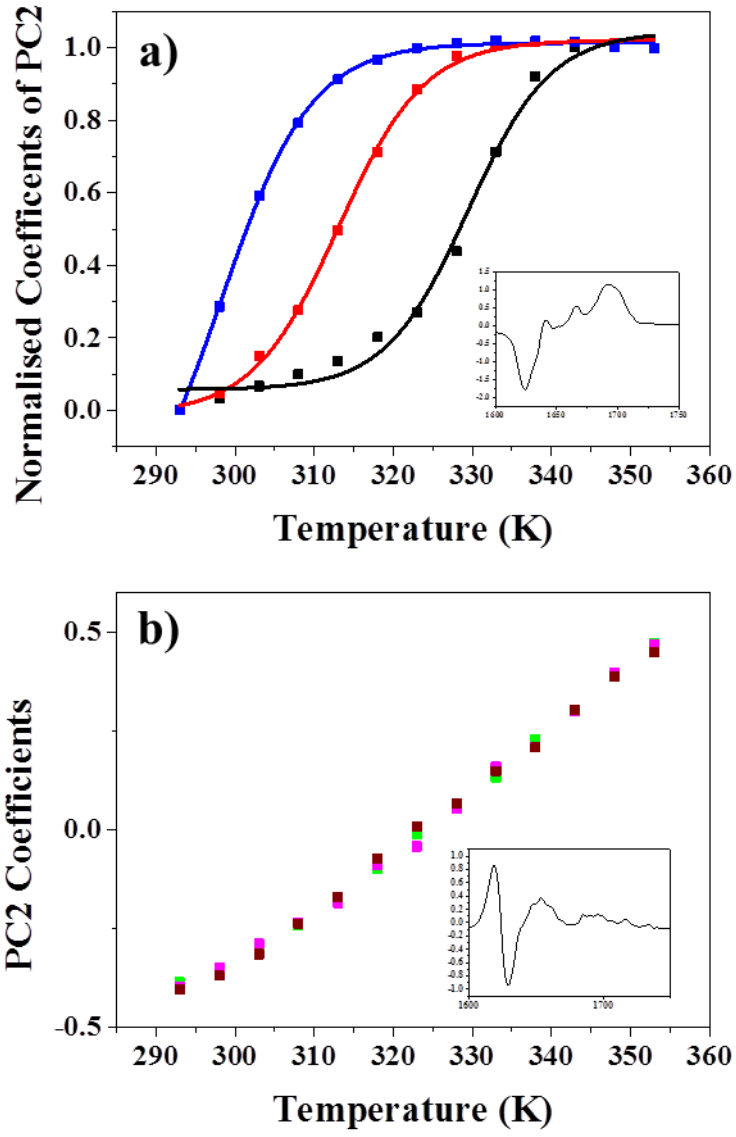

Figure 5.5 *– a) Melting curves obtained from PCA analysis fit with Boltzmann sigmoids for AT 15mer (black), AT 10mer (red) and AT 6mer (blue) sequences. b) Melting curves obtained from PCA analysis for AT 4mer (green), AT 2mer (pink) and TMP (brown) sequences. The inset in both a) and b) shows the spectral contributions of PC2 that represent the changes in the FTIR spectra for each of the sequences upon melting.*

The FTIR spectra of the six sequences could be grouped into two distinct groups and the melting behaviour of each of the sequences further supports this grouping. The AT 15mer AT 10mer and AT 6mer sequences all exhibit sigmoidal melting profiles (Figure 5.5a), although it appears that the lower temperature region of the AT 6mer is not well defined. Melting temperatures were extracted for each of these sequences, the T_m of the AT 15mer was found to be 329 ±2 K, for the AT 10mer the T_m was found to be 313 ±2 K and the T_m for the AT 6mer was found to be 298 ±2 K. The T_m decreases as the length of sequence decreases. This result would be expected as fewer base pairs would means less hydrogen bonds holding together the duplex and therefore less energy is required to disrupt all of these hydrogen bonds. It is clear that for each of these sequences that at 293 K the sample can be considered to contain ds-DNA while at 353 K the sample contains ss-DNA. However, it should be noted that from the melting curve for the AT 6mer is already exhibiting the transition from ds- to ss- even at room temperature. This implies that even at the lowest temperatures measured the AT 6mer sample will likely contain a significant amount of ss-DNA.

The melting profiles obtained for the AT 4mer, AT 2mer and TMP samples do not follow this pattern (Figure 5.5b). Instead of a sigmoidal profile, the value of PC2 returned form the PCA varies linearly with temperature for each of the three short sequences. This indicates that any changes in the spectrum upon heating are not due to melting, these are perhaps due to heating effects causing some small shifts or broadening of the spectral features, and these samples can be considered to contain ss-DNA at all temperatures. Note also the figures inset in Figure 5.5a) and b), these show the returned PC2 spectra from the PCA of the AT 10mer and AT 4mer respectively, indicating the changes in the spectrum with increasing temperature. The Figure 5.5a) inset of the AT 10mer is comparable to that already shown in Chapter (3) for the AT 15mer, highlighting a decrease in the intensity of the band at 1622 cm^{-1} with temperature and an increase in intensity of the band at 1693 cm^{-1}. For the AT 4mer inset shown in Figure 5.5b), it can be seen that the changes are represented predominantly by a shift of the 1625 cm^{-1} band, shown in the PC2 spectrum by a gain in intensity on the lower frequency portion of the band and an equal decrease in intensity of the band on the higher frequency side. This helps to support that for the sequences 4 bases or fewer in length, changes in the FTIR spectrum are not attributable to melting behaviour.

5.4.2 Base Region 2D-IR Spectroscopy

2D-IR spectra have been recorded at 293 K and 353 K, temperatures at which the sequences can be defined as being in either double stranded or single stranded conformation, at a series of waiting times for each of the six DNA sequences. Figure 5.6 shows an example of spectra recorded in both the base region and phosphate off-diagonal region for the AT 10mer sequence along with accompanying IR absorption spectra. In the base region 2D-IR spectrum at low temperature (Figure 5.6d), four negative features (red) are found along the spectrum diagonal corresponding to the v=0-1 transition of each of the four bands discussed in the linear IR spectrum. Each negative feature is accompanied by a positive feature (blue) due to the v=1-2 transition of the modes. These features are shifted downwards in frequency due to the anharmonicity of the modes. Off-diagonal features are in the spectrum are also consistent with that observed previously for the AT 15mer. The spectrum shown in Figure 5.6d) is also representative of the AT 15mer and AT 6mer spectra which show comparable features.

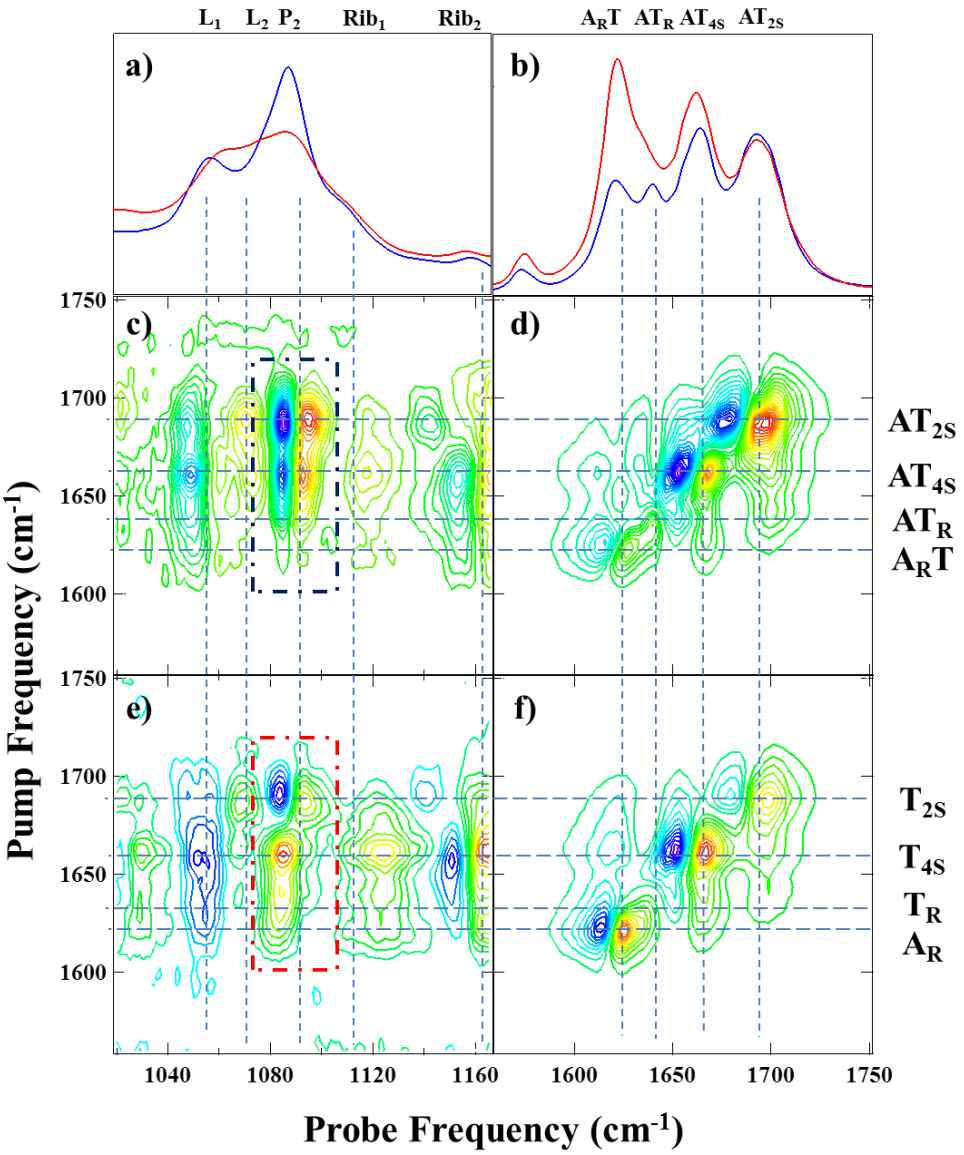

Figure 5.6 *– a) AT 10mer phosphate region FTIR spectra at 293 K (blue) and 353 K (red), b) AT 10mer base region FTIR spectra at 293 K (blue) and 353 K (red), (c-f) Phosphate and Base region 2D-IR spectra of AT-10mer sequence at 293 K (c,d) and at 353 K (e,f), highlighted regions in spectra c) and e) show off-diagonal coupling patterns characteristic of duplex and single strand DNA.*

Upon heating to 353 K (Figure 5.6f), changes are observed which are characteristic of the transition from double to single stranded DNA. The A_RT/A_R on-diagonal features increases intensity upon melting while the AT_{2S}/T_{2S} mode decreases in intensity. The AT_R/T_R mode also shifts down in frequency towards the A_R mode and there is a loss of off-diagonal features that link the A_RT/A_R mode with each of the three T modes. The changes in the

spectral features described here for the AT 10mer sequence are also applicable for the base region 2D-IR spectra of the AT 15mer and AT 6mer sequences.

The features observed in the base region 2D-IR spectra for the shorter AT 4mer, AT 2mer and TMP sequences are comparable to the ss-DNA spectrum shown in Figure 5.6f) at both low and high temperatures. Diagonal features of the A_R, T_{4S} and T_{2S} modes are clearly visible and the features of the A_R mode are the display the greatest amplitude as in the ss-DNA spectra for the longer sequences. The T_R mode is visible as a shoulder on the AR features however they are less well defined than in the longer sequences at low temperature.

Overall the patterns observed for the IR absorption spectra are holding true in the 2D spectra. The data can be clearly separated into two groups, the longer sequences (6 bases or longer in length) which exhibit on and off-diagonal peaks characteristic of ds-DNA, and the shorter sequences (4 bases or shorter in length) which the 2D-IR spectra all closely resemble the high temperature spectra of the longer sequences. Given the presence or lack thereof of the off-diagonal features identified in Chapter (3) as characteristic of the presence of double stranded duplex DNA then these two groups can also be considered to be characteristic of those DNA sequences that can form a DNA double helix and those that cannot.

5.4.3 Backbone Region 2D-IR Spectra

The backbone region 2D-IR spectra for the AT 10mer sequence is also shown in Figure 5.6. In the lower frequency portion of Figure 5.6c) features linking each of the base modes to the phosphodiester linkages L_2 (left of the blue box Figure 5.6c) as well as the P_2 mode (marked within the blue box Figure 5.6c) can be seen. Features linking the base modes to the L_1 mode are not well resolved due to overlap of the features linking to the L_2 and P_2 modes. Moving to the higher frequency portion of the spectrum (>1100 cm^{-1}), features linking each of the base modes to the Rib_1 and Rib_2 modes can now also be observed (right of the blue box Figure 5.6c). As for the base region spectra, the AT 10mer spectrum is also representative of features observed in the AT 15mer and AT 6mer spectra.

Upon heating there are significant changes in the backbone region (Figure 5.6e) which are primarily located on the P_2 features (highlighted in the blue and red boxes of 5.6c and 6e). Changes in the coupling pattern upon melting of the DNA duplex are observed between the A_RT/A_R, AT_R/T_R and AT_{4S}/T_{4S} base modes and the P_2 mode with these features being lost and

the only remaining P_2 off-diagonal belonging linking to the T_{2S} base mode. Features linking the base modes to the L_2, L_1 modes as well as the newly observed Rib_1 and Rib_2 off-diagonal features appear to be insensitive to heating the sample. This is consistent with changes observed in the previous chapter of the AT 15mer (with the exception of the now resolved Rib_1 and Rib_2 features) which describes conformation dependent off-diagonal patterns in this spectral region.[33]

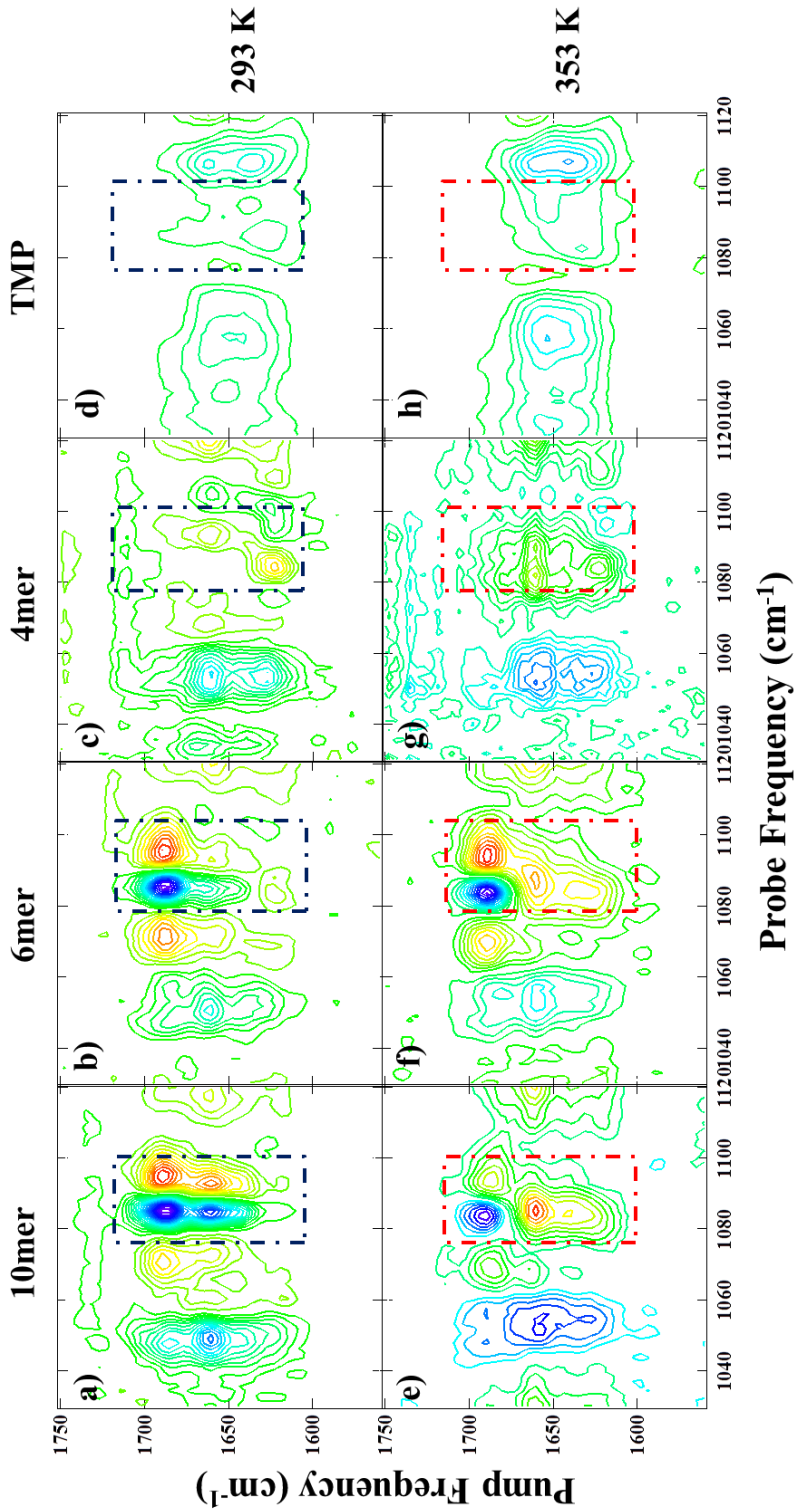

Figure 5.7 *– Phosphate region 2D-IR spectra at Tw=0.4 ps for AT 10mer, AT 6mer, AT 4mer and TMP DNA sequences at 293 K (a-d) and 353 K (e-h).*

Comparison of the backbone region 2D-IR spectra measured at both low and high temperatures for each of the new sequences in this study are shown in 5.7. The only exceptions are the AT 2mer which showed poor signal to noise ratio and the AT 15mer spectra which has been presented in Chapter (4). Due to low signal to noise achieved for the AT 2mer data, quantitative information has not been extracted however qualitatively the observable features in the data compare well with the TMP data. While the backbone spectra of the AT 10mer and AT 6mer can be observed to be very similar in Figure 5.7 at both low (Figure 5.7a) and b)) and high temperature (Figure 5.7e) and f)), clear differences are observed for in the spectra of the shorter sequences.

In each spectrum of Figure 5.7 the coupling pattern of the base modes coupling to the P_2 mode are highlighted in the blue and red boxes. The distinctive T_{2S}-P_2 off-diagonal that has been consistent in the longer sequences at low and high temperatures is no longer present in the spectra of sequences 4 bases or less in length. This feature discussed for the AT 15mer in Chapter (4) appears to be insensitive to DNA strand conformation in the AT 10mer and AT 6mer data. However for the shorter sequences this feature linking the T_{2S} and P_2 modes is no longer present indicative of a minimum sequence length required to facilitate the link between these two modes.

In particular upon heating of the AT 4mer this feature (visible in at the top of the blue boxes in Figures 5.7a) and b) but not observed in the same blue boxes in Figures 5.7c) and d)) is also not present, indicating some point of difference between the 4mer and the longer sequences in terms of the ability for the base and backbone modes to communicate. There are some changes that occur upon heating of the AT 4mer that appear in the lower pump frequencies within the red box (Figure 5.7g). Features at pump frequencies between 1620 cm^{-1} and 1660 cm^{-1} appear consistent with the longer sequences at high temperature.

The final two spectra in Figure 5.7 (d,h) are of the single thymine monomer unit TMP. In these spectra there is little evidence of interaction between the base modes and the P_2 mode. Features linking the base modes to the phosphodiester modes as well as the ribose modes are still present. These features are now more prominent than in the longer sequences due to the decrease the number of features observed in this spectral region.

5.4.4 Dynamics

5.4.4.1 Base Relaxation Dynamics

2D-IR spectra have been recorded for each of the six sequences at a series of waiting times, this allowed for extraction of vibrational relaxation times by extracting the peak amplitudes of the diagonal modes as a function of T_W and fitting the resulting plot with single exponential decays to extract the timescale of the relaxation. The vibrational relaxation time (T_1) was taken as the average of the decay times of the v=0-1 and v=1-2 features. Parameters extracted from the spectra recorded at 293 K are listed in Table 5.4. An example of the kinetic traces obtained from extraction of peak amplitudes for the AT 10mer is shown in Figure 5.8 below. Extracted values of T_1 showed only slight variation with increasing sequence length.

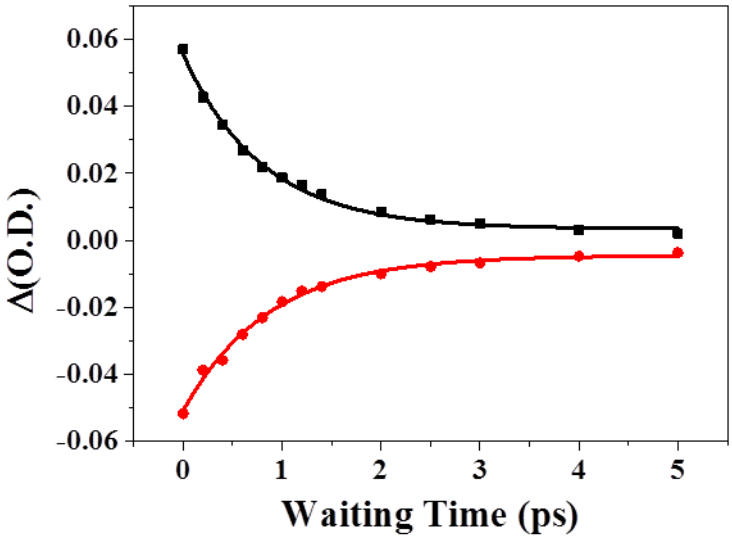

Figure 5.8 *- Kinetics extracted from following peak amplitudes for the A_RT features of the AT 10mer sequence. v=0-1 kinetics are shown in red while the v=1-2 kinetics are shown in black. Timescales extracted via fitting of single exponential decay.*

Sequence	Assignment	T_1 (fs)
AT 15mer	AT_{2S}	580 ± 30
	AT_{4S}	550 ± 30
	AT_R	520 ± 70
	A_RT	680 ± 50
AT 10mer	AT_{2S}	590 ±20
	AT_{4S}	560 ± 20
	AT_R	-
	A_RT	830 ± 50
AT 6mer	AT_{2S}	600 ± 30
	AT_{4S}	570 ± 30
	AT_R	360 ± 50
	A_RT	710 ± 30
AT 4mer	T_{2S}	630 ± 10
	T_{4S}	600 ± 40
	T_R	-
	A_R	710 ± 40
AT 2mer	T_{2S}	620 ± 50
	T_{4S}	650 ± 40
	T_R	-
	A_R	810 ± 30
TMP	T_{2S}	640 ± 30
	T_{4S}	590 ± 40
	T_R	530 ± 50

Table 5.4 *– Vibrational relaxation times for the base vibrational modes for each of the six DNA sequences used in this study at 293 K.*

5.4.4.2 Backbone Relaxation Dynamics

Backbone region 2D-IR spectra have also been recorded for each of the six sequences used in this study. This allowed for comparison of the relaxation dynamics shown in the previous Chapter for the AT 15mer for sequences of varying length. Dynamics are obtained from the spectra by extracting the peak amplitude of a particular spectral feature as a function of

waiting time. Example dynamics for the AT 10mer taken at a pump slice corresponding to excitation of the AT_{4S} base mode is shown in Figure 5.9 below.

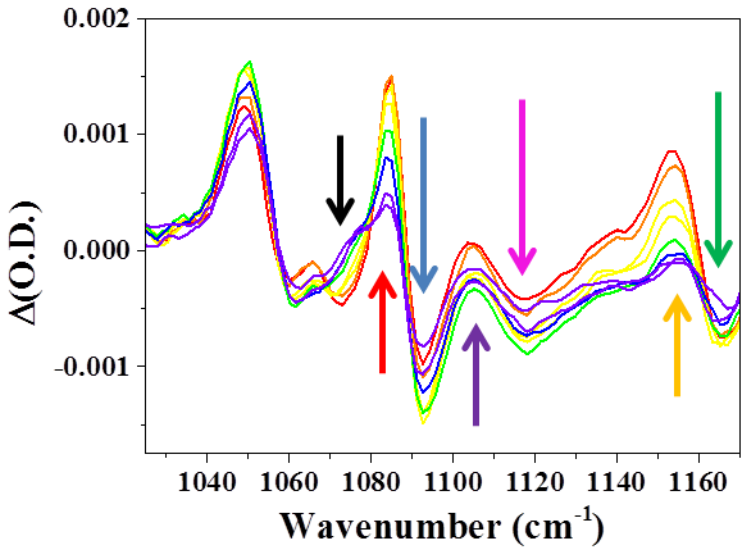

Figure 5.9 *– Pump slices at a series of waiting times from 0.4 ps (red) to 5 ps (purple) taken from the AT 10mer backbone region 2D-IR spectrum at 293 K. Arrows referred to in the text.*

Overall the relaxation dynamics observed in the backbone region for the AT 10mer are comparable to those observed for the AT 15mer sequence in Chapter (4). Three features linking to the P_2 mode are observed, a v=0-1 feature (blue arrow Figure 5.9) that shows an initial rise in amplitude followed by a long decay. The v=1-2 feature however has two components as observed in Chapter (4). A narrow component (red arrow Figure 5.9) shifted to lower frequency with respect to the corresponding v=0-1 feature by around 5 cm^{-1} and a broader component shifted to lower probe frequency (black arrow Figure 5.9) with respect to the corresponding v=0-1 feature by 12-15 cm^{-1}. As discussed at length in Chapter (4), the features marked by the blue and black arrows in Figure 5.9 are indicative of energy transfer as they display a clear rise in amplitude with increasing waiting time and also have peak separation comparable to the diagonal anharmonicty of the receiving mode in the energy transfer. The narrow feature marked with the red arrow in Figure 5.9 is indicative of coupling as the feature is present from the earliest recorded waiting times and decays exponentially. Comparing the observations made for the AT 10mer to those made for the AT 15mer previously, points to the suggested energy transfer mechanism, in Chapter 4,

holding true for this sequence also. Population relaxation from the base modes allows for energy transfer between coupled modes of the DNA back bone.

To compare timescales between the different sequences the kinetic traces obtained were normalised to negate differences in relative signal sizes between the sequences. The average kinetic trace for a given feature across all the sequences where that feature appeared was then calculated from the normalised data.

The first set of dynamics considered are those associated with off-diagonal features to the P_2 mode. Dynamics have been observed for these features before for the AT 15mer in the previous chapter[33] (Chapter 4.4.3). Here we report similar kinetics for the 15mer, 10mer and 6mer sequences. A kinetic profile for the v=0-1 feature (blue arrow Figure 9) that displayed an initial rise in intensity on a time scale of around 700 fs. The corresponding v=1-2 feature was more complicated with the main band (red arrow Figure 5.9) exhibiting behaviour indicative of coupling in terms of kinetics with little evidence of an increase in intensity, however a red-shifted shoulder (black arrow Figure 5.9) to this feature which grew in as a function of time indicating an energy transfer component was also observed for these three sequences. An average rise time of the v=0-1 features for each of the three sequences was extracted by fitting to a single exponential and was found to be on the order of 500 fs. The spread in the average across the sequences is indicated by the error bars calculated as the standard deviation in the average value obtained at each point. An average relaxation time for the coupling feature of the v=1-2 components of the sequences was found to be much longer on the order of 5000 fs. Dynamics were not extracted from the red-shifted shoulder. As coupling to the P_2 mode was not observed in the 4mer or TMP spectra then no dynamics are reported for these modes. The average kinetics for the T_{2S}-P_2 and T_{4S}-P_2 features for the AT 15mer, AT10mer and AT 6mer sequences are shown in Figure 5.10 below.

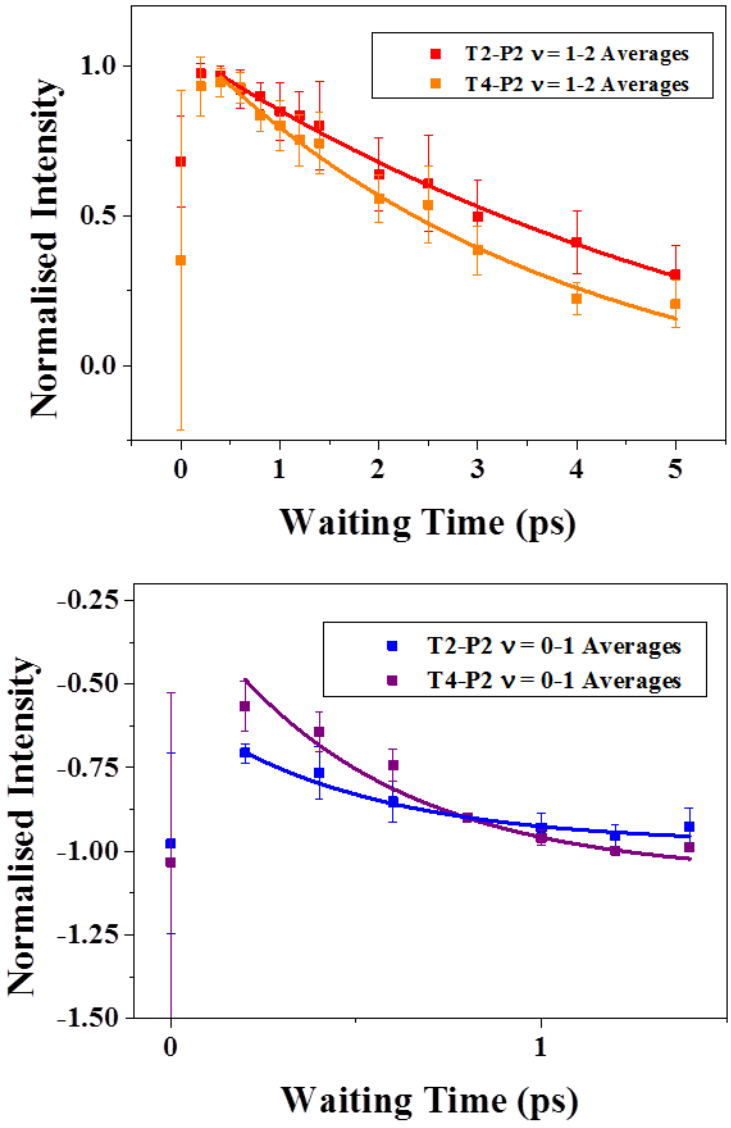

Figure 5.10 *– Off-diagonal kinetics between the base modes and the P_2 mode. Fitted regions in the data used to extract dynamic timescales.*

In the same manner as used for the P_2 off-diagonal features, temporal dynamics have also been extracted for the newly measured Rib_1 and Rib_2 off-diagonal features. The v=1-2 features between the Rib_1 mode and the base modes (purple arrow Figure 5.9) were observed for the AT 15mer on the very edge of the recorded spectra. There appears to be an initial increase in amplitude at short waiting times; however, this is within the timescale of the laser pulse duration. As such, placing a timescale on a rise time is not possible, but it is clear that these features are present in the spectra at the earliest recorded waiting times. The amplitude of these features then decay over a time scale which is mode-dependent

however, an average decay time of 700 fs represents well the dynamics across the sequences measured.

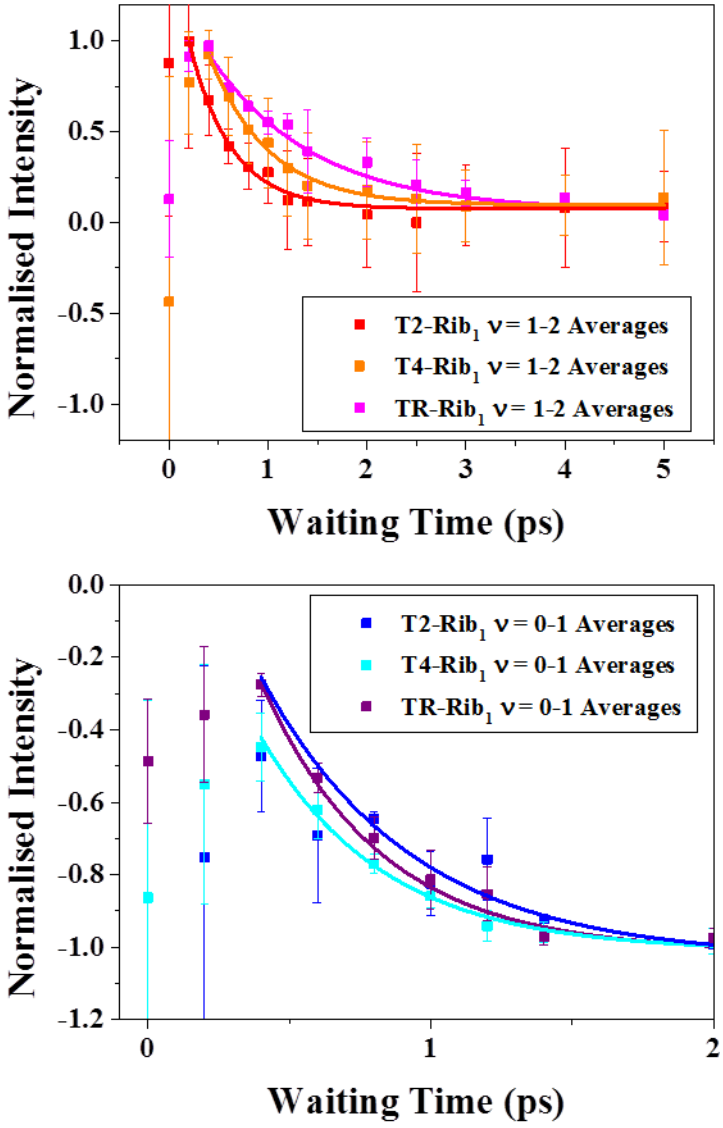

Figure 5.11 *– Off-diagonal kinetics between the base modes and the Rib_1 mode. Fitted regions in the data used to extract dynamic timescales.*

The v=0-1 features for the Rib_1 mode (pink arrow Figure 5.9) were outwith the detection window in the previous experiments. In this study we have measured the temporal dynamics for these features. These features displayed a profile similar to that observed for the P_2 mode, an average initial rise time of around 460 fs across the sequences, is then followed by a long decay time which extends longer than the longest waiting times

measured (5 ps). Average dynamics for Rib_1 modes across the sequences measured is shown in Figure 5.11.

Average temporal dynamics recovered for the Rib_2 off diagonal features are shown in Figure 5.12. Features attributed to v=1-2 transitions (orange arrow Figure 5.9) have a similar profile to those for the Rib_1 mode. At the earliest waiting times amplitudes show a slight increase although again laser pulse overlap effects make it difficult to quantify this rise. An exponential decay in the amplitude of these features follows on a timescale of 1200-1600 fs depending on the base mode. The accompanying v=0-1 features (green arrow Figure 5.9) for this mode display different behaviour to those of the Rib_1 mode. Instead of the relatively slow rise in amplitude observed for the Rib_1 features, the temporal behaviour is more similar to the v=1-2 features, a fast rise not clearly resolvable due to the duration of the laser pulses used in the experiment, followed by a decay. An average timescale of 660 fs for this decay was recorded for the T_{4S}-Rib_2 features across the sequences while the T_R-Rib_2 modes, although displaying qualitatively similar behaviour to the T_{4S}-Rib_2 features, did not fit well to an exponential and are not shown here.

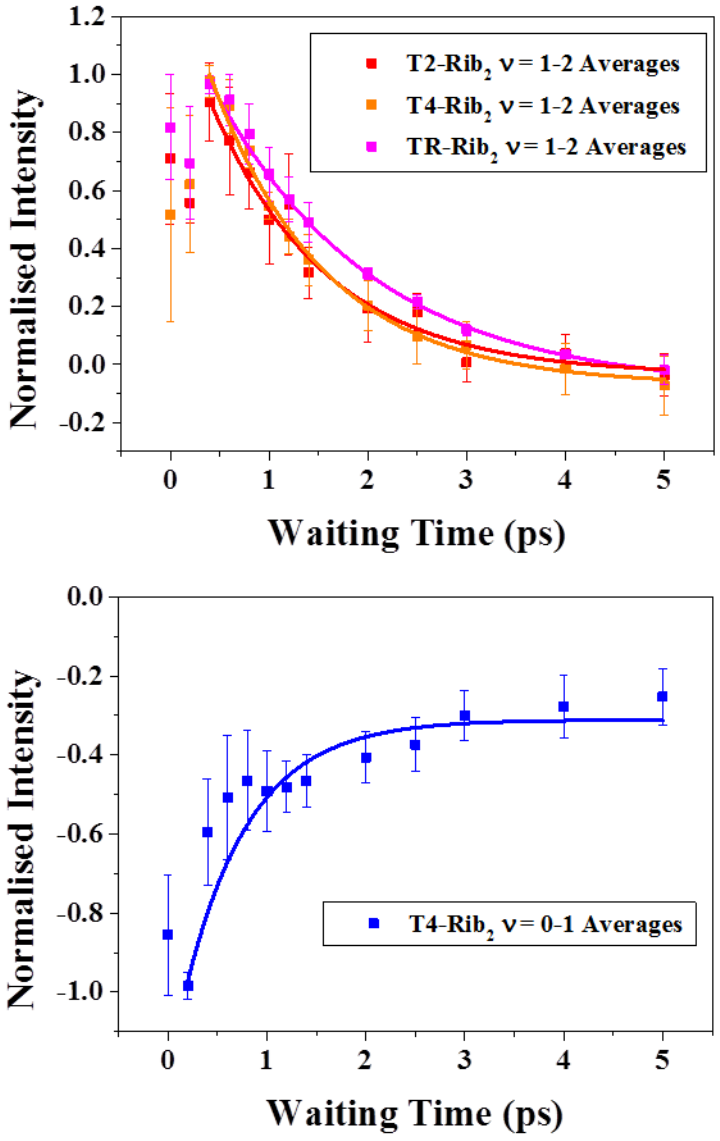

Figure 5.12 *– Off-diagonal kinetics between the base modes and the Rib_2 mode. Fitted regions in the data used to extract dynamic timescales.*

5.5 Discussion

There are two main areas of discussion from the results presented here. Firstly the impact of sequence length on the off-diagonal features produced between the base and backbone vibrational modes. The second area is the discussion of how the dynamics of the off-diagonal modes help to determine the role played by each of the modes in the vibrational energy relaxation mechanism described in Chapter (4).

5.5.1 Sequence Length Dependent Off-diagonal Features

For all the sequences measured in this study, off-diagonal features in the backbone region 2D-IR spectra linking the L_2, L_1, Rib_1 and Rib_2 modes and the base modes are largely unaffected by heating of the sample. These features are therefore insensitive to oligomer conformation and are consistent for longer oligomers as well as single mononucleotide building blocks. Therefore the interactions between base and backbone moieties in DNA appear to have fundamental roots in their building blocks and remain largely unchanged as the oligomer increases in length.

It is clear from the data presented here that the AT 15mer, AT 10mer and AT 6mer show similar behaviour in the backbone off-diagonal region at both low temperatures (ds-DNA) as well as at elevated temperatures sufficient to induce melting (ss-DNA). In ds-DNA clear off-diagonal features between the P_2 backbone mode and each of the four base modes is present. Upon melting of the DNA duplex these features are no longer present with the exception of those connecting the T_{2S} and P_2 modes. This means that for DNA sequences of length sufficient to form a stable DNA duplex (6 bases or more in length), interaction between the A_RT, AT_R and AT_{4S} modes with the P_2 mode is dependent on the DNA strands being in double stranded conformation and therefore must represent inter-strand interactions while the interaction between the AT_{2S}/T_{2S} base mode and P_2 mode is facilitated by intra-strand interactions.

The shorter sequences used in this study do not follow the same behaviour. In the AT 4mer sequence there is some indication of interaction between the T_{4S} mode and the P_2 mode; however, the amplitude of this feature is very small compared to other features in the spectrum. Upon heating of the sample this feature is also lost as is the case in the 2D-IR spectra of the longer sequences. This change in the spectrum points to some change in the conformation in the AT 4mer upon heating despite the FTIR and base region 2D-IR spectrum indicating that the AT 4mer can be considered to be ss-DNA at all temperatures. With DNA oligomers four base pairs in length, the number of bases required needed for a full turn in a double helix is 10,[39] there is some possibility of weak base pairing between the oligomers which would be disrupted at high temperatures. In the TMP spectra there are no features coupling the base modes to the P_2 mode and there is little change to the spectra upon heating. As no base pairing is possible with only single thymine bases present in the sample then no changes upon heating are expected.

A notable difference in the spectra between the shorter and longer sequences lies in the absence of features linking the T_{2S} and P_2 modes. It was observed in the previous chapter for this spectral region that even for single DNA strands, features linking the T_{2S} and P_2 modes remain present,[33] indicating this feature is not conformation dependent. The absence of this feature in the sequences with 4 or fewer bases indicates that this feature could require a minimum oligomer length in order to facilitate the coupling between the two vibrational modes. These features can also serve as markers which indicate that DNA is of sufficient length to form a double-stranded helix which from the data presented here is 6 bases or more.

There is also a remarkable drop in the amplitude of any off-diagonal features from the T_{2S} base mode in the sequences with 4 or fewer bases. It is notable that in the FTIR spectra for these shorter sequences that the T_{2S} mode is clearly the smallest absorption band compared to the others in this spectral region. This feature is also clearly broader in the spectra for sequences with four or fewer bases. The lack of off-diagonal features linking this particular base mode with the backbone modes could be a result of reduced transition dipole strength in these shorter sequences due to a lack of excitonic vibrational coupling between the transition dipoles as observed in α-helical peptides.[40] Another possibility could be that in the shorter sequences, energy from the T_{2S} mode is preferentially dissipated via interaction with the solvent environment in proximity with this C=O group. The broadening of features in the FTIR spectra is indicative of increased interaction with the solvent and this direct interaction with the solvent may prove to be a more efficient path way for vibrational relaxation than observed in the longer sequences.

5.5.2 Role of Backbone Modes in Vibrational Relaxation Pathways

Across the range of modes for which dynamics have been measured in this data, it is clear that no significant variation in timescales between the DNA sequences used in this study exists. In general the spread in the kinetics throughout the sequences represented by error bars in Figures 5.10, 5.11 and 5.12, are generally small and therefore an average timescale presented for the dynamics is a reasonable representation of the data.

In general there is a transition in the behaviour of the off-diagonal features as the frequency of the modes decreases. The highest frequency modes (Rib_2) appear to act as an initial conduit for energy absorbed by the bases and interact with them via a coupling

interaction. The features in the middle of the spectrum (P_2, Rib_1) exhibit dynamic behaviour indicative of both coupling interactions as well as energy transfer between the base and back bone modes. Finally the lowest frequency modes observed (L_1, L_2) appear to be dominated by energy transfer dynamics. In total the data points to a general pathway for energy transport in DNA oligomers that support the conclusions made in the previous chapter for the AT 15mer. Population relaxation from the bases to the ribose backbone modes facilitates vibrational transfer between the coupled backbone modes followed by subsequent dissipation of energy to the solvent environment via vibrations of the DNA backbone.

The average relaxation dynamics for the P_2 off-diagonal features compare well with that observed in the previous chapter. An increase in amplitude of the v=0-1 features peaking between 1 and 2 ps indicating prevalent energy transfer processes accompanied by more complex v=1-2 features which have a narrow component that decays accompanied by a lower frequency shoulder that grows in with increased T_W. Loss of some of these P_2 off-diagonals following melting indicates that their interaction is dependent on conformation of the DNA oligomers. Quantitatively the timescales for the rise times of v=0-1 modes we have observed in this study (500 fs) compare well with that observed previously (650 fs). Decay times of the narrow coupling v=1-2 features also compared well, in all cases being long decays on a timescale of 5-10 picoseconds.

Dynamics for the Rib_1 off-diagonals show somewhat similar behaviour to the P_2 features with v=0-1 features growing in on a timescale of 400-500 fs and v=1-2 features which are dominated by an exponential decay from early times on a 500-1000 fs timescale indicative of coupling. A rapid increase in amplitude of the v=1-2 modes may be present; however, quantification of this is not possible due to the temporal duration of the laser pulses used. This behaviour indicates that the interaction between the base modes and the Rib_1 mode is similar to those with the P_2 mode and is a combination of coupling and energy transfer processes. These features are also insensitive to DNA melting and as such do not rely on DNA being in the duplex conformation in order to facilitate the energy relaxation mechanism. Another difference between the Rib_1 and P_2 features is that the v=1-2 features do not exhibit the complex lineshape of a broadened and narrow components. Although, given the similarity of the rest of the dynamics of these modes compared to those of the P_2, it is possible that a positive red-shifted component may be hidden by overlap with the

negative v=0-1 P_2 features, though this is unlikely, given the visibility of the red-shifted component of the P_2 feature despite close proximity to the L_1 features.

Rib_2 dynamics do not follow the same behaviour as the other features in this region. For off-diagonal features to this mode, both v=0-1 and v=1-2 features display relaxation dynamics that show a potential short initial rise that is unclear due to the temporal resolution of the experiment, followed by an exponential decay. This behaviour is indicative of coupling and or rapid energy transfer that again cannot be reliably extracted from the data. There is a difference in the timescales between the v=0-1 and v=1-2 features, the former of which decay rapidly and the average time is not well defined for the TR-Rib2 modes but the T4-Rib2 modes have an average decay time of around 700 fs. The v=1-2 features have a notable longer delay time which is mode dependent but has an average value of 1200-1600 fs. The lineshape of the Rib2 features may attribute to the longer lived timescale of the v=1-2 modes. A shoulder is visible on the lower frequency side of these features similar to that observed in the P_2 off-diagonals. However, unlike those in the P_2 off-diagonals, these features do not grow in over time. If this shoulder is indicative of an overlapping feature partially obscured by the Rib2 features then it would appear that it also interacts with the base modes via a coupling interaction as opposed to energy transfer.

5.6 Conclusions

Extension of the work in Chapter (4) uses 2D-IR to study long-range interactions in DNA and has been performed on a range of DNA sequences of various lengths. Structure dependent coupling features between the base A_RT, AT_R and AT_{4S} modes and the P_2 backbone mode were found to be in good agreement for AT 15mer, AT 10mer and AT 6mer sequences. This pattern begins to break down as the sequence length is decreased further to four bases, and the same coupling patterns are no longer observed. The model completely breaks down for two-base and single mononucleotides where a change in off-diagonal features in the backbone spectra upon heating of the sample are not observed. This result supports the notion that the minimum length of DNA oligomer required to form a stable DNA duplex is 6 bases long.

Dynamic information was extracted from backbone off-diagonal 2D-IR spectra from an expanded detection window compared to that in the experiments in the previous chapter.

The expanded detection window allowed observation of dynamics from two previously undetected off-diagonal features. These modes are assigned to vibrations located on the deoxyribose moiety. The dynamic information from these modes point to an energy transfer pathway facilitated by coupling between the base modes and the higher frequency modes of the DNA backbone before undergoing energy transfer between the modes.

Sequence dependence of the observed dynamics has also been investigated. In general, comparable temporal dynamics of off-diagonal features found in DNA sequences from 1 to 15 bases in length remain largely unchanged with decreasing oligomer length. This results indicated that the energy transfer mechanism between base and backbone vibrational modes are rooted in the individual DNA mononucleotides and as such the base-sugar-phosphate unit acts as an efficient mechanism for dissipation of excess energy absorbed by DNA bases to prevent subsequent damage to DNA sequences.

5.7 References

1. Houlihan, G., Arangundy-Franklin, S. & Holliger, P. Exploring the Chemistry of Genetic Information Storage and Propagation through Polymerase Engineering. *Acc. Chem. Res.* **50,** 1079–1087 (2017).

2. Watson, J. & Crick, F. Molecular structure of nucleic acids. *Nature* **171,** 737–738 (1953).

3. Zhou, B. S. & Elledge, S. J. Checkpoints in perspective. *Nature* **408,** 433–439 (2000).

4. Jackson, S. & Bartek, J. The DNA-damage response in human biology and disease. *Nature* **461,** 1071–1078 (2009).

5. Ma, H., Wan, C., Wu, A. & Zewail, A. H. DNA folding and melting observed in real time redefine the energy landscape. *Proc. Natl. Acad. Sci. U. S. A.* **104,** 712–716 (2007).

6. Towrie, M. *et al.* ps-TRIR covers all the bases – recent advances in the use of transient IR for the detection of short-lived species in nucleic acids. *Analyst* **134,** 1265–1273 (2009).

7. Doorley, G. W. *et al.* Tracking DNA excited states by picosecond-time-resolved

infrared spectroscopy: Signature band for a charge-transfer excited state in stacked adenine-thymine systems. *J. Phys. Chem. Lett.* **4,** 2739–2744 (2013).

8. Adamczyk, K. *et al.* The effect of point mutation on the equilibrium structural fluctuations of ferric Myoglobin. *Phys. Chem. Chem. Phys.* **14,** 7411–7419 (2012).

9. Simpson, N. & Hunt, N. T. Ultrafast 2D-IR spectroscopy of haemoproteins. *Int. Rev. Phys. Chem.* **34,** 361–383 (2015).

10. Baiz, C. R., Peng, C. S., Reppert, M. E., Jones, K. C. & Tokmakoff, A. Coherent two-dimensional infrared spectroscopy: quantitative analysis of protein secondary structure in solution. *Analyst* **137,** 1793–1799 (2012).

11. Chung, J. K., Thielges, M. C. & Fayer, M. D. Dynamics of the folded and unfolded villin headpiece (HP35) measured with ultrafast 2D IR vibrational echo spectroscopy. *Proc. Natl. Acad. Sci. U. S. A.* **108,** 3578–3583 (2011).

12. Krummel, A. T., Mukherjee, P. & Zanni, M. T. Inter and Intrastrand Vibrational Coupling in DNA Studied with Heterodyned 2D-IR Spectroscopy. *J. Phys. Chem. B* **107,** 9165–9169 (2003).

13. Krummel, A. T. & Zanni, M. T. DNA vibrational coupling revealed with two-dimensional infrared spectroscopy: insight into why vibrational spectroscopy is sensitive to DNA structure. *J. Phys. Chem. B* **110,** 13991–14000 (2006).

14. Lee, C., Park, K.-H. & Cho, M. Vibrational dynamics of DNA. I. Vibrational basis modes and couplings. *J. Chem. Phys.* **125,** 114508 (2006).

15. Lee, C. & Cho, M. Vibrational dynamics of DNA. II. Deuterium exchange effects and simulated IR absorption spectra. *J. Chem. Phys.* **125,** 114509 (2006).

16. Lee, C., Park, K.-H., Kim, J.-A., Hahn, S. & Cho, M. Vibrational dynamics of DNA. III. Molecular dynamics simulations of DNA in water and theoretical calculations of the two-dimensional vibrational spectra. *J. Chem. Phys.* **125,** 114510 (2006).

17. Lee, C. & Cho, M. Vibrational dynamics of DNA: IV. Vibrational spectroscopic characteristics of A-, B-, and Z-form DNA's. *J. Chem. Phys.* **126,** 145102 (2007).

18. Sanstead, P. J., Stevenson, P. & Tokmakoff, A. Sequence-Dependent Mechanism of

DNA Oligonucleotide Dehybridization Resolved through Infrared Spectroscopy. *J. Am. Chem. Soc.* **138,** 11792–11801 (2016).

19. Hithell, G. *et al.* Ultrafast 2D-IR and Optical Kerr Effect Spectroscopy Reveal the Impact of Duplex Melting on the Structural Dynamics of DNA. *Phys. Chem. Chem. Phys.* **19,** 10333–10342 (2017).

20. Ramakers, L. A. I. *et al.* Optimised DNA Minor Groove Binding Follows an Induced Fit Model. *J. Phys. Chem. B* **121,** 1295–1303 (2017).

21. Peng, C. S., Jones, K. C. & Tokmakoff, A. Anharmonic vibrational modes of nucleic acid bases revealed by 2D IR spectroscopy. *J. Am. Chem. Soc.* **133,** 15650–15660 (2011).

22. Dwyer, J. R. *et al.* Ultrafast Vibrational Dynamics of Adenine-Thymine Base Pairs in DNA Oligomers Ultrafast Vibrational Dynamics of Adenine-Thymine Base Pairs in DNA Oligomers. *J. Phys. Chem. B Lett.* **112,** 11194–11197 (2008).

23. Kozich, V., Szyc, L., Nibbering, E. T. J., Werncke, W. & Elsaesser, T. Ultrafast redistribution of vibrational energy after excitation of NH stretching modes in DNA oligomers. *Chem. Phys. Lett.* **473,** 171–175 (2009).

24. Szyc, Ł., Dwyer, J. R., Nibbering, E. T. J. & Elsaesser, T. Ultrafast dynamics of N-H and O-H stretching excitations in hydrated DNA oligomers. *Chem. Phys.* **357,** 36–44 (2009).

25. Szyc, Ł., Yang, M. & Elsaesser, T. Ultrafast Energy Exchange via Water-Phosphate Interactions in Hydrated DNA. *J. Phys. Chem. B* **114,** 7951–7957 (2010).

26. Szyc, Ł., Yang, M., Nibbering, E. T. J. & Elsaesser, T. Ultrafast vibrational dynamics and local interactions of hvdrated DNA. *Angew. Chemie - Int. Ed.* **49,** 3598–3610 (2010).

27. Yang, M. *et al.* Dynamics and couplings of N-H stretching excitations of guanosine-cytidine base pairs in solution. *J. Phys. Chem. B* **115,** 5484–5492 (2011).

28. Yang, M., Szyc, Ł. & Elsaesser, T. Femtosecond two-dimensional infrared spectroscopy of adenine-thymine base pairs in DNA oligomers. *J. Phys. Chem. B* **115,**

1262–1267 (2011).

29. Greve, C. *et al.* N-H stretching modes of adenosine monomer in solution studied by ultrafast nonlinear infrared spectroscopy and ab initio calculations. *J. Phys. Chem. A* **116,** 7636–7644 (2012).

30. Greve, C. *et al.* N-H stretching excitations in adenosine-thymidine base pairs in solution: Pair geometries, infrared line shapes, and ultrafast vibrational dynamics. *J. Phys. Chem. A* **117,** 594–606 (2013).

31. Siebert, T., Guchhait, B., Liu, Y., Costard, R. & Elsaesser, T. Anharmonic Backbone Vibrations in Ultrafast Processes at the DNA–Water Interface. *J. Phys. Chem. B* **119,** 9670–9677 (2015).

32. Guchhait, B., Liu, Y., Siebert, T. & Elsaesser, T. Ultrafast vibrational dynamics of the DNA backbone at different hydration levels mapped by two-dimensional infrared spectroscopy. *Struct. Dyn.* **3,** 43202 (2016).

33. Hithell, G. *et al.* Long-Range Vibrational Dynamics Are Directed by Watson–Crick Base Pairing in Duplex DNA. *J. Phys. Chem. B* **120,** 4009–4018 (2016).

34. González-jiménez, M. *et al.* Observation of coherent delocalised phonon-like modes in DNA under physiological conditions. *Nat. Commun.* **7,** 1–8 (2016).

35. Deflores, L. P., Nicodemus, R. a & Tokmakoff, A. Two-dimensional Fourier transform spectroscopy in the pump-probe geometry. *Opt. Lett.* **32,** 2966–2968 (2007).

36. Shim, S.-H., Strasfeld, D. B., Ling, Y. L. & Zanni, M. T. Automated 2D IR spectroscopy using a mid-IR pulse shaper and application of this technology to the human islet amyloid polypeptide. *Proc. Natl. Acad. Sci. U. S. A.* **104,** 14197–14202 (2007).

37. Greetham, G. M. *et al.* A 100 kHz time-resolved multiple-probe femtosecond to second infrared absorption spectrometer. *Appl. Spectrosc.* **70,** 645–653 (2016).

38. Banyay, M., Sarkar, M. & Graslund, A. A library of IR bands of nucleic acids in solution. *Biophys. Chem.* **104,** 477–488 (2003).

39. Seeman, N. C. An overview of structural DNA nanotechnology. *Mol. Biotechnol.* **37,** 246–257 (2007).

40. Hamm, P. & Zanni, M. T. *Concepts and Methods of 2D Infrared Spectroscopy*. (Cambridge University Press: Cambridge, 2011).

6. Conclusions and Future Work

In Chapter (1) 2D-IR spectroscopy was highlighted as a valuable technique for examining the ultrafast dynamics that underpin the biological mechanisms of DNA. The sensitivity to changes in molecular structure along with sub-picosecond temporal resolution make 2D-IR spectroscopy an ideal method for providing new dynamic insights into processes involving biomacromolecules that can serve to complement current information obtained from X-ray diffraction and NMR studies. In particular the process of DNA melting was highlighted as an area that current lacked 2D-IR studies in the literature and yet is a crucial step in a biological processes involving DNA.

Two laser systems based at the Rutherford Appleton Laboratories were used to carry out the majority of the experiments presented in this thesis and the details of operation and data acquisition of each of these systems is presented in Chapter (2).

In Chapter (3) the impact of DNA melting on the features observed in the 2D-IR spectrum of a DNA sequence containing only AT base pairs is presented. A number of previous 2D-IR studies of DNA point to a significant degree of delocalistion of vibrational modes, necessitating that a rigorous assignment of the features in the 2D-IR spectrum is performed. A number of off-diagonal coupling features linking a vibrational mode originating from the Adenine base to three vibrational modes originating from the Thymine base that are conformation dependent have been identified. These features further support the idea of delocalisation of vibrational modes of DNA bases across the hydrogen-bonded base pair. Time-resolved 2D-IR spectra have also been recorded to allow observation of solvation dynamics for the AT DNA sequence under both double and single-stranded conditions. Spectral diffusion was measured for the $A_{R1}T$ and AT_{2S} base vibrational modes. Under double-stranded conditions, little change in spectral diffusion is observed for these two modes and upon melting of the DNA duplex a significant increase in spectral diffusion is seen on a timescale of 500-1000 fs. Data presented in this study highlights the possibility of using the T_2 carbonyl group as a probe of solvation dynamics in the DNA minor groove.

Chapter (4) explores the extent of the delocalisation of vibrational modes in DNA. The study utilises 'Two-Colour' 2D-IR spectroscopy to excite the same base vibrational modes

observed in Chapter (3) before probing both the base region as well as the spectral region where vibrational modes located on the DNA backbone are located. A number of off-diagonal features linking each of the base vibrational modes excited to modes represented by vibrations of the phosphodiester linkages (L_1 and L_2 modes) and symmetric stretching vibration of the phosphate moiety (P_2 mode) have been observed for the first time. Conformation dependent couping patterns have been observed in particular for off-diagonal features linking the base modes to the P_2 mode. This indicates that the delocalisation across base pairs observed in Chapter (3) extends further in the DNA double helix. Relaxation dynamics of the off-diagonal features between the base and backbone modes indicate a pathway through which energy absorbed by the DNA bases can relax through to the backbone vibrations and be dissipated into the solvent environment. We propose that mechanism is facilitated by population relaxation from the base modes to lower frequency modes located on the deoxyribose moiety which are in turn coupled to the backbone modes.

In Chapter (5) the observations of Chapter (4) are extended by applying the same experimental methodology to a number of AT DNA sequences that vary in length from a single DNA mononucleotide to 15 base pairs. Off-diagonal features observed linking the base and backbone modes observed in the Chapter (4) for the AT 15mer sequence are also found to be consistent in AT 10mer and AT 6mer sequences. However for sequences shorter than this, the off-diagonal features observed begin to differ, in particular those linking the base modes to the P_2 backbone mode which were shown in Chapter (4) to be sensitive to DNA conformation. The data supports the idea of a minimum DNA sequence length required to form a DNA duplex where the minimum number of bases required appears to be six. Relaxation dynamics were also recorded for each of the AT DNA sequences. Little variation in the timescales of the relaxation dynamics were observed in comparable off-diagonal features for each of the sequence. The lack of dependence on sequence length highlights that the energy transfer mechanism proposed for dissipation of excess energy absorbed in the bases has roots in a single DNA mononucleotide building block.

The studies presented in this thesis have also provided the basis for further studies based on the observations made here. The identification of signatures of DNA melting provides a platform for studying binding of drug type small molecules to the DNA minor groove or

alternatively proteins and peptides to the DNA major groove. In particular temperature-jump 2D-IR, which has recently been demonstrated to study DNA melting by Tokmakoff and co-workers, would be a powerful tool with the temporal resolution to observe the interaction between DNA and the binding molecule in real-time. Determination of exact modes of binding would allow for improved design of drug-molecules to increase binding affinities and subsequently increase drug effectiveness.

Further exploration into the energy relaxation pathway from the DNA bases to the DNA backbone is also encouraged by the studies presented. Firstly, observation of intermediate features that link the bases to the backbone could lie in deoxyribose modes found in the 1300-1500 cm^{-1} region would help isolate the exact mechanism through which the relaxation mechanism is facilitated. Another experiment of interest would be an alternate 'two colour' 2D-IR experiment where the excitation of the backbone modes followed by probing the interaction with base modes in reverse may also provide further insight into the exact nature of the interaction between the different DNA moieties.

Acknowledgements

Thanks first of all must go to my PhD supervisor, Neil. His guidance throughout the course of my PhD has been invaluable and I greatly appreciate his door always being open for discussion of data analysis or experiments. Thank you also for the proofreading and feedback you have given me through the course of writing this thesis, it has truly been invaluable and always timely. A note of thanks also here must go to Sue for passing on some of this feedback when you were out of the country.

Thanks must also go to all the members of the UCP group that I have had the pleasure of working with over the years. From former group members, Marco, Katrin, Danny and Pim who I met through my undergraduate and early PhD work, Niall who has been present for nearly my entire tenure with the group, through to current members Lucy, Robby, Sam and Lennart who have all helped make this experience truly enjoyable and made some long and trying nights at RAL more bearable. I also appreciate our mutual enjoyment of cake and there has been little shortage of that during my time with the group.

On the subject of RAL, I must also offer a huge amount of thanks to our collaborators based there who have made this work possible. To Tony, Greg, Paul, Igor, Ian and Mike, thank you for all your help in acquiring the mountain of data I have been able to accumulate during my PhD and for providing truly insightful discussion in terms of data interpretation and the nuances of the ULTRA and LIFEtime laser systems. Special thanks also to Tony for taking us for the occasional curry and pint (when the lasers were out of action of course).

To my second supervisor Glenn, thank you for all your help, despite starting this project with little more than high school level education in chemistry and biology I have learned a great deal from you about these aspects of my project.

To the other PhD students I have met at Strathclyde through my PhD, in particular those from the Photophysics group who I have spent a lot of time with over the years. Thank you for all the Friday lunches and distractions from work when needed, my repertoire of places to eat in Glasgow is now truly astonishing. To Ben in particular, our time through the entirety of university has been shared and it has been made all the more enjoyable with you close by to discuss food, video games and anything else that comes up (mostly food). I

will uphold my end of the deal (even though you didn't hold up yours) by simply saying – 'Shop?'

To my parents. You have always provided me with every opportunity to achieve in anything I have chosen to pursue. Please know that without your support I would not be the person I am today. Thank you for everything you have done for me, not least putting up with me for the last 27 years (which I appreciate can't be easy at times). To my Grandparents who sadly will not be able to see my time in education come to an end. I must also say thank you for everything you did for me, time spent with you all in my formative years taught me a number of important lessons (not least finishing my sandwiches before my crisps at lunchtime) that I will carry with me forever.

I am extremely fortunate to have met a number of truly incredible people in my life that I now consider to be very close friends. From those that I have known since before primary school, to the close friendships I made through high school, to those that I have met during my time at university. Thank you all for putting up with me in general, but in particular more recently when the demands of thesis writing have limited my time with you. Know that sharing a few pints together; going for food, sitting watching TV or even having a good blether has often been a light at the end of the tunnel for me through the dark days of thesis writing. You are all truly amazing people.

Finally, I would like to say thank you to my girlfriend Dawn. Your constant positivity and belief that I will be able to achieve anything is a constant source of inspiration to me. I am truly grateful for all the support you have given me, even during times when I felt like the world was collapsing. I look forward to all the adventures we are going to get to share together in the future.